UCLA
UCLA Electronic Theses and Dissertations

Title
The mechanism of action and regulation of hepcidin

Permalink
https://escholarship.org/uc/item/1g13b208

Author
Aschemeyer, Sharraya

Publication Date
2017

Peer reviewed|Thesis/dissertation

eScholarship.org Powered by the California Digital Library
University of California

UNIVERSITY OF CALIFORNIA

Los Angeles

The mechanism of action and regulation of hepcidin

A dissertation submitted in partial satisfaction of the

requirements for the degree Doctor of Philosophy

in Molecular Biology

by

Sharraya Lynn Aschemeyer

2017

ABSTRACT OF THE DISSERTATION

The mechanism of action and regulation of hepcidin

by

Sharraya Lynn Aschemeyer

Doctor of Philosophy in Molecular Biology

University of California, Los Angeles, 2017

Professor Tomas Ganz, Chair

Iron is vital for bodily function but is potentially toxic and accordingly, tightly controlled in the body. Systemic iron homeostasis is regulated by the liver-produced hormone hepcidin which controls cellular iron efflux through ferroportin, the only known iron exporter. Ferroportin delivers iron into the plasma from duodenal enterocytes which absorb dietary iron, from macrophages in the spleen and the liver which recycle iron from senescent erythrocytes, and from hepatocytes in the liver which store iron and deliver it to plasma when systemic iron requirements increase. Ferroportin is the hepcidin receptor: hepcidin binds to ferroportin, leading to its endocytosis and degradation, thus preventing the entry of iron into plasma.

Regulation of hepcidin production is crucial for iron homeostasis. Iron, inflammation, and erythropoiesis are three factors which regulate hepcidin transcription. Iron and inflammation

increase hepcidin expression whereas erythropoiesis suppresses it. Dysregulation of hepcidin leads to iron disorders. Hepcidin deficiency causes unrestrained iron absorption resulting in iron overloading disorders, such as hereditary hemochromatosis and β-thalassemia. However, hepcidin excess leads to iron restriction causing anemia, such as iron-refractory iron deficiency anemia.

Neither the mechanism of hepcidin action nor the regulation of hepcidin is completely understood, and these are the two areas on which I focused my research. Chapter 1 elucidates the structural basis of hepcidin-Fpn interaction whereas Chapters 2 and 3 examine potential signaling pathways which regulate hepcidin transcription. More specifically, Chapter 1A examines the structural basis of genetic resistance to hepcidin and details an alternative hepcidin mechanism of action. Chapter 1B provides preclinical support for a potential therapy to treat a genetic iron overload disease caused by resistance to hepcidin. Chapter 2 examines the signaling pathway used by erythroferrone, a protein hormone involved in hepcidin regulation by erythropoiesis, and Chapter 3 examines a candidate hepcidin regulator, Nrf2, a transcription factor induced by oxidative stress.

In summary, this body of work examines the structural basis of hepcidin action, the mechanism of its regulation by iron and erythropoiesis, and a potential therapeutic application to a genetic iron overload disorder.

The dissertation of Sharraya Lynn Aschemeyer is approved.

Donald Barry Kohn

Gregory S. Payne

James Akira Wohlschlegel

Elizabeta Nemeth

Tomas Ganz, Committee Chair

University of California, Los Angeles

2017

TABLE OF CONTENTS

VITA

University of California, Los Angeles 2011-2017
Los Angeles, CA
PhD candidate

University of Michigan 2010-2011
Ann Arbor, MI
Post-baccalaureate program (Michigan PREP)

University of California, San Diego 2006-2010
La Jolla, Ca
B.S. in Biochemistry/Chemistry
Psychology Minor

FELLOWSHIPS

NRSA NIH F31 grant award: HL129760 2015-2017

Cell and Molecular Biology Training Grant: Ruth L. Kirschstein National Research Service Award: GM007185 2012-2015

PUBLICATIONS

Aschemeyer S, Gabayan V, Ganz T, Nemeth E, Kautz L. Erythroferrone and matriptase-2 independently regulate hepcidin expression. Am J Hematol. 2017 Feb 10. doi:10.1002/ajh.24672.

Sandoval S, Mendez N, Alfaro JG, Yang J, **Aschemeyer S**, Liberman A, Trogler WC, Kummel AC. Quantification of endocytosis using a folate functionalized silica hollow nanoshell platform. J Biomed Opt. 2015 Aug;20(8):88003. doi: 10.1117/1.JBO.20.8.088003.

Yang J, Sandoval S, Alfaro JG, **Aschemeyer S**, Liberman A, Martin DT, Makale M, Kummel AC, Trogler WC. Red-luminescent europium (III) doped silica nanoshells: synthesis, characterization, and their interaction with HeLa cells. J Biomed Opt. 2011 Jun;16(6):066012. PMCID:PMC3133801

Yang J, **Aschemeyer S**, Martinez HP, and Trogler WC. Hollow Silica Spheres Encapsulating Silafluorene-fluorene Conjugated Polymer for aqueous TNT Detection. ChemComm. 46(36):6804-6, 2010. PMID: 20737079

PRESENTATIONS

Aschemeyer S, Qiao B, Ruwe T, Vieth K, Jormakka M, Mackenzie B, Ganz T, Nemeth E. Evidence that hepcidin occludes ferroportin to inhibit iron export. Oral presentation presented at the International Bioiron Society, Los Angeles, CA, April 2017.

Aschemeyer S, Qiao B, Sek A, Jormakka M, Ganz T, Nemeth E. Structure-function study of the ferroportin-hepcidin interaction. Poster presented at UCLA's Department of Medicine Day. Los Angeles, CA September 2016.

Aschemeyer S, Qiao B, Ganz T, Nemeth E. The structure-function study of the ferroportin-hepcidin interaction. Poster presented at the Scientific Innovation Through Diverse Perspectives Conference, Rochester, MN May 2016.

Aschemeyer S, Qiao B, Sek A, Jormakka M, Ganz T, Nemeth E. Characterization of ferroportin disease-related residues predicted to confer hepcidin resistance. Poster presented at UCLA's Department of Medicine Day. Los Angeles, CA October 2015.

Aschemeyer S, Qiao B, Sek A, Jormakka M, Ganz T, Nemeth E. Characterization of ferroportin disease-related residues predicted to confer hepcidin resistance. Poster presented at the International Bioiron Society, Hangzhou, China September, 2015

Aschemeyer S, Qiao B, Ganz T, and Nemeth E. Defining the mechanism of hepcidin-induced ferroportin endocytosis. Poster presented at the International Bioiron Society, London, UK, April 2013.

Aschemeyer S, Clapp KM, Lau M, Peng HM, Morishima Y, and Osawa Y. "Time- and Concentration-Dependent Inactivation of Neuronal NO-Synthase by Cobalt Protoporphyrin IX." Oral Presentation at the 38th Annual Pharmacology Research Colloquium, Toledo, OH, June 2011.

Aschemeyer S, Clapp KM, Lau M, Peng HM, Morishima Y, and Osawa Y. Time-dependent inactivation of neuronal NO-synthase, a P450-like hemeprotein, by cobalt protoprohyrin IX. . Poster presented at the Great Lakes Drug Metabolism Conference, Madison, Wisconsin, May 2011.

Aschemeyer S, Yang J, Sandoval S, Alfaro J, Kummel A, Trogler WC. Gold doped hollow silica nanoshells for imaging and drug delivery. . Poster presented at the ACS Conference, San Francisco, CA, March 2010.

Aschemeyer S, Yang J, Sandoval S, Alfaro J, Kummel A, Trogler WC. Folate conjugated PLGA Silica coreshell nanoparticles for drug delivery. Poster presented at the AACR Conference, Washington, DC, April 2010.

OVERVIEW: IRON HOMEOSTASIS

1. Elemental Iron

Comprising eighty-nine percent of the Earth's core and approximately five percent of the Earth's crust, iron is one of the most abundant elements. (1, 2). Iron is a transition metal with 8 oxidation states ranging from -2 to 6.

2. Iron and biology

In biology, iron is found predominately in two forms: ferrous (II) and ferric (III) (2). Though iron is essential for most living organisms, the focus of this thesis is on iron in mammalian biological systems.

2.1 Physiological importance of iron in the body

Iron is involved in many chemical reactions within the body because of its redox potential, which allows it to donate or accept an electron under conditions prevailing in biological organisms. Iron participates in prosthetic groups such as heme which is composed of ferric iron and a porphyrin ring (protophoryrin IX) (3) and iron sulfur clusters which are various arrangements of iron and sulfur atoms covalently bound together (4). Additionally, iron ions can directly bind proteins; these metalloproteins are known as ferroproteins.

ISCs, heme, and ferroproteins are essential for vital cellular processes. For example, oxidative phosphorylation requires proteins containing ISCs, because they shuttle electrons through the electron transport chain. ISCs are also involved in DNA replication since DNA polymerase requires ISCs as a cofactor to form its active complex (5, 6). Additionally, iron in the form of heme is necessary for oxygen transport, because heme binds to oxygen in hemoglobin (7). Many enzymes utilize iron to catalyze reactions ranging from amino acid (aromatic amino acid hydroxylase and glutamate synthase), carbohydrate (glycerol phosphate dehydrogenase and

phosphoenolpyruvate dehydrogenase) and lipid metabolism (fatty acid desaturase), oxygen sensing (prolyl hydroxylases), and drug metabolism (cytochrome P450s) (8). Lastly, iron-binding proteins are also necessary for iron storage and protection from oxidative damage (ferritin) or for iron delivery to cells (transferrin) which will be discussed later in the introduction.

2.2. Bioavailability of iron

Despite being abundant on the Earth's crust and essential for proper bodily function, iron is not readily available to organisms because of oxygen-containing atmosphere oxidizing ferrous iron to ferric iron, which is essentially insoluble (9). The bioavailability of medicinal ferric iron when administered orally is 3-4 fold less than ferrous iron (10). Ferric iron is not efficiently absorbed by the gut, unless the ferric iron is complexed with a protein or chemical scaffold, such as protoporphyrin, or converted to ferrous iron by ferric reductases at the mucosal surface (11). Most humans only absorb 10-15% of iron from their diet (10).

2.3 Body iron distribution

An average adult contains around 3-4 g of iron. About 1-2 mg of dietary iron per day is absorbed in the duodenum by enterocytes but about 20-25 mg daily is needed, mostly for hemoglobin synthesis. The iron requirement is provided mostly by recycling heme iron from senescent erythrocytes within macrophages in the spleen and the liver. This recycling distributes around 20-25 mg of iron per day into the circulation. Transferrin, the main iron carrier in the body, binds about 2-4 mg of this circulating iron. Most of the iron in the body (2-3 g) is stored in erythrocytes. 1 g of iron is stored within ferritin in hepatocytes in the liver and macrophages in the spleen (11-13) (Figure 1). Only 1-2 mg of iron is lost per day due to enterocyte and epithelial shedding or minor blood loss; dietary iron absorption compensates for these losses.

Though body iron distribution is similar between mice and humans, there is a species difference in the iron turnover and absorption rate. As mentioned above, humans replenish their daily iron requirement by recycling heme iron, whereas mice eat more relative to their body mass and absorb enough iron from their diet to meet about half of the daily iron requirement, with the other half generated by recycling. Thus, mice readily become anemic or iron overloaded depending on the iron content of their diet (12). This is an important species difference to note since Chapters 2 and 3 involve iron overloaded mouse models.

3. Iron transport

Iron transport mechanisms have evolved at both the systemic and cellular level to meet our daily iron requirement needs.

3.1 Systemic iron transport

Iron that circulates in the plasma is derived from three sources. Once source is dietary iron, which is absorbed in the duodenum by enterocytes. Another source is recycled iron from macrophages that extract iron from senescent red blood cells in the spleen and the liver. The last source is the mobilization of stored iron from ferritin in the liver. From each of these sources, iron is exported into the plasma by the only known iron exporter, ferroportin (Fpn). Once in the plasma, iron is bound by transferrin and is shuttled to the bone marrow and other tissues that use iron (12) (Figure 1).

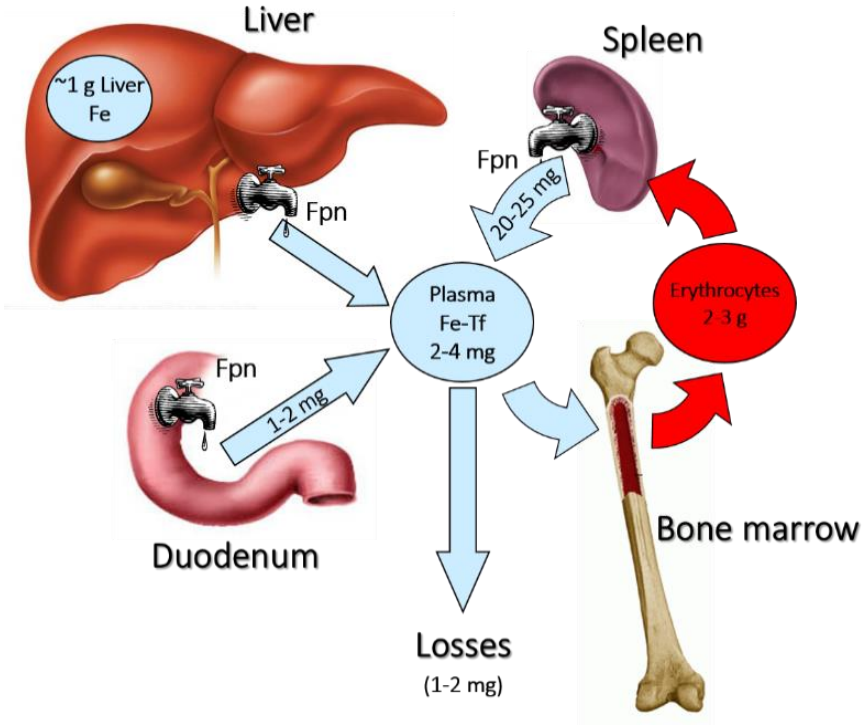

Figure 1 (Adapted from (11)): Body iron distribution in an average adult. Ferroportin (Fpn), the only known iron exporter, exports iron into the plasma from three main sources: duodenum, liver, and spleen. Dietary iron (1-2 mg/day) is transferred from the duodenum into plasma, and 20-25 mg/day of recycled iron is delivered to plasma by macrophages in the spleen. The liver stores ~1 g of iron for utilization when necessary. Most of the iron in the body (2-3 g) is located in circulating erythrocytes and erythroid precursors in the bone marrow. Only a small amount of iron is lost from the body by minor blood loss and epithelial shedding (1-2 mg/day).

3.2 Cellular iron transport

All cells require iron for their vital cellular processes. Some cell types (duodenal enterocytes, splenic and liver macrophages, and hepatocytes) are involved in processing large amounts of iron to supply the rest of the organism.

3.2.1 Iron transport in enterocytes

In duodenal enterocytes, apical uptake of iron is achieved by coordinated action of duodenal cytochrome B (DcytB), a ferrireductase, which reduces iron in the diet from ferric iron to ferrous iron, followed by ferrous iron transport via divalent metal transporter 1 (DMT1) across the membrane into the enterocyte cytoplasm. Heme can also be transported into the enterocyte by an unknown heme transporter and then degraded by heme oxygenase to release the iron (11). Regardless of which apical mechanism provides the iron, Fpn exports the iron across the

basolateral membrane of the enterocyte where the iron is oxidized by the GPI-linked ferroxidase, hephaestin, before entering the bloodstream and binding the carrier protein transferrin (14). The enterocyte only lives for 2-6 days and is then sloughed off and excreted with its iron content. This is unique, because iron from other cell types is recycled (15) (Figure 2).

3.2.2 Generic cellular iron transport

In circulation, transferrin binds one or two iron atoms, and the diferric form is referred to as holotransferrin (holo-tf). Holo-tf circulates until it binds to transferrin receptor 1 (TfR1) in the cell membrane. TfR1 is ubiquitously expressed, although the highest expression is in erythroblasts. TfR1 is regulated post-transcriptionally by cellular iron content: cellular iron deficiency results in stabilization of TfR1 mRNA to increase iron uptake (16). When holo-tf binds to TfR1, the complex is endocytosed. The endosome becomes acidified by proton pumps (17) which dissociates ferric iron from the TfR1-holo-tf complex. Then a ferrireductase, such as STEAP3 (Six-transmembrane epithelial antigen of the prostate 3), reduces ferric iron to ferrous iron. STEAP3 is expressed in macrophages, hepatocytes, and erythroblasts, but it is unclear how generic this ferrireductase is (18, 19). Next, DMT1 exports the iron out of the endosome and into the cytosol where it is referred to as the labile iron pool (LIP). The LIP is poorly characterized since it is difficult to probe experimentally without changing its composition. Most agree that the LIP is composed mainly of loosely coordinated ferrous iron and potentially some ferric iron (~10%). The ferrous iron is likely complexed with reduced glutathione (GSH) present at high concentrations in the cytosol, which prevents the oxidation of iron (20). This ferrous iron can either be stored in the form of ferritin (after it has been oxidized by ferritin heavy chain), shuttled into the mitochondria to generate heme and iron sulfur clusters, used for cytoplasmic ferroprotein synthesis, or exported out of the cell by Fpn (21). In mammals, poly C binding proteins 1 and 2 (PCBP1&2) bind iron in the LIP and

deliver it to ferritin and ferroproteins. PCBPs likely also deliver iron to ferroportin for export and potentially to the mitochondria as well (20). After Fpn exports ferrous iron, it is oxidized to ferric iron by the ferroxidase ceruloplasmin, expressed either as a GPI-membrane bound or as a plasma protein depending on the cell type (22, 23).

Though not as common as iron import by TfR1, many cell types can also import heme. Free plasma heme is bound by hemopexin, a heme scavenger, and then binds to its receptor, low-density lipoprotein receptor-related protein 1 (LRP1) (24). The ligand-receptor complex is endocytosed and degraded in lysosomes. Heme is then exported out of the lysosome by HGR1 (heme responsive gene-1), where either heme oxygenase will degrade heme to free the iron or the heme can be exported out of the cell by FLVCR1 (feline leukemia virus, subgroup C, receptor) (25). These are the generic mechanisms for iron transport utilized by many cells (Figure 2).

3.2.3 Iron transport in hepatocytes

Hepatocytes have the same iron transport mechanism as above, except for two additions. They not only import iron via TfR1, but also TfR2, and they import another form of iron known as non-transferrin bound iron (NTBI). NTBI is iron that is complexed with citrate, albumin, acetate, or glutathione. It is taken up into hepatocytes by ZIP 14 (Zrt–Irt-like protein 14), a transporter that can also transport zinc or manganese. Hepatocytes in the liver are the main importers of NTBI, but the pancreas and heart import NTBI as well (26, 27) (Figure 2).

3.2.4 Iron transport in macrophages

Macrophages have specialized mechanisms to recycle large amounts of iron. Like other cells they can import transferrin-bound iron using TfR1 but, unlike most cells, can also take up heme from plasma hemopexin using LRP1 (also known as CD91). Macrophages also import plasma hemoglobin bound to haptoglobin, a hemoglobin scavenger, via the haptoglobin receptor,

CD163, which is endocytosed. The hemoglobin undergoes proteolysis and the heme is exported by HGR1 out of the endosome. (25). Finally, macrophages also ingest senescent red cells by erythrophagocytosis. When a macrophage engulfs an aged red blood cell, it degrades it in the phagolysosome. Heme is then transported into the cytosol by HGR1 and the free heme is either utilized, degraded to iron, or exported (11) (Figure 2).

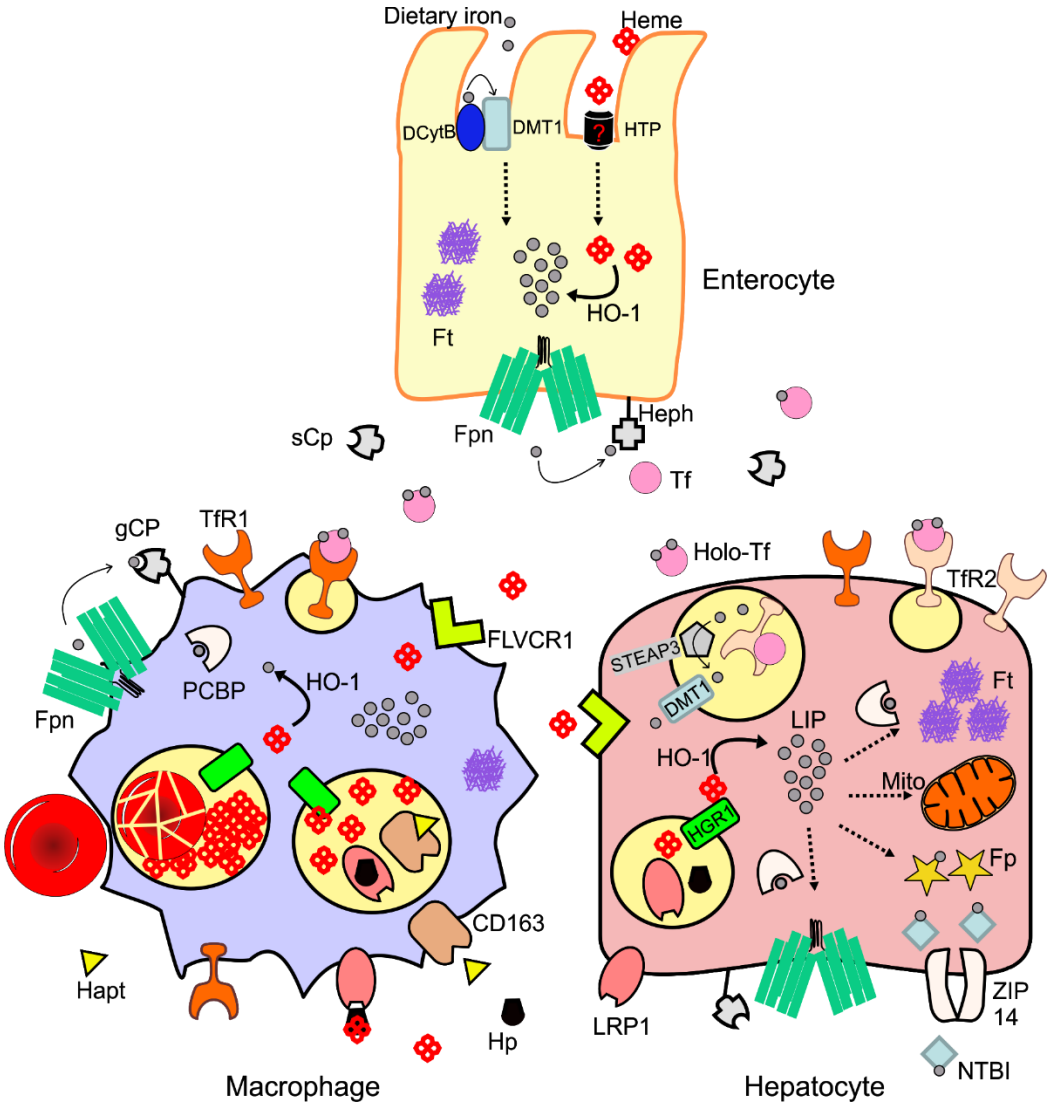

Figure 2 Cellular iron transport. Duodenal cytochrome B (DCtyB) reduces iron in the duodenum, and divalent metal transporter 1 (DMT1) transports the iron into the enterocyte. Heme is also transported into the enterocyte by an unknown heme transporter (HTP) and then degraded by heme oxygenase (HO-1) to release the iron. Ferroportin (Fpn) exports the iron out of the enterocyte where hephaestin (Heph), a ferroxidase tethered to the basolateral membrane by a glycophosphatidylinositol (GPI) anchor, oxides the iron to ferric iron which transferrin (Tf) binds.

When two iron atoms in the plasma bind to transferrin, it is referred to as holo-transferrin (holo-Tf). In hepatocytes, holo-tf binds to its receptor, either transferrin receptor 1 or 2 (TfR1 or TfR2) on the cell surface, causing the complex to be endocytosed into endosomes. The endosome is then acidified which dissociates ferric iron from the transferrin-TfR complex. STEAP3 reduces the iron to its ferrous form and DMT1 exports the iron into the cytoplasm. Additionally, heme binds to hemopexin (Hp), a heme scavenger, and the heme-hemopexin complex binds to its receptor, LRP1, which is then endocytosed. LRP1 degrades in the endosome and the heme is exported by HGR1. The heme is either utilized, exported by FLVCR1, or degraded by HO-1 to free the iron, which then pools in the cytosol. This pooled iron, also known as the labile iron pool (LIP), is bound by PCBPs, iron chaperones, which carry the iron to either be stored in ferritin (Ft), shuttled to the mitochondria (Mito) to form heme or iron sulfur clusters, incorporated by ferroproteins (Fp), or exported from the cell by Fpn. When exported by Fpn, the iron is then reduced by ceruloplasmin either bound to the cell membrane (gCP) or circulating in the plasma (sCP), depending on the cell type. Additionally, non-transferrin bound iron (NTBI) is transported by ZIP14 into the cell. On macrophages, haptoglobin (Hapt), a hemoglobin scavenger, binds to hemoglobin and is recognized by its receptor, CD163. The receptor-ligand-hemoglobin complex is endocytosed and degraded, allowing heme to exit the endosome via HGR1. Additionally, macrophages erythrophagocytose and degrade aged red blood cells, freeing heme which is also transported into the cytosol by HGR1.

4. Toxic effects of iron

Even though iron is required for many essential processes, once it enters the bloodstream there is no way to excrete it (28). Free iron is highly reactive, with ferrous iron being more labile than ferric iron (29). Therefore, iron in the body is usually bound to proteins or is stored within ferritin in its ferric form (30). Having excess iron is toxic, because all iron storage or usage pools become saturated and labile iron accumulates within cells (31). Labile ferrous iron forms hydroxyl radicals via the Fenton reaction (see below), which leads to generation of reactive oxygen species (ROS), such as superoxides via the Haber-Weiss reaction (32). Antioxidant mechanisms to eliminate ROS also become saturated. ROS oxidize lipids and generate lipid peroxides leading to lipid membrane damage. Furthermore, Lipid by-products oxidize amino acids in proteins and nucleic acids in DNA, resulting in further destruction on a microscale and ultimately, tissue damage on a macroscale (31). This occurs in iron overload diseases such as hereditary

hemochromatosis, iron-loading anemias, or transfusion-dependent iron overload (refer to the section 8).

Fenton's reaction: $Fe^{2+} + H_2O2 \rightarrow Fe^{3+} + OH^- + OH\cdot$ (33)

5. Systemic iron regulation

As mentioned above, although iron is essential for life, it is toxic in excess, which necessitates a close coordination between its absorption and utilization. Iron is systemically regulated by hepcidin, which is a 25 amino acid peptide hormone predominately produced by hepatocytes in the liver and is conserved in vertebrates (34). Hepcidin is the central regulator for iron absorption, regulating the iron exported into the plasma by Fpn from the duodenum, liver, and spleen (Figure 1). Hepcidin binds to ferroportin causing ferroportin to be ubiquitinated, endocytosed, and degraded in lysosomes (Figure 3) (35). When hepcidin is low, ferroportin accumulates in the cell membrane and exports iron into the plasma from the duodenum, liver, and spleen, causing an increased influx of iron into blood plasma. Thus, iron deficiency suppresses hepcidin allowing an influx of iron into circulation. Conversely, decreased ferroportin (caused by high hepcidin production or non-functional ferroportin) results in less iron absorption in the duodenum and more iron retention in macrophages, decreasing the flow of iron into blood plasma and decreasing plasma iron concentration. When the body is iron-loaded, hepcidin is increased preventing further iron flows into plasma, preventing further iron absorption from the diet to maintain total body iron balance (12).

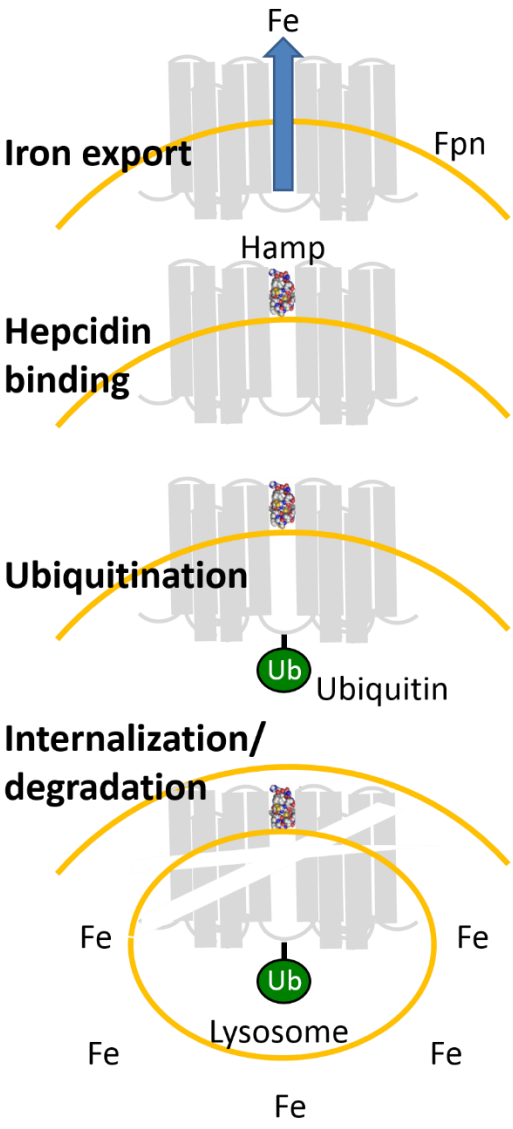

Figure 3: Regulation of Fpn by hepcidin. Under baseline conditions, Fpn exports iron out of the cell. In the presence of hepcidin, hepcidin binds to Fpn causing Fpn to undergo a conformational change that leads to the ubiquitination of Fpn's intracellular loop. The ubiquitin tag triggers Fpn to endocytose and degrade in lysosomes. As a consequence, iron export is inhibited and iron accumulates in the cell.

6. Structural studies of ferroportin and hepcidin

The structural features of hepcidin and Fpn determine the hepcidin-Fpn interaction. Therefore, analysis of both their structures is necessary for the understanding of how hepcidin regulates Fpn.

6.1 Ferroportin Structure

Fpn is a 62 kDa, 12 transmembrane protein encoded by the SLC40A1 gene. Based on analysis of its amino acid sequence, Fpn is a member of the major facilitator superfamily (MFS) (36, 37). Most of what we understand about Fpn structure has come from studying other MFS proteins, since crystalizing human Fpn has been a difficult task. Based on the MFS, Fpn is symmetric; the N-terminal six helices of Fpn form a bundle that is connected by a long intracellular loop to the C-terminal six helix bundle. It is expected that Fpn exports iron similarly to how other MFS proteins transport substrate, via the alternating access transport mechanism (also known as the rocker-switch model) (37). This model suggests that Fpn exports iron by alternating between three states: inward-open, occluded, and outward-open. When Fpn is in its inward-open conformation, its iron binding site is accessible and iron binds Fpn. This binding transitions Fpn to an intermediate state known as the occluded state which is a neutral state that is not open to either the cytoplasm or extracellular space. Then Fpn undergoes a conformational change to its outward-open state. In this state, iron is released into the extracellular space (37) (Figure 4).

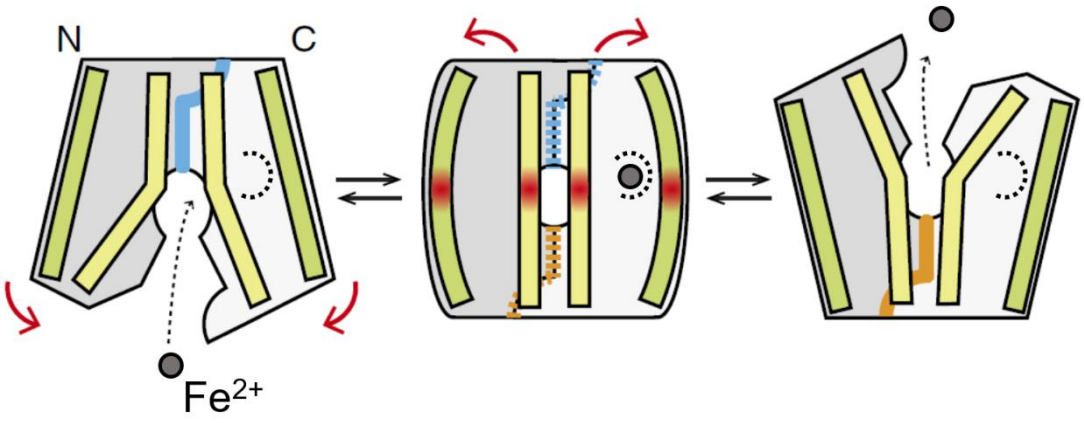

Figure 4: Alternating access iron transport mechanism adapted from (38). Iron binds to Fpn in its inward open state. Then the structure of Fpn changes to the occluded state where the iron in Fpn is not accessible to either side of the membrane. Lastly, Fpn transitions to its outward open state, releasing the iron into the extracellular space.

Fpn is a large transmembrane protein with many disordered regions. Thus, expressing Fpn in mammalian or insect systems has proven laborious with low yields and relatively poor crystal formation (39, 40). As a result, computational human Fpn models were based on crystal structures of known MFS proteins that are similar in sequence to Fpn (39, 41, 42). Recently, however, Taniguchi et al. crystalized the structure of a Fpn homolog, BdFpn (Bdellovibrio Fpn), from the bacterium Bdellovibrio bacteriovorus both in its inward-open and outward-open state (38). This was an important advance in the MFS field since this was the first member to have been crystalized in both conformations from same organism (36).

Although BdFpn gives insight into the structure of Fpn, it is much less informative about the hepcidin-Fpn interaction because it lacks the hepcidin-binding site, which has only evolved in vertebrates. Nevertheless, modeling of human Fpn based on the similarity to BdFpn structure predicted that hepcidin should bind inside the Fpn central cavity, but the experimental evidence has been lacking. All previous models suggested that hepcidin binds on an extracellular loop near the opening of the Fpn cavity (41-46). Chapter 1 provides evidence that hepcidin binds in the central cavity of human Fpn and proposes an alternative mechanism of hepcidin action that supplements the endocytic mechanism documented by our laboratory earlier (35).

6.2 Hepcidin structure

The structure of hepcidin has also been important to advancing our understanding about the hepcidin-Fpn interaction. Human hepcidin is a 2.5 kDa peptide with amino acid sequence DTHFPICIFCCGCCHRSKCGMCCKT (47). Its structure was solved by NMR (48) and crystallography (49). Hepcidin is a hairpin shape β sheet (Figure 5). The curved hairpin bends towards the C-and N-termini with the curvature stabilized by two disulfide bonds. In total, hepcidin contains 4 disulfide bonds (49).

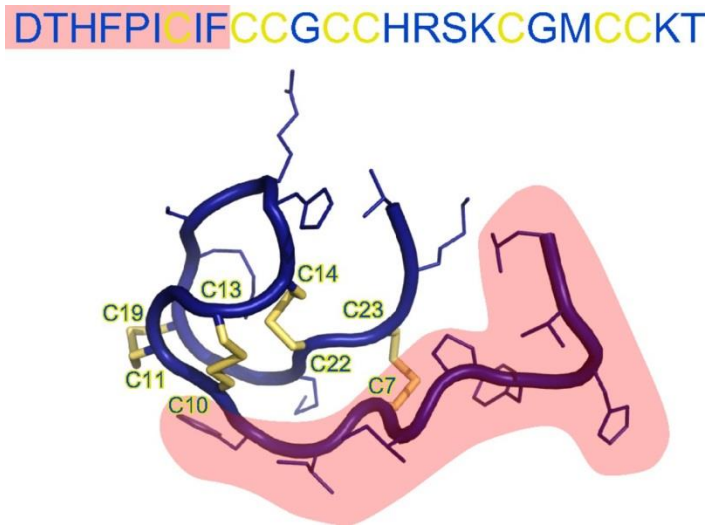

Figure 5 (from (11)): Hepcidin amino acid sequence (top) and structure (bottom). Hepcidin is a 25 amino acid peptide with 4 disulfide bonds. The cysteines for each of the disulfide bonds are in yellow. Hepcidin's structure is hairpin shaped and its turn bends towards the C- and N-termini. The pink highlight indicates the N-terminus of hepcidin that is crucial for hepcidin activity.

The extent to which the thiols in hepcidin interact with Fpn is still poorly understood. Clark et al. changed the 4 disulfide bonds in hepcidin to diselenide bonds to make the bonds more resistant to reduction. This mutated hepcidin had similar activity to native hepcidin (50). The diselenide bonds were more resistant to reduction and exchange than the disulfide bonds, but they still were reduced in the presence of dithiothreitol (DTT) (50). Further examination included performing pairwise substitutions from cysteines to alanines for each of the disulfide bonds. The 4 pairwise disulfide bond mutants had a similar loss in hepcidin activity compared to native hepcidin, but none of them were crucial for activity (51). Based on these experiments, no individual disulfide bond appears necessary for hepcidin activity.

However, C326S, a Fpn mutant found in a family with hereditary hemochromatosis, is hepcidin-resistant, because it cannot bind hepcidin despite being an isosteric substitution. The thiol requirement on the Fpn side suggests that some type of thiol interaction occurs between hepcidin

and Fpn (52). Furthermore, hepcidin remains bound to Fpn even after protein extraction, immunoprecipitation, and SDS-PAGE, unless treated with DTT before SDS-PAGE (51). Though individual disulfide bonds in hepcidin are not required for activity, there is evidence to support hepcidin interacting with Fpn by thiol-disulfide exchange. However, Chapter 1B provides evidence that thiol-disulfide exchange is not necessary for hepcidin mimics (refer to section 9).

The most flexible region of hepcidin is at the N-terminus (49). Nemeth et al. discovered the N-terminus was critical for activity, but the first 3-6 amino acids alone were not sufficient for activity (47). More specifically, amino acids: H3, F4, I6, and F9 in the N-terminus are crucial to hepcidin activity, presumably because their hydrophobic (and for F possibly aromatic) properties are necessary for the hepcidin-Fpn interaction (50, 51).

Another notable feature about hepcidin is that it aggregates (51). Hunter et al. hypothesized that this aggregation is likely due to the phenylalanine at position 4 forming a π-interaction with the phenylalanine at position 9 on another hepcidin (48). It is unknown whether aggregates of hepcidin are more or less active than hepcidin monomers.

7. Regulation of hepcidin

Regulation of hepcidin production is critical for maintenance of iron homeostasis, and for response to erythropoietic stress or infection. Iron, inflammation, and erythropoiesis are three main factors that transcriptionally regulate hepcidin. Both iron and inflammation stimulate, and erythropoiesis suppresses hepcidin production (Figure 6).

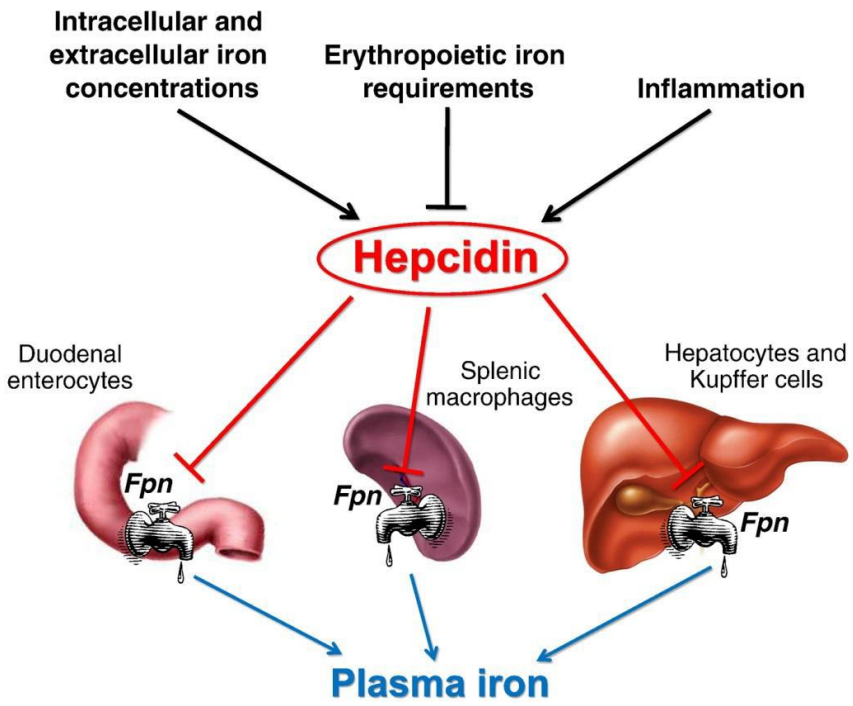

Figure 6 (From (12)): Regulation of hepcidin ensures maintenance of iron homeostasis. Intracellular iron, extracellular iron, and inflammation increase hepcidin transcription (black arrows), whereas erythropoiesis suppresses it. Increased hepcidin expression will degrade Fpn on enterocytes, macrophages in the spleen, and hepatocytes and Kupffer cells in the liver to lower plasma iron (blue arrows). Conversely, a decrease in hepcidin increases plasma iron.

7.1 Hepcidin regulation by iron

Two distinct iron signals that regulate hepcidin are extracellular and intracellular iron. The iron-sensing and signaling system is built around the BMP (bone morphogenetic protein) pathway. The BMP pathway involves BMP ligands and their receptors that trigger the phosphorylation of SMADs (suppressor of mothers against decapentaplegic proteins) and other SMAD-independent pathways. However, the signal for hepcidin regulation is SMAD-dependent. BMP ligands are members of the TGF-β (transforming growth factor- β) family. There are over 20 BMP-related ligands, but the ones known to be involved in hepcidin regulation are BMP 2 and 6. They bind to BMP receptors (BMPRs) which have serine/threonine kinase activity. There are two types of BMPRs: type I and II. The type I receptors include Alk 1 (activin receptor-like kinase 1), Alk2,

Alk3, and Alk6. The type II receptors include BMPR2, ActRIIa (activin receptor type IIa), and ActRIIb. The BMPRs involved in hepcidin regulation are Alk2, Alk 3, ActIIRA, and BMPR2 (53). The physiologic function of BMP receptors requires heterodimeric complexes of type I and type II receptors; Type I receptors heterodimerize with type II receptors. Type II receptors are constitutively active and phosphorylate type I receptors upon ligand binding which then activates type I receptors (54, 55). In the context of hepcidin regulation, when type I receptors are activated, they phosphorylate SMADs 1,5, and 8. Once phosphorylated, they heterodimerize with SMAD4 and translocate to the nucleus to bind to the hepcidin promoter to increase hepcidin transcription (56).

7.1.1 Extracellular iron-sensing pathway

Remarkably, signaling by BMP receptors in the context of iron regulation is strongly modulated by iron-specific receptors and adaptors. The iron-mediated activation of the BMP/SMAD pathway begins with holo-transferrin (transferrin-bound iron). Holotransferrin (holo-tf) is the extracellular form of iron that is sensed by TfR1 and TfR2 on hepatocytes. TfR2 is a homolog of TfR1 but has a lower affinity (~30x) for transferrin than TfR1, and its expression is restricted predominately to hepatocytes (57). Another difference between these two extracellular iron sensors is that holo-tf binding to TfR2 in itself stabilizes membrane TfR2 protein by redirecting TfR2 to recycling endosomes instead of lysosomes for degradation. This effect was not seen with TfR1 (58, 59). Additionally, iron regulates TfR1 by increasing TfR1 mRNA stability, whereas it does not for TfR2 (60).

When holo-tf concentrations are low, TfR1 is complexed with HFE, an MHC class I-like protein. However, when holo-tf binds to TfR1, it displaces HFE from TfR1, allowing it to interact with TfR2. TfR2 and HFE then potentiate the BMP signaling, possibly by forming a supercomplex

with a BMP co-receptor, hemojuvelin (HJV) (61), BMP6 and/or BMP2, a heterodimer of BMP receptors, and neogenin (62-64). This is an attractive model, but has not been fully experimentally verified. HFE was also shown to interact with Alk3 and prevent its ubiquitination (65), and there is controversy in the field as to how TfR2 interacts with the BMP receptor complex, if it does at all (66). Furthermore, it is not well understood what function neogenin performs in the receptor complex, except that it potentiates the BMP signal (67). What is known is that the BMP receptor complex phosphorylates SMADs 1, 5, and 8. (Figure 7). The BMP signaling pathway leads to the transcription of other genes besides hepcidin, including ATOH8 and ID1 (68), as discussed further in Chapter 2.

7.1.1a Negative regulators of extracellular iron-sensing

There also are multiple mechanisms in the extracellular iron-sensing pathway that negatively regulate the BMP/SMAD signal. Soluble HJV (sHJV), a shed inactive form of HJV as a result of furin (a protease) and matriptase-2 (MT-2) cleavage, negatively regulates the BMP/SMAD pathway by binding to BMP 6 (69). MT-2 is a serine protease that dampens the BMP signal by cleaving HJV and thus, decreasing hepcidin transcription. Also, MT-2 itself is regulated by iron. Iron deficiency (low intracellular iron) stabilizes MT-2 on the hepatic membrane surface to dampen hepcidin, allowing plasma iron to increase (70).

A direct negative regulator of the SMAD4 complex signal is SMAD7. The BMP signaling pathway prompts SMAD4 complex translocation into the nucleus to bind to the SMAD7 promoter to increase SMAD7 transcription (68, 71). SMAD7, a negative feedback regulator, either competes with SMAD4 complexes to bind to the hepcidin promoter, binds to a different region on the promoter, or does a combination of both, which inhibits transcription leading to a dampening of the BMP/SMAD signal (72) (73).

7.1.1b Inappropriate extracellular iron-sensing

Mutations in multiple components of this pathway results in inappropriate sensing of iron and hepcidin dysregulation. HFE (74), HJV (75), and TfR2 (76) KO mice are hepcidin deficient, resulting in the genetic iron overload disease known as hereditary hemochromatotsis (refer to the section 8.2.1). Additionally, neogenin (67), Alk2, Alk3 (64), BMP6 (77), BMP2 conditional KO (78) and SMAD1/5 conditional KO (79) mice all lead to hepcidin deficiency and iron overload. Mutations in Tmprss6, the gene encoding MT-2, results in excessive hepcidin production and iron-refractory iron deficiency anemia (IRIDA) (refer to section 8.1.2) (80).

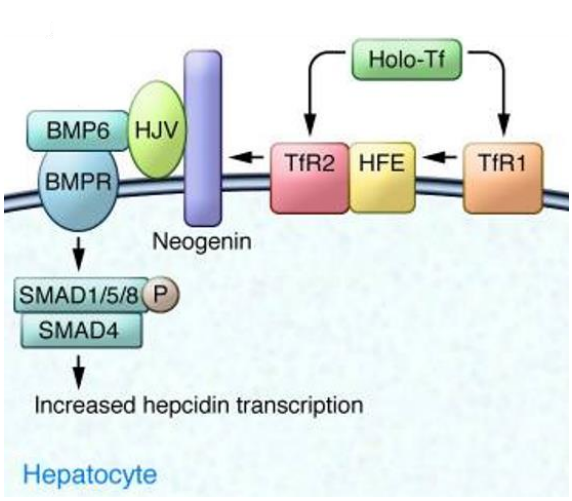

Figure 7 (Adapted from (56)): Current model of hepcidin regulation by iron. A) Holo-transferrin (Holo-Tf) binds to transferrin receptors 1 and 2 (TfR1 and TfR2). When transferrin binds TfR1, HFE dissociates from TfR1 and interacts with TfR2. HFE/TfR2 will interact with the BMP complex, consisting of hemojuvelin (HJV), neogenin, BMP6 (or other BMP ligands), and the BMP receptor (BMPR). The BMPR is formed by heterodimers of ActRIIa or BMPR2 with Alk2 or Alk3. This complex triggers the phosphorylation of SMADs 1, 5, and 8. These SMADs heterodimerize with SMAD4 and translocate into the nucleus to bind to the hepcidin promoter and increase hepcidin transcription. The intracellular iron sensor is unknown, but its signaling pathway probably overlaps the extracellular iron-sensing pathway, except BMP ligand expression increases as a result from rising intracellular iron concentrations.

7.1.2 Intracellular iron-sensing pathway

The intracellular iron sensor is less understood. BMP6 is proposed to be an important mediator of the signal as production of BMP6 in the liver correlates with hepatic iron loading. Both HJV knockout (KO) and BMP6 KO mice placed on a chronic iron loading diet have a blunted increase in hepcidin transcription indicating that they play a role in this circuitry. However, the

signaling pathway is not fully dependent on these molecules as both KO mice still partially increase hepcidin after being chronically iron loaded compared to their wildtype (WT) controls (81). Recently, Koch et al. discovered that BMP2 modulates iron homeostasis in a manner that is nonredundant with BMP6 (78). Thus, BMP2 is also likely involved in the intracellular iron-sensing pathway. Sinusoidal endothelial cells in the liver produce BMP6 and BMP2, which interact with the BMP receptor complex on hepatocytes to induce BMP/SMAD signaling, thereby increasing hepcidin transcription (78, 82). It is unknown how and where intracellular iron signals for the production of BMP6 and BMP2. Chapter 3 examines a potential intracellular iron sensor.

7.2 Hepcidin regulation by inflammation

7.2.1 Interleukin-6 (IL-6) pathway

Inflammation also increases hepcidin expression (Figure 8). Inflammatory cells produce IL-6, an inflammatory cytokine, which binds to the IL-6 receptor on the hepatocyte to induce the JAK2-STAT3 (janus kinase 2-signal transducer and activator of transcription 3) signaling pathway. STAT3 binds to its STAT3 domain in the hepcidin promoter to induce hepcidin transcription (83).

7.2.2 BMP pathway

Activin B, another inflammatory cytokine, was proposed to be an important inflammatory mediator of increased hepcidin transcription via the BMP/SMAD 1/5/8 signaling cascade (84, 85) (Figure 8). However, the biological role of this mechanism has recently been questioned. Besson-Fournier et al. concluded that Activin B is a biomarker of bacterial infection rather than a regulator of hepcidin in response to inflammation since Activin B (*Inhbb*) KO mice infected with either LPS or E. coli do not have blunted hepcidin transcription compared to their WT controls (86).

7.2.3 Cross talk between the IL-6 and BMP pathways

Additionally, there is cross talk between BMP and IL-6 pathways. Mice lacking Tmprss6 are unresponsive to LPS, an inflammatory stimulus, because these KO mice have very high levels of baseline hepcidin caused by an overstimulation of the BMP pathway (87). Additionally, inflammation decreases MT-2 expression due to a decrease in STAT5 signaling, which dampens the BMP signal (88). Thus, the BMP pathway functions synergistically with the IL-6 pathway to mediate hepcidin transcription.

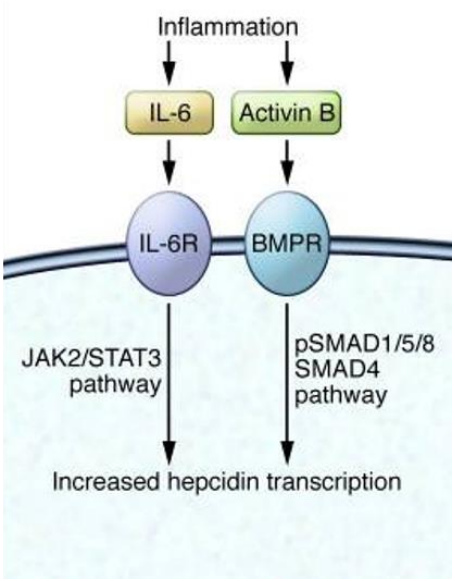

Figure 8 (Adapted from (56)): Current model of hepcidin regulation by inflammation. Inflammation induces interleukin 6 (IL-6) which interacts with its receptor, IL-6R, and triggers the JAK2/STAT3 signaling pathway to increase hepcidin transcription. In addition, inflammation also induces Activin B, another inflammatory cytokine, to increase hepcidin transcription via the BMP/SMAD pathway, but its role in regulating hepcidin in response to inflammation *in vivo* has recently been challenged (86).

7.3 Hepcidin regulation by erythropoiesis

7.3.1 Baseline erythropoiesis

Furthermore, erythropoiesis inhibits hepcidin transcription. Iron is an essential functional component of heme within hemoglobin and is required for erythropoiesis. Since erythroid precursors are the main consumers of iron, iron bound by transferrin flows mostly to the bone marrow for erythrocyte production (12, 89). During heightened red cell production, intestinal iron absorption and the release of iron from stores increase, facilitating the production of new

erythrocytes. In the absence of regulatory responses, even a moderate increase in erythropoiesis would rapidly deplete the iron in the transferrin compartment and limit not only hemoglobin synthesis, but also all other iron-dependent processes (89). Thus, erythropoiesis suppresses hepcidin in order to maintain red cell production.

7.3.2 Stress erythropoiesis

Stress erythropoiesis is different from basal red blood cell production, because it occurs in response to specific types of stimuli such as hemorrhage, hemolysis, hypoxia, or erythropoietin treatment (90). During such stress, hemoglobin synthesis is greatly enhanced which increases iron usage in the bone marrow up to 10x over the normal requirement (89). To meet this iron demand, hepcidin is suppressed, allowing iron influx from the diet and release of iron from macrophages, and from ferritin in the liver. Thus, hepcidin is low in patients who develop an erythropoietic response to anemia and especially low in patients with ineffective erythropoiesis, a condition in which the erythropoietic response develops but does not result in proportional production of mature erythrocytes (91).

7.3.3 Mechanism of hepcidin regulation by stress erythropoiesis

The mechanism which stress erythropoiesis regulates hepcidin transcription is beginning to be understood. Blood loss leads to anemia and renal hypoxia. Erythropoietin-producing cells in the kidneys sense the decrease in oxygen levels and secrete erythropoietin (EPO), a hormone that activates JAK2-STAT5 signaling in cell types equipped with erythropoietin receptors (EPOR), mainly erythroid precursors. This signaling pathway induces a recently described erythroid regulator of hepcidin, erythroferrone (ERFE) (92), produced in erythroblasts and secreted from the bone marrow and the spleen (in mice). ERFE belongs to the C1q-TNF related family of proteins. Once in circulation, ERFE acts on hepatocytes to decrease hepcidin by an unknown mechanism

(92). It has recently been shown that ablation of SMAD1/5 prevents both EPO and ERFE treatment from suppressing hepcidin (79). Therefore, ERFE suppresses hepcidin by dampening SMAD1/5 signaling, but the mechanism by which this occurs is unknown. Chapter 2 provides evidence that ERFE signaling does not involve MT-2.

7.3.4 Physiological and pathological role of erythroferrone

Though the detailed mechanism of ERFE action is unknown, its physiological and pathological role is known. ERFE KO mice are phenotypically normal unless they are stressed. When stressed by either phlebotomy or EPO injection, ERFE KO mice fail to suppress hepcidin (92). Additionally, ERFE has a pathological role in β-thalassemia, a disease characterized by ineffective erythropoiesis. ERFE mRNA levels are remarkably elevated in the bone marrow and the spleen of β-thalassemia intermedia ($Hbb^{th3/th3}$) mice and ablation of ERFE in these mice restored hepcidin levels to normal and reduced the liver iron content (93). These results suggest that ERFE is one of the long-sought erythroid regulators responsible for hepcidin suppression and iron overload in patients with hereditary iron-loading anemias.

8. Iron disorders

8.1 Anemias

The most common type of anemia worldwide is iron-deficiency anemia. However, there are other anemias resulting from genetic mutations, such as β-thalassemia and iron-refractory iron deficiency anemia.

8.1.1 β-thalassemia (iron-loading anemia)

β-thalassemia is an iron-loading anemia characterized by ineffective erythropoiesis. β-thalassemia is caused by mutations in the gene encoding beta-globin, leading to decreased

production of the protein (94). Depending on the degree of beta-globin deficiency and modifying factors, there are three clinically-defined types of β-thalassemia: major, intermedia, and minor (94). The manifestations of the disease are progressively worse when examining minor, intermediate, and major β-thalassemia patients. Hemoglobin is made up of four subunits: 2 subunits of α-globin and 2 subunits of β-globin. When there is little or no β-globin to dimerize to α-globin, the α-globin aggregates become insoluble and forms precipitates in the red blood cell that leads to oxidative damage, causing a shortened lifespan and hemolysis of mature erythrocytes (95). The α-globin aggregates also affect erythrocyte precursors by causing most of them to undergo apoptosis at the erythroblast stage. Thus, erythrocyte precursors massively expand but do not mature into erythrocytes, causing ineffective erythropoiesis as seen in β-thalassemia major and intermedia patients (96). As a result of both hemolysis and ineffective erythropoiesis, the patients become anemic. Their erythropoietic organs (marrow and spleen), under constant pressure to produce more red blood cells, greatly expand but fail to compensate for ineffective erythropoiesis. In both β-thalassemia intermedia and major, an increase in ineffective erythropoiesis suppresses hepcidin and induces enhanced iron absorption from the diet. Since there is no net increase in red cell mass, the additional iron is not utilized for red blood cell formation, and it deposits in the liver, heart, and endocrine tissues (97). If the patients are treated with frequent blood transfusions (β-thalassemia major), the hepcidin-suppressive effect of erythropoiesis is partially ameliorated, but the added iron load of each unit of erythrocytes (200-250 mg of iron) (98) exacerbates the iron overload. Ultimately, β-thalassemia intermedia and major patients will die early from iron-induced cardiomyopathy and heart failure it not treated (99). If treated with iron chelators, they can live into their fifties and sixties (100).

8.1.2 Iron-refractory iron deficiency anemia (IRIDA)

IRIDA is a hereditary iron disorder that results from mutations in Tmprss6, the gene encoding MT-2. IRIDA patients have normal to high hepcidin despite low transferrin saturation, and suffer from severe microcytic hypochromic anemia, low reticulocyte count, and increased red blood cell number (101). The disease is iron-refractory, meaning that oral iron treatment does not improve a patient's iron deficiency because inappropriately elevated hepcidin levels block medicinal iron absorption. Even intravenous (IV) iron only partially corrects the anemia in these patients because of hepcidin-induced iron-trapping in macrophages, and the patient's response to IV iron is slow (101). Thus, a treatment that decreases hepcidin levels would be beneficial for these patients.

8.2 Iron overload disorders

8.2.1 Hereditary Hemochromatosis

Hereditary hemochromatosis (HH) is an autosomal recessive genetic iron overload disorder caused by mutations in genes involved in iron homeostasis. There are 4 different types of HH that are categorized by the gene causing the disease. Five mutated genes that lead to HH are: HFE (type I), HJV (type IIa), Hamp (hepcidin, type IIb), TfR2 (type III), and SLC40A1 (refer to section 8.2.2) (type IV). Adult HH, also known as classical HH type I and III, is characterize by late onset of symptoms occurring after the age of 40, gradual iron loading, and progressive liver damage. Juvenile HH, also known as type II HH, is more a severe form of HH and is characterized by early onset of symptoms occurring between ages 20-30, rapid iron loading, liver damage, and heart complications, such as arrhythmias and heart failure (102).

8.2.2 Ferroportin Disease

Ferroportin Disease, also known as Hereditary Hemochromatosis type IV, is a rare iron overload disorder caused by point mutations in SLC40A1, the gene encoding Fpn, leading to either a gain of, or loss of Fpn function. Accordingly, there are two subtypes of Ferroportin Disease (FD): classical (loss-of-Fpn function) and non-classical (gain-of-Fpn function). Classical FD is characterized by high serum ferritin and normal transferrin saturation resulting from hypofunctional Fpn (103). Non-classical FD on the other hand resembles classical hemochromatosis and is characterized by high serum ferritin and high transferrin saturation due to hepcidin resistance (104). This disease is caused by heterozygous mutations with a dominant effect. Even though the wild-type Fpn copy will degrade in the presence of hepcidin, the mutant Fpn copy will continue to export iron into the blood circulation, causing hyperabsorption of dietary iron and eventually iron overload (105, 106). The most severe non-classical FD mutation, C326S, is a hepcidin-nonbinding mutant (52). One C326S Fpn mutant patient exhibited arthritis when only 16 years old and another had liver cirrhosis at age 35 due to iron overload (107). This and other gain-of-function Fpn mutations are categorized, experimentally analyzed, and discussed further in Chapter 1.

9. Minihepcidins as a therapeutic intervention for iron overload

Patients with iron overload need better therapies. The current treatment for patients with hereditary hemochromatosis is blood-letting (phlebotomy) to remove the excess iron. The treatment of anemic β-thalassemic patients involves transfusions and iron chelators (97, 108). Though these treatments are effective, phlebotomies are inconvenient requiring the patient to visit the hospital weekly or every two weeks during the initial de-ironing and multiple times a year for

the rest of their life (109). Furthermore, many patients prescribed iron chelators suffer from side effects and are noncompliant (51).

Unfortunately, native hepcidin is an imperfect therapeutic candidate, because it is difficult to refold after chemical synthesis and has a short half-life in circulation (51, 110). Minihepcidins are hepcidin agonists which consist of 7-9 amino acids comprising the N-terminal region of hepcidin (51). They are further modified by substitutions of unnatural amino acids to make them resistant to proteolysis, and they are PEGylated and/or derivatized with fatty acids to increase their half-life by decreasing renal clearance. These peptides interact with ferroportin causing endocytosis and thus iron restriction, similarly to hepcidin (51). Minihepcidins prevented iron overload in a hereditary hemochromatosis mouse model (111) and improved anemia and iron overload in a β-thalassemia intermedia mouse model (112). There are other therapies that are in clinical trials or progressing towards clinical trials including: other hepcidin agonists, Fpn antagonists, and drugs enhancing hepcidin transcription (113, 114), but none are FDA approved yet. Chapter 1B provides evidence that minihepcidins could potentially be developed for the treatment of patients with non-classical Ferroportin Disease.

10. Summary

The work in this dissertation provides new insights about the hepcidin-Fpn interaction (Chapter 1) and the regulation of hepcidin by erythropoiesis and iron (Chapters 2 and 3). Chapter 1A provides evidence for an alternative mechanism of hepcidin action, and Chapter 1B provides preliminary evidence that minihepcidins could treat non-classical Ferroportin Disease patients. Chapter 2 examines a potential signaling pathway of a recently discovered hepcidin suppressor, erythroferrone, and Chapter 3 examines a candidate intracellular iron sensor, Nrf2.

REFERENCES

1. Morgan JW, Anders E. Chemical composition of Earth, Venus, and Mercury. *Proc. Natl. Acad. Sci. U. S. A.* 1980; 77(12)**:** 6973-6977.

2. Beard JL, Dawson H, Pinero DJ. Iron metabolism: a comprehensive review. *Nutr. Rev.* 1996; 54(10)**:** 295-317.

3. Layer G, Reichelt J, Jahn D, Heinz DW. Structure and function of enzymes in heme biosynthesis. *Protein Sci.* 2010; 19(6)**:** 1137-1161. doi: 10.1002/pro.405

4. Fontecave M. Iron-sulfur clusters: ever-expanding roles. *Nat. Chem. Biol.* 2006; 2(4)**:** 171-174. doi: 10.1038/nchembio0406-171

5. Beinert H, Holm RH, Munck E. Iron-sulfur clusters: nature's modular, multipurpose structures. *Science* 1997; 277(5326)**:** 653-659.

6. Netz DJ, Stith CM, Stumpfig M, Kopf G, Vogel D, Genau HM *et al.* Eukaryotic DNA polymerases require an iron-sulfur cluster for the formation of active complexes. *Nat. Chem. Biol.* 2011; 8(1)**:** 125-132. doi: 10.1038/nchembio.721

7. Geissler C, Singh M. Iron, meat and health. *Nutrients.* 2011; 3(3)**:** 283-316. doi: 10.3390/nu3030283 [doi];nutrients-03-00283 [pii]

8. Gropper S, Smith J, Carr T. *Advanced Nutrition and Human Metabolism*, 7 edn Cengage Learning, 2018.

9. Nakamori M, Hien VT, Khan NC, Lam NT, Dung NT, Uotsu N *et al.* Difructose anhydride III enhances bioavailability of water-insoluble iron in anemic Vietnamese women. *J. Nutr. Sci. Vitaminol. (Tokyo)* 2010; 56(3)**:** 191-197.

10. Santiago P. Ferrous versus ferric oral iron formulations for the treatment of iron deficiency: a clinical overview. *ScientificWorldJournal* 2012; 2012**:** 846824. doi: 10.1100/2012/846824

11. Ganz T. Systemic iron homeostasis. *Physiol Rev.* 2013; 93(4)**:** 1721-1741. doi: 93/4/1721 [pii];10.1152/physrev.00008.2013 [doi]

12. Ganz T, Nemeth E. Hepcidin and iron homeostasis. *Biochim.Biophys.Acta* 2012; 1823(9)**:** 1434-1443. doi: S0167-4889(12)00016-X [pii];10.1016/j.bbamcr.2012.01.014 [doi]

13. Ganz T, Nemeth E. Regulation of iron acquisition and iron distribution in mammals. *Biochim.Biophys.Acta* 2006; 1763(7)**:** 690-699.

14. Petrak J, Vyoral D. Hephaestin--a ferroxidase of cellular iron export. *Int. J. Biochem. Cell Biol.* 2005; 37(6)**:** 1173-1178. doi: 10.1016/j.biocel.2004.12.007

15. Mayhew TM, Myklebust R, Whybrow A, Jenkins R. Epithelial integrity, cell death and cell loss in mammalian small intestine. *Histol. Histopathol.* 1999; 14(1)**:** 257-267.

16. Hentze MW, Muckenthaler MU, Andrews NC. Balancing acts: molecular control of mammalian iron metabolism. *Cell* 2004; 117(3)**:** 285-297.

17. Van Dyke RW. Acidification of lysosomes and endosomes. *Subcell. Biochem.* 1996; 27**:** 331-360.

18. Zhang F, Tao Y, Zhang Z, Guo X, An P, Shen Y *et al.* Metalloreductase Steap3 coordinates the regulation of iron homeostasis and inflammatory responses. *Haematologica* 2012; 97(12)**:** 1826-1835. doi: 10.3324/haematol.2012.063974

19. Blanc L, Papoin J, Debnath G, Vidal M, Amson R, Telerman A *et al.* Abnormal erythroid maturation leads to microcytic anemia in the TSAP6/Steap3 null mouse model. *Am. J. Hematol.* 2015; 90(3)**:** 235-241. doi: 10.1002/ajh.23920

20. Philpott CC, Ryu MS. Special delivery: distributing iron in the cytosol of mammalian cells. *Front. Pharmacol.* 2014; 5**:** 173. doi: 10.3389/fphar.2014.00173

21. Graham RM, Chua AC, Herbison CE, Olynyk JK, Trinder D. Liver iron transport. *World J Gastroenterol.* 2007; 13(35)**:** 4725-4736.

22. Mostad EJ, Prohaska JR. Glycosylphosphatidylinositol-linked ceruloplasmin is expressed in multiple rodent organs and is lower following dietary copper deficiency. *Exp. Biol. Med.* 2011; 236(3)**:** 298-308.

23. Marques L, Auriac A, Willemetz A, Banha J, Silva B, Canonne-Hergaux F *et al.* Immune cells and hepatocytes express glycosylphosphatidylinositol-anchored ceruloplasmin at their cell surface. *Blood Cells.Mol.Dis.* 2012; 48(2)**:** 110-120. doi: S1079-9796(11)00233-6 [pii];10.1016/j.bcmd.2011.11.005 [doi]

24. Tolosano E, Fagoonee S, Morello N, Vinchi F, Fiorito V. Heme scavenging and the other facets of hemopexin. *Antioxid Redox Signal* 2010; 12(2)**:** 305-320. doi: 10.1089/ars.2009.2787

25. Gammella E, Buratti P, Cairo G, Recalcati S. Macrophages: central regulators of iron balance. *Metallomics* 2014; 6(8)**:** 1336-1345. doi: 10.1039/c4mt00104d

26. Liuzzi JP, Aydemir F, Nam H, Knutson MD, Cousins RJ. Zip14 (Slc39a14) mediates non-transferrin-bound iron uptake into cells. *Proc. Natl. Acad. Sci. U. S. A.* 2006; 103(37)**:** 13612-13617. doi: 10.1073/pnas.0606424103

27. Brissot P, Ropert M, Le LC, Loreal O. Non-transferrin bound iron: A key role in iron overload and iron toxicity. *Biochim. Biophys. Acta* 2012; 1820(3)**:** 403-410. doi: S0304-4165(11)00180-2 [pii];10.1016/j.bbagen.2011.07.014 [doi]

28. Green R, Charlton R, Seftel H, Bothwell T, Mayet F, Adams B *et al.* Body iron excretion in man : A collaborative study. *The American Journal of Medicine* 1968; 45(3)**:** 336-353.

29. Gupta A, Pratt RD, Crumbliss AL. Ferrous iron content of intravenous iron formulations. *Biometals* 2016; 29(3)**:** 411-415. doi: 10.1007/s10534-016-9923-7

30. Liu J, Chakraborty S, Hosseinzadeh P, Yu Y, Tian S, Petrik I *et al.* Metalloproteins containing cytochrome, iron-sulfur, or copper redox centers. *Chem. Rev.* 2014; 114(8)**:** 4366-4469. doi: 10.1021/cr400479b

31. Pietrangelo A. Mechanisms of iron hepatotoxicity. *J. Hepatol.* 2016; 65(1)**:** 226-227. doi: 10.1016/j.jhep.2016.01.037

32. Haber F, Weiss J. The catalytic decomposition of hydrogen peroxide by iron salts. *Proc. R. Soc.* 1934; (147).

33. Wardman P, Candeias LP. Fenton chemistry: an introduction. *Radiat. Res.* 1996; 145(5)**:** 523-531.

34. Hilton KB, Lambert LA. Molecular evolution and characterization of hepcidin gene products in vertebrates. *Gene* 2008; 415(1-2)**:** 40-48.

35. Nemeth E, Tuttle MS, Powelson J, Vaughn MB, Donovan A, Ward DM *et al.* Hepcidin regulates cellular iron efflux by binding to ferroportin and inducing its internalization. *Science* 2004; 306(5704)**:** 2090-2093.

36. Quistgaard EM, Low C, Guettou F, Nordlund P. Understanding transport by the major facilitator superfamily (MFS): structures pave the way. *Nat. Rev. Mol. Cell Biol.* 2016; 17(2)**:** 123-132. doi: 10.1038/nrm.2015.25

37. Yan N. Structural Biology of the Major Facilitator Superfamily Transporters. *Annu Rev Biophys* 2015; 44**:** 257-283. doi: 10.1146/annurev-biophys-060414-033901

38. Taniguchi R, Kato HE, Font J, Deshpande CN, Wada M, Ito K *et al.* Outward- and inward-facing structures of a putative bacterial transition-metal transporter with homology to ferroportin. *Nat Commun* 2015; 6**:** 8545. doi: 10.1038/ncomms9545

39. Rice AE, Mendez MJ, Hokanson CA, Rees DC, Bjorkman PJ. Investigation of the biophysical and cell biological properties of ferroportin, a multipass integral membrane protein iron exporter. *J Mol.Biol* 2009; 386(3)**:** 717-732. doi: S0022-2836(08)01596-9 [pii];10.1016/j.jmb.2008.12.063 [doi]

40. Carpenter EP, Beis K, Cameron AD, Iwata S. Overcoming the challenges of membrane protein crystallography. *Curr. Opin. Struct. Biol.* 2008; 18(5)**:** 581-586. doi: 10.1016/j.sbi.2008.07.001

41. Wallace DF, Harris JM, Subramaniam VN. Functional analysis and theoretical modeling of ferroportin reveals clustering of mutations according to phenotype. *Am. J. Physiol. Cell Physiol.* 2010; 298(1)**:** C75-C84.

42. Bonaccorsi di Patti MC, Polticelli F, Cece G, Cutone A, Felici F, Persichini T *et al.* A structural model of human ferroportin and of its iron binding site. *FEBS J* 2014; 281(12)**:** 2851-2860. doi: 10.1111/febs.12825

43. Liu XB, Yang F, Haile DJ. Functional consequences of ferroportin 1 mutations. *Blood Cells Mol. Dis.* 2005; 35(1)**:** 33-46.

44. Ganz T, Nemeth E. The hepcidin-ferroportin system as a therapeutic target in anemias and iron overload disorders. *Hematology.Am.Soc Hematol.Educ.Program* 2011; 2011**:** 538-542. doi: 2011/1/538 [pii];10.1182/asheducation-2011.1.538 [doi]

45. Le Gac G, Ka C, Joubrel R, Gourlaouen I, Lehn P, Mornon JP *et al.* Structure-function analysis of the human ferroportin iron exporter (SLC40A1): effect of hemochromatosis type 4 disease mutations and identification of critical residues. *Hum. Mutat.* 2013; 34(10)**:** 1371-1380. doi: 10.1002/humu.22369

46. Preza GC, Ruchala P, Pinon R, Qiao B, Peralta M, Sharma S *et al.* Analysis of the hepcidin-ferroportin interface yields minihepcidins, small peptides for the treatment of iron overload. In, 2011.

47. Nemeth E, Preza GC, Jung CL, Kaplan J, Waring AJ, Ganz T. The N-terminus of hepcidin is essential for its interaction with ferroportin: structure-function study. *Blood* 2006; 107(1)**:** 328-333. doi: 2005-05-2049 [pii];10.1182/blood-2005-05-2049 [doi]

48. Hunter HN, Fulton DB, Ganz T, Vogel HJ. The solution structure of human hepcidin, a peptide hormone with antimicrobial activity that is involved in iron uptake and hereditary hemochromatosis. *J. Biol. Chem.* 2002; 277(40)**:** 37597-37603.

49. Jordan JB, Poppe L, Haniu M, Arvedson T, Syed R, Li V *et al.* Hepcidin revisited, disulfide connectivity, dynamics, and structure. *J. Biol. Chem.* 2009; 284(36)**:** 24155-24167. doi: M109.017764 [pii];10.1074/jbc.M109.017764 [doi]

50. Clark RJ, Tan CC, Preza GC, Nemeth E, Ganz T, Craik DJ. Understanding the structure/activity relationships of the iron regulatory peptide hepcidin. *Chem.Biol* 2011; 18(3)**:** 336-343. doi: S1074-5521(10)00481-3 [pii];10.1016/j.chembiol.2010.12.009 [doi]

51. Preza GC, Ruchala P, Pinon R, Ramos E, Qiao B, Peralta MA *et al.* Minihepcidins are rationally designed small peptides that mimic hepcidin activity in mice and may be useful

for the treatment of iron overload. *J Clin.Invest* 2011; 121(12)**:** 4880-4888. doi: 57693 [pii];10.1172/JCI57693 [doi]

52. Fernandes A, Preza GC, Phung Y, De Domenico I, Kaplan J, Ganz T *et al.* The molecular basis of hepcidin-resistant hereditary hemochromatosis. *Blood* 2009; 114(2)**:** 437-443. doi: blood-2008-03-146134 [pii];10.1182/blood-2008-03-146134 [doi]

53. Mayeur C, Leyton PA, Kolodziej SA, Yu B, Bloch KD. BMP type II receptors have redundant roles in the regulation of hepatic hepcidin gene expression and iron metabolism. *Blood* 2014; 124(13)**:** 2116-2123. doi: 10.1182/blood-2014-04-572644

54. Sieber C, Kopf J, Hiepen C, Knaus P. Recent advances in BMP receptor signaling. *Cytokine Growth Factor Rev.* 2009; 20(5-6)**:** 343-355. doi: S1359-6101(09)00082-3 [pii];10.1016/j.cytogfr.2009.10.007 [doi]

55. Miyazono K, Maeda S, Imamura T. BMP receptor signaling: transcriptional targets, regulation of signals, and signaling cross-talk. *Cytokine Growth Factor Rev.* 2005; 16(3)**:** 251-263. doi: 10.1016/j.cytogfr.2005.01.009

56. Zhao N, Zhang AS, Enns CA. Iron regulation by hepcidin. *J. Clin. Invest.* 2013; 123(6)**:** 2337-2343. doi: 67225 [pii];10.1172/JCI67225 [doi]

57. Andrews NC. Molecular control of iron metabolism. *Best.Pract.Res.Clin.Haematol.* 2005; 18(2)**:** 159-169.

58. Johnson MB, Enns CA. Diferric transferrin regulates transferrin receptor 2 protein stability. *Blood* 2004; 104(13)**:** 4287-4293.

59. Chen J, Wang J, Meyers KR, Enns CA. Transferrin-directed internalization and cycling of transferrin receptor 2. *Traffic* 2009; 10(10)**:** 1488-1501. doi: 10.1111/j.1600-0854.2009.00961.x

60. Owen D, Kuhn LC. Noncoding 3' sequences of the transferrin receptor gene are required for mRNA regulation by iron. *EMBO J.* 1987; 6(5)**:** 1287-1293.

61. D'Alessio F, Hentze MW, Muckenthaler MU. The hemochromatosis proteins HFE, TfR2, and HJV form a membrane-associated protein complex for hepcidin regulation. *J Hepatol.* 2012; 57(5)**:** 1052-1060. doi: S0168-8278(12)00441-2 [pii];10.1016/j.jhep.2012.06.015 [doi]

62. Xia Y, Babitt JL, Sidis Y, Chung RT, Lin HY. Hemojuvelin regulates hepcidin expression via a selective subset of BMP ligands and receptors independently of neogenin. *Blood* 2008; 111(10)**:** 5195-5204. doi: blood-2007-09-111567 [pii];10.1182/blood-2007-09-111567 [doi]

63. Babitt JL, Huang FW, Wrighting DM, Xia Y, Sidis Y, Samad TA *et al.* Bone morphogenetic protein signaling by hemojuvelin regulates hepcidin expression. *Nat. Genet.* 2006; 38(5)**:** 531-539.

64. Steinbicker AU, Bartnikas TB, Lohmeyer LK, Leyton P, Mayeur C, Kao SM *et al.* Perturbation of hepcidin expression by BMP type I receptor deletion induces iron overload in mice. *Blood* 2011; 118(15)**:** 4224-4230. doi: blood-2011-03-339952 [pii];10.1182/blood-2011-03-339952 [doi]

65. Wu XG, Wang Y, Wu Q, Cheng WH, Liu W, Zhao Y *et al.* HFE interacts with the BMP type I receptor ALK3 to regulate hepcidin expression. *Blood* 2014; 124(8)**:** 1335-1343. doi: 10.1182/blood-2014-01-552281

66. Worthen CA, Enns CA. The role of hepatic transferrin receptor 2 in the regulation of iron homeostasis in the body. *Front Pharmacol.* 2014; 5**:** 34. doi: 10.3389/fphar.2014.00034 [doi]

67. Lee DH, Zhou LJ, Zhou Z, Xie JX, Jung JU, Liu Y *et al.* Neogenin inhibits HJV secretion and regulates BMP-induced hepcidin expression and iron homeostasis. *Blood* 2010; 115(15)**:** 3136-3145. doi: blood-2009-11-251199 [pii];10.1182/blood-2009-11-251199 [doi]

68. Kautz L, Meynard D, Monnier A, Darnaud V, Bouvet R, Wang RH *et al.* Iron regulates phosphorylation of Smad1/5/8 and gene expression of Bmp6, Smad7, Id1, and Atoh8 in the mouse liver. *Blood* 2008; 112(4)**:** 1503-1509.

69. Andriopoulos B, Jr., Corradini E, Xia Y, Faasse SA, Chen S, Grgurevic L *et al.* BMP6 is a key endogenous regulator of hepcidin expression and iron metabolism. *Nat. Genet.* 2009; 41(4)**:** 482-487. doi: ng.335 [pii];10.1038/ng.335 [doi]

70. Zhao N, Nizzi CP, Anderson SA, Wang J, Ueno A, Tsukamoto H *et al.* Low intracellular iron increases the stability of matriptase-2. *J. Biol. Chem.* 2015; 290(7)**:** 4432-4446. doi: 10.1074/jbc.M114.611913

71. Mleczko-Sanecka K, Casanovas G, Ragab A, Breitkopf K, M++ller A, Boutros M *et al.* SMAD7 controls iron metabolism as a potent inhibitor of hepcidin expression. *Blood* 2010; 115(13)**:** 2657-2665. doi: 10.1182/blood-2009-09-238105

72. Zhang S, Fei T, Zhang L, Zhang R, Chen F, Ning Y *et al.* Smad7 antagonizes transforming growth factor beta signaling in the nucleus by interfering with functional Smad-DNA complex formation. *Mol. Cell. Biol.* 2007; 27(12)**:** 4488-4499. doi: 10.1128/MCB.01636-06

73. Nagarajan RP, Zhang J, Li W, Chen Y. Regulation of Smad7 promoter by direct association with Smad3 and Smad4. *J. Biol. Chem.* 1999; 274(47)**:** 33412-33418.

74. Zhou XY, Tomatsu S, Fleming RE, Parkkila S, Waheed A, Jiang J *et al.* HFE gene knockout produces mouse model of hereditary hemochromatosis. *Proceedings of the National Academy of Sciences* 1998; 95(5)**:** 2492-2497.

75. Huang FW, Pinkus JL, Pinkus GS, Fleming MD, Andrews NC. A mouse model of juvenile hemochromatosis. *J Clin.Invest* 2005; 115(8)**:** 2187-2191. doi: 10.1172/JCI25049 [doi]

76. Fleming RE, Ahmann JR, Migas MC, Waheed A, Koeffler HP, Kawabata H *et al.* Targeted mutagenesis of the murine transferrin receptor-2 gene produces hemochromatosis. *Proceedings of the National Academy of Sciences* 2002; 99(16)**:** 10653-10658.

77. Meynard D, Kautz L, Darnaud V, Canonne-Hergaux F, Coppin H, Roth MP. Lack of the bone morphogenetic protein BMP6 induces massive iron overload. *Nat. Genet.* 2009; 41(4)**:** 478-481. doi: ng.320 [pii];10.1038/ng.320 [doi]

78. Koch PS, Olsavszky V, Ulbrich F, Sticht C, Demory A, Leibing T *et al.* Angiocrine Bmp2 signaling in murine liver controls normal iron homeostasis. *Blood* 2017; 129(4)**:** 415-419. doi: 10.1182/blood-2016-07-729822

79. Wang CY, Core AB, Canali S, Zumbrennen-Bullough KB, Ozer S, Umans L *et al.* Smad1/5 is required for erythropoietin-mediated suppression of hepcidin in mice. *Blood* 2017. doi: 10.1182/blood-2016-12-759423

80. Folgueras AR, de Lara FM, Pendas AM, Garabaya C, Rodriguez F, Astudillo A *et al.* Membrane-bound serine protease matriptase-2 (Tmprss6) is an essential regulator of iron homeostasis. *Blood* 2008; 112(6)**:** 2539-2545. doi: blood-2008-04-149773 [pii];10.1182/blood-2008-04-149773 [doi]

81. Ramos E, Kautz L, Rodriguez R, Hansen M, Gabayan V, Ginzburg Y *et al.* Evidence for distinct pathways of hepcidin regulation by acute and chronic iron loading in mice. *Hepatology* 2011; 53(4)**:** 1333-1341. doi: 10.1002/hep.24178 [doi]

82. Canali S, Zumbrennen-Bullough KB, Core AB, Wang CY, Nairz M, Bouley R *et al.* Endothelial cells produce bone morphogenetic protein 6 required for iron homeostasis in mice. *Blood* 2017; 129(4)**:** 405-414. doi: 10.1182/blood-2016-06-721571

83. Wrighting DM, Andrews NC. Interleukin-6 induces hepcidin expression through STAT3. *Blood* 2006; 108(9)**:** 3204-3209.

84. Besson-Fournier C, Latour C, Kautz L, Bertrand J, Ganz T, Roth MP *et al.* Induction of activin B by inflammatory stimuli upregulates expression of the iron-regulatory peptide hepcidin through Smad1/5/8 signaling. *Blood* 2012; 120(2)**:** 431-439. doi: blood-2012-02-411470 [pii];10.1182/blood-2012-02-411470 [doi]

85. Canali S, Core AB, Zumbrennen-Bullough KB, Merkulova M, Wang CY, Schneyer AL *et al.* Activin B Induces Noncanonical SMAD1/5/8 Signaling via BMP Type I Receptors in

Hepatocytes: Evidence for a Role in Hepcidin Induction by Inflammation in Male Mice. *Endocrinology* 2016; 157(3)**:** 1146-1162. doi: 10.1210/en.2015-1747

86. Besson-Fournier C, Gineste A, Latour C, Gourbeyre O, Meynard D, Martin P *et al.* Hepcidin upregulation by inflammation is independent of Smad1/5/8 signaling by activin B. *Blood* 2017; 129(4)**:** 533-536. doi: 10.1182/blood-2016-10-748541

87. Pagani A, Nai A, Corna G, Bosurgi L, Rovere-Querini P, Camaschella C *et al.* Low hepcidin accounts for the proinflammatory status associated with iron deficiency. *Blood* 2011; 118(3)**:** 736-746. doi: blood-2011-02-337212 [pii];10.1182/blood-2011-02-337212 [doi]

88. Meynard D, Sun CC, Wu Q, Chen W, Chen S, Nelson CN *et al.* Inflammation regulates TMPRSS6 expression via STAT5. *PLoS One* 2013; 8(12)**:** e82127. doi: 10.1371/journal.pone.0082127

89. Kautz L, Nemeth E. Molecular liaisons between erythropoiesis and iron metabolism. *Blood* 2014; 124(4)**:** 479-482. doi: blood-2014-05-516252 [pii];10.1182/blood-2014-05-516252 [doi]

90. Paulson RF, Shi L, Wu DC. Stress erythropoiesis: new signals and new stress progenitor cells. *Curr. Opin. Hematol.* 2011; 18(3)**:** 139-145. doi: 10.1097/MOH.0b013e32834521c8

91. Ganz T, Nemeth E. Hepcidin and disorders of iron metabolism. *Annu.Rev.Med.* 2011; 62**:** 347-360. doi: 10.1146/annurev-med-050109-142444 [doi]

92. Kautz L, Jung G, Valore EV, Rivella S, Nemeth E, Ganz T. Identification of erythroferrone as an erythroid regulator of iron metabolism. *Nat. Genet.* 2014; 46(7)**:** 678-684. doi: ng.2996 [pii];10.1038/ng.2996 [doi]

93. Kautz L, Jung G, Du X, Gabayan V, Chapman J, Nasoff M *et al.* Erythroferrone contributes to hepcidin suppression and iron overload in a mouse model of beta-thalassemia. *Blood* 2015; 126(17)**:** 2031-2037. doi: 10.1182/blood-2015-07-658419

94. Origa R. beta-Thalassemia. *Genet. Med.* 2016. doi: 10.1038/gim.2016.173

95. Brunori M, Falcioni G, Fioretti E, Giardina B, Rotilio G. Formation of Superoxide in the Autoxidation of the Isolated Alpha and Beta Chains of Human Hemoglobin and Its Involvement in Hemichrome Precipitation. *Eur. J. Biochem.* 1975; (53)**:** 99-104.

96. Centis F, Tabellini L, Lucarelli G, Buffi O, Tonucci P, Persini B *et al.* The importance of erythroid expansion in determining the extent of apoptosis in erythroid precursors in patients with b-thalassemia major. *Blood* 2000; 96(10)**:** 3624-3629.

97. Wood JC. Diagnosis and management of transfusion iron overload: the role of imaging. *Am. J. Hematol.* 2007; 82(12 Suppl)**:** 1132-1135. doi: 10.1002/ajh.21099

98. Amatto M, Acharya H. Secondary hemochromatosis as a result of acute transfusion-induced iron overload in a burn patient. *Burns Trauma* 2016; 4**:** 10. doi: 10.1186/s41038-016-0034-z

99. Hahalis G, Alexopoulos D, Kremastinos DT, Zoumbos NC. Heart failure in beta-thalassemia syndromes: a decade of progress. *Am. J. Med.* 2005; 118(9)**:** 957-967. doi: 10.1016/j.amjmed.2005.02.021

100. Vitrano A, Calvaruso G, Lai E, Colletta G, Quota A, Gerardi C *et al.* The era of comparable life expectancy between thalassaemia major and intermedia: Is it time to revisit the major-intermedia dichotomy? *Br. J. Haematol.* 2017; 176(1)**:** 124-130. doi: 10.1111/bjh.14381

101. De Falco L, Sanchez M, Silvestri L, Kannengiesser C, Muckenthaler MU, Iolascon A *et al.* Iron refractory iron deficiency anemia. *Haematologica* 2013; 98(6)**:** 845-853. doi: 10.3324/haematol.2012.075515

102. Pietrangelo A. Hereditary hemochromatosis--a new look at an old disease. *The New England Journal of Medicine* 2004; 350(23)**:** 2383-2397.

103. Sabelli M, Montosi G, Garuti C, Caleffi A, Oliveto S, Biffo S *et al.* Human macrophage ferroportin biology and the basis for the ferroportin disease. *Hepatology* 2017. doi: 10.1002/hep.29007

104. Pietrangelo A. The ferroportin disease. *Blood Cells Mol. Dis.* 2004; 32(1)**:** 131-138.

105. Schimanski LM, Drakesmith H, Merryweather-Clarke AT, Viprakasit V, Edwards JP, Sweetland E *et al.* In vitro functional analysis of human ferroportin (FPN) and hemochromatosis-associated FPN mutations. *Blood* 2005; 105(10)**:** 4096-4102. doi: 10.1182/blood-2004-11-4502

106. Cemonesi L, Forni GL, Soriani N, Lamagna M, Fermo I, Daraio F *et al.* Genetic and clinical heterogeneity of ferroportin disease. *Br. J. Haematol.* 2005; 131(5)**:** 663-670.

107. Sham RL, Phatak PD, West C, Lee P, Andrews C, Beutler E. Autosomal dominant hereditary hemochromatosis associated with a novel ferroportin mutation and unique clinical features. *Blood Cells Mol. Dis.* 2005; 34(2)**:** 157-161.

108. Fleming RE, Ponka P. Iron overload in human disease. *N. Engl. J. Med.* 2012; 366(4)**:** 348-359. doi: 10.1056/NEJMra1004967

109. Barton JC, McDonnell SM, Adams PC, Brissot P, Powell LW, Edwards CQ *et al.* Management of hemochromatosis. Hemochromatosis Management Working Group. *Ann. Intern. Med.* 1998; 129(11)**:** 932-939.

110. Luo X, Jiang Q, Song G, Liu YL, Xu ZG, Guo ZY. Efficient oxidative folding and site-specific labeling of human hepcidin to study its interaction with receptor ferroportin. *FEBS J* 2012; 279(17)**:** 3166-3175. doi: 10.1111/j.1742-4658.2012.08695.x

111. Ramos E, Ruchala P, Goodnough JB, Kautz L, Preza GC, Nemeth E *et al.* Minihepcidins prevent iron overload in a hepcidin-deficient mouse model of severe hemochromatosis. *Blood* 2012; 120(18)**:** 3829-3836. doi: blood-2012-07-440743 [pii];10.1182/blood-2012-07-440743 [doi]

112. Casu C, Goldberg A, Nemeth E, Ganz T, Gardenghi S, MacDonald B *et al.* Treatment With Minihepcidin Peptide Improves Anemia and Iron Overload In a Mouse Model Of Thalassemia Intermedia. *Blood* 2013; 122(21)**:** 431.

113. Vyoral D, Jiri P. Therapeutic potential of hepcidin - the master regulator of iron metabolism. *Pharmacol. Res.* 2017; 115**:** 242-254. doi: 10.1016/j.phrs.2016.11.010

114. Liu J, Sun B, Yin H, Liu S. Hepcidin: A Promising Therapeutic Target for Iron Disorders: A Systematic Review. *Medicine (Baltimore)* 2016; 95(14)**:** e3150. doi: 10.1097/MD.0000000000003150

CHAPTER 1A:

Structure-function study of the ferroportin-hepcidin interaction defines the hepcidin-binding site and a new mechanism of hepcidin action

Manuscript submitted:

ANALYSIS OF HEPCIDIN-RESISTANT FERROPORTINS DEFINES THE HEPCIDIN-BINDING SITE AND A NEW MECHANISM OF HEPCIDIN ACTION

Sharraya Aschemeyer, Bo Qiao, Erika V. Valore, Albert C. Sek, T. Alex Ruwe, Kyle R. Vieth, Mika Jormakka, Bryan Mackenzie, Tomas Ganz, and Elizabeta Nemeth

ABSTRACT

Non-classical Ferroportin Disease is a form of hereditary hemochromatosis caused by mutations in the iron transporter ferroportin (Fpn), resulting in parenchymal iron overload. Fpn is regulated by the hormone hepcidin, which induces Fpn endocytosis and cellular iron retention. We characterized 11 clinically-relevant and 5 nonclinical Fpn mutations using stably transfected, inducible, isogenic cell lines. All clinical mutants were functionally resistant to hepcidin as a consequence of either impaired hepcidin binding or impaired hepcidin-dependent ubiquitination despite intact hepcidin binding. Mapping the residues onto two computational models of the human Fpn structure indicated that i) mutations that caused ubiquitination-resistance were positioned at helix-helix interfaces, likely preventing the hepcidin-induced conformational change, ii) hepcidin binding occurred within the central cavity of Fpn, iii) hepcidin interacted with up to 4 helices, and iv) hepcidin binding should occlude Fpn and interfere with iron export independently of endocytosis. We experimentally confirmed in HEK293 cells that hepcidin at high concentrations and minihepcidins at 10x lower concentrations blocked iron export by occlusion in K8R Fpn, an endocytosis-defective mutant. Similarly, iron export by *Xenopus* oocytes expressing WT or K8R Fpn was inhibited at high hepcidin concentrations by occlusion without Fpn endocytosis.

We conclude that non-classical Ferroportin Disease is caused by Fpn mutations that decrease hepcidin binding or hinder conformational changes required for ubiquitination and endocytosis of Fpn. The newly documented ability of hepcidin and its agonists to occlude iron

transport may facilitate the development of broadly effective treatments for hereditary iron overload disorders.

INTRODUCTION

Ferroportin Disease (FD) is a rare autosomal dominant iron disorder caused by mutations in the cellular iron exporter Fpn. “Classical” FD is characterized by hyperferritinemia with normal-to-low transferrin saturation that arises from Fpn mutations that cause decreased iron export ("loss-of-function"), and iron accumulates primarily in macrophages, which normally export very high amounts of iron after erythrophagocytosis. Here we focused on “non-classical” FD, characterized by hyperferritinemia with high transferrin saturation attributed to Fpn “gain-of-function,” causes iron overload primarily in hepatocytes.(1, 2)

We examined the structural and functional characteristics of clinical "gain-of-function" Fpn mutants associated with both hyperferritinemia and transferrin saturation greater than 60% (Table 1, References S1-S14). Additional nonclinical mutants were generated to probe the hepcidin-binding region in greater detail.

Our study builds on two important technical advances: improved cellular modeling of Fpn mutants and updated structural Fpn data. To avoid the limitations of transiently transfected cells with large variations of Fpn expression between individual cells and mutants (2-11), we established stable, inducible mammalian cell lines expressing wild-type or mutant Fpn from a defined genomic location, a Flp-In recombination locus. This allowed for a more accurate comparison and quantification of the mutation effects on iron export, Fpn stability, hepcidin binding, and hepcidin-induced Fpn ubiquitination and degradation, steps that could not be individually assessed in earlier studies of hepcidin resistance (2-11).

Mutant	Serum ferritin (μg/L)	Transferrin saturation (%)	Examples of pathological findings	References	Number of adult patients
WT	15-200F 40-300M	15-45 both M and F		(S1)	
C326Y	481-552F 4,232-4,326M	94-80F 96-100M		(S1)	2F, 2M
C326S	-	-	Cirrhosis and arthritis	(S2)	1M
Y501C	43-199F 568-642M	35-64F 94-104M	Asthenia, arthralgia, and hepatomegaly	(S3)	2F, 2M
D504N	1,514-1,605M	89-102M	Hepatomegaly and moderate drinking	(S4)	2M
N144D	7,500F 10,510M	99M	Iron loading in hepatocytes and BDECs, cirrhosis	(S5)	1F, 1M
V72F	27-174F 195-1,091M	31-35F 53-81M	Iron loading primarily in hepatocytes, but also in Kupffer cells, BDECs, and PTMs, fibrosis, and hepatic steatosis	(S6)	2F, 3M
Y64N	176-513F 647-2,812M	47-86F 91-98M	Iron loading in Kupffer cells and hepatocytes, fatigue and tremors	(S7)	3F, 5M
H507R	233F 785-3,751M	46F 93-100M	Iron loading in hepatocytes, mild steatosis, and siderosis	(S8, S9)	1F, 3M
S71F	5,500	70	Uncharacterized	(S10)	1*
G204S	4-5236F 508-3755M	2-100F 27-91M	Mixed iron loading, but mainly hepatocytes heterogeneous phenotype	(S10, S11)	3F, 5M
D270V	<1,000F 353-559M**	78F 37-41M**	Fatigue, fibrosis, iron loading in hepatocytes and Kupffer cells, hepatitis C	(S12, S13)	1F, 1M
S338R	1,990M	90M	Iron loading in hepatocytes, Kupffer cells, and PTMs, mild steatosis	(S14)	1M

Table 1: Non-classical Ferroportin Disease mutations.
Based on the literature, the 12 Fpn mutations listed in the table are associated with elevated serum ferritin and transferrin saturation, although not every subject carrying the mutation had abnormal biochemical parameters or related pathology. The color code was assigned retrospectively based on the results of our study. Red/pink colors represent mutants in which hepcidin binding is impaired; the green colors represent mutants in which binding is normal, but hepcidin-mediated ubiquitination is impaired. The bolder colors represent more severe impairment. Adult = > 18 years, BDECs = bile duct epithelial cells, PTMs = portal tract macrophages, M= male, F= female, * = source did not cite gender and **= the patient's parameters were recorded at two different times.

The lack of information about Fpn structure has also hampered understanding of the hepcidin-Fpn interaction (9, 12-14). Recently, Taniguchi et al. identified the prokaryotic protein, BdFPN, from the bacterium *Bdellovibrio bacteriovorus* as an ortholog of Fpn and obtained its structure by X-ray crystallography (15). However, hepcidin itself and the hepcidin-binding site within Fpn are found only in vertebrates (16), so in this context, the BdFPN structure can only

serve as a modeling constraint. We therefore used the available structural data from related members of the major facilitator superfamily, including eventually BdFPN, and incorporated the experimental results from the Fpn mutant analysis to develop a new model of the hepcidin-Fpn interaction, which segregates Fpn residues important for hepcidin-induced conformational change from those critical for hepcidin binding. As predicted by the model, our experiments also demonstrated that hepcidin can occlude Fpn and prevent iron export even in the absence of endocytosis.

MATERIALS AND METHODS

Reagents were obtained from Sigma–Aldrich or Research Products International unless otherwise indicated.

Site-directed mutagenesis

Human Fpn-GFP in the pGFP-N3 vector (7) was transferred into the pcDNA5/FRT/TO vector (Invitrogen). Single mutations were introduced using QuikChange Lightning Site-Directed Mutagenesis Kit (Agilent Technologies) and confirmed by sequencing. Mutagenesis primers are listed in Table S1.

Stably transfected inducible cell lines

All mutant human Fpn-GFP pcDNA5/FRT/TO vector constructs were verified by sequencing. Using the Flp-In T-Rex system (Invitrogen K5600-01), HEK293T cells were transfected with the pcDNA5/FRT/TO vector encoding WT or mutant Fpn and pOG44 vector. Stable cell lines were established according to the manufacturer's protocol. Doxycycline (dox) was used to induce expression of Fpn-GFP.

Microscopy in mammalian cells

Cells were induced with 100 ng/ml dox overnight in 12-well poly-D-lysine coated plates (BD). Cells were washed with PBS, and treated with 25 μM ferric ammonium citrate (FAC) ±1 μg/ml hepcidin (Peptide International) for 24 hours. Cells were visualized with an epifluorescence microscope (Nikon Eclipse), and images were acquired with a 40x objective, SPOT camera, and SPOT Advanced Imaging Software (Diagnostic Instruments).

Fpn membrane localization in mammalian cells

Cells were seeded on 6-well poly-D-lysine coated plates (BD) and induced with 500 ng/ml doxycycline for 24 hours. Cells were washed 3x with PBS, and treated with EZ-link maleimide PEG-2-biotin in PBS for 30 minutes at 4 C. Cells were then washed with 1x PBS, solubilized in RIPA (Boston BioProducts) with protease inhibitors, and Fpn-GFP was immunoprecipitated with anti-GFP Ab as described previously (17). Blots were probed with Streptavidin-HRP (Pierce) and total Fpn was detected with anti-GFP Ab (Roche). To adjust for variations between individual Western blots, we normalized band intensity to WT Fpn sample within the same blot.

Ferritin assay

Cells were processed the same as in the microscopy section. After 24 hours of treatment, cells were washed with PBS and harvested in RIPA with protease inhibitors. Ferritin levels were determined by an ELISA assay (Ramco Laboratories) according to the manufacturer's instructions and were normalized to the total protein concentration in each sample (BCA assay, Pierce). To adjust for variations of the absolute ferritin values between multiple experiments, we expressed the measurements as the relative change in ferritin, according to the formula I/U, where I is the ferritin value for the induced cell line and U is the ferritin value for the uninduced cell line. For hepcidin-treated cells, we expressed the ferritin measurements as (H-I)/U, where H refers to the ferritin value for the induced cells treated with hepcidin.

Hepcidin binding

Cells were treated with 3 μg/ml N-terminally biotinylated hepcidin (Peptides International) for 30 min at 37°C. Protein lysates were immunoprecipitated with anti-GFP Ab (Abcam)(17) and blotted with Streptavidin-HRP (Pierce) and total Fpn was blotted with anti-GFP Ab (Roche). To adjust for variations between Western blots, we normalized the values from Fpn mutants to those of WT Fpn within the same blot.

Immunoprecipitation and Western blotting for ubiquitination

Immunoprecipitation was performed as previously (17), except the gel-loading dye contained 5% 2-mercaptoethanol. To adjust for variations between Western blots, we normalized the mutant ubiquitination values to those of the WT within the same blot.

Computational modeling

Structural models of human Fpn (hFpn) were generated using I-TASSER (Iterative Threading ASSEmbly Refinement) (18, 19). This server predicted the protein structure and function of hFpn by threading hFpn onto program-selected crystal structures of other members of the major facilitator superfamily (PDB entries: 4IKV, 3WDO, 4AV3, and 4M64), either not including (Figure 1A-3) or including (Figure S7) the BdFPN crystal structure (PDB entry: 5AYM) as a template. The models without and with the BdFPN template were generated respectively on 6/18/2015 and 1/20/2016.

Radioactive iron export

Adherent cells were loaded with 2 mM ^{55}Fe (Perkin Elmer) for 48 hours, washed 3x with medium, re-plated, induced overnight, washed 2x with medium, and ±3 μg/ml of hepcidin was added to the wells. Aliquots of the medium were taken at 0.5, 2, 4, and 8 hours to measure iron export. The "uninduced" measurement at each time point was subtracted as background. The slope

for each of the lines ("induced" and "induced+hepcidin") was determined and used to calculate the percent iron export by comparing to untreated WT.

Fpn Western blot

Protein was measured by BCA assay, 6x SDS-loading buffer was added to lysates which were then separated by SDS-PAGE on 4-20% Mini-PROTEAN TGX Precast Gels (BioRad), and transferred to PVDF membranes using Trans-Blot Turbo (Bio-Rad). Blocking was performed overnight at 4°C in 5% milk in TBST (50mM Tris-HCl, pH7.5, 150mM NaCl, 0.1% Tween 20). Anti-GFP (Roche) was used to detect Fpn and anti-GAPDH-HRP (Cell Signaling) were used for normalization.

Functional expression of hFpn in *Xenopus* oocytes

We performed laparotomy and ovariectomy on adult female *Xenopus laevis* frogs (Nasco) under 2-aminoethylbenzoate methanesulfonate anesthesia (0.2%, by immersion, to effect) following a protocol approved by the University of Cincinnati Institutional Animal Care and Use Committee. The pOX(+) oocyte expression plasmid vectors containing human WT or K8R Fpn-GFP were used to synthesized RNA *in vitro*. We examined the functional expression of hFpn-GFP and K8R-hFpn-GFP in RNA-injected *Xenopus* oocytes as described (20) except for the following modifications. RNA-injected oocytes were stored at 17 °C in modified Barths' medium (MBM) containing 50 $mg.l^{-1}$ dox, and incubated 4–5 days before being used in functional assays.

We treated oocytes for 0−4 h with 10 μM hepcidin in MBM prior to assaying iron efflux. Oocytes were injected with 50 nl of 5 μM ^{55}Fe, added as Fe^{3+} (Perkin-Elmer Life Science Products) in a vehicle of composition 250 mM KCl, 5 mM nitrilotriacetic acid trisodium salt, 4 mM 2-(*N*-morpholino)ethanesulfonic acid (GFS Chemicals). To initiate the efflux assay, we placed oocytes in efflux medium of composition 100 mM NaCl, 1 mM KCl, 2 mM $CaCl_2$, 1 mM $MgCl_2$, 0.5 mM

bathophenanthroline disulfonic acid, 1 mM nitrilotriacetic acid trisodium salt, 50 μg.ml^{-1} apotransferrin (R&D Systems), buffered with 2.5 mM 1,4-diethylpiperazine (Alfa Aeser) and approximately 2.5 mM 2-(*N*-morpholino)ethanesulfonic acid to obtain pH 7.5. We obtained the first-order rate constants (k) describing iron efflux over 30 min determined for individual oocytes as described (20). Live-cell imaging of Fpn-GFP in oocytes before and after 30-min 10 μM hepcidin treatment was performed as described (20).

Statistical analysis

We set critical significance level, $\alpha = 0.05$, and expressed our data as mean, SD for *n* observations. Statistical analyses employed the two-tailed t-test (normally distributed data) or Mann-Whitney rank sum test (data with non-normal distribution), the two-tailed one-sample t-test (normally distributed data) or the two-tailed one-sample signed rank test (data with non-normal distribution) compared with a reference of 1, and 2-way analysis of variance (ANOVA). (SigmaPlot version 12.5, Systat Software).

RESULTS

Fpn-GFP mutants localize to cell membrane and export iron

We first examined whether "gain-of-function" mutations (Table 1) caused increased expression of Fpn on the cell membrane or increased baseline iron export. Mutants were visualized by microscopy to assess membrane localization. Green fluorescence was visible on the cell membrane for all mutants (Figure S1). To quantify the amount of Fpn present on the cell surface compared to the total Fpn amount, we performed cell surface thiol-specific biotinylation targeting the Fpn C326 residue. All mutants were expressed on the cell surface similarly to, or only marginally less, than WT (quantitation shown in Figure 1A-1A, representative Western blots in

Figure S2). As expected, C326S mutant showed essentially no biotinylation, confirming the specificity of the method. We next assessed the iron-exporting function of the mutants by measuring intracellular ferritin as an index of remaining cellular iron stores. All mutants exported iron similarly or with moderate impairment compared to WT, but none exported more than WT (Figure 1A-1B). Thus, the gain-of-function phenotype cannot be explained by the cell membrane expression or transport properties of these Fpn mutants.

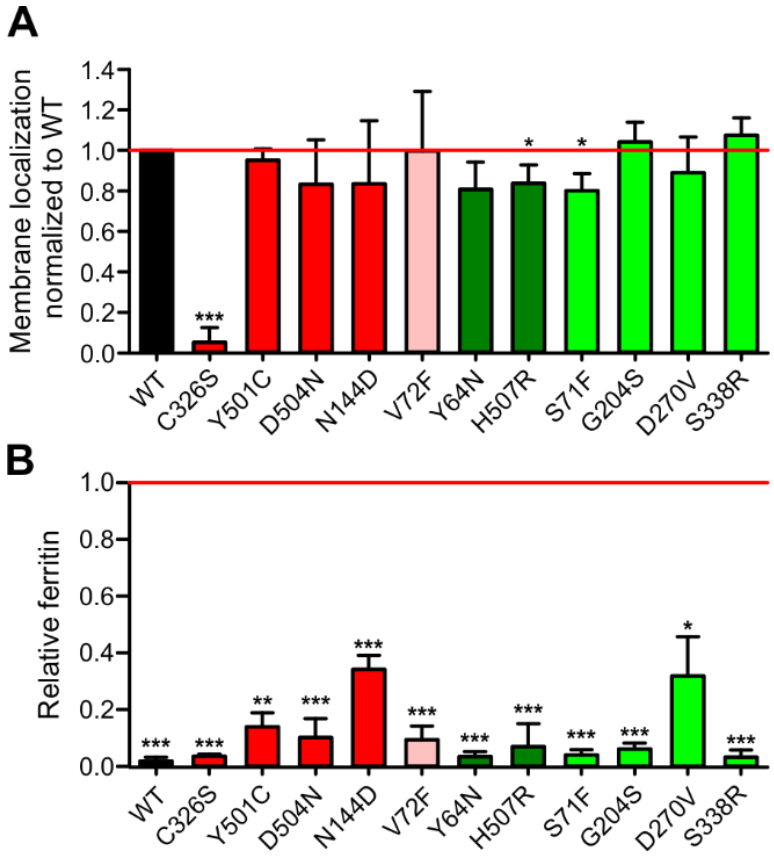

Figure 1A-1: Fpn-GFP mutants localize to the cell membrane and export iron. A) HEK293T cells stably transfected with hFpn-GFP mutants or WT were induced with doxycycline (dox) to express Fpn, surface-thiol biotinylated for 30 minutes, immunoprecipitated with anti-GFP antibody (Ab), and immunoblotted with streptavidin-HRP or anti-GFP Ab. Band intensity was normalized to total GFP and then further normalized to WT Fpn on each blot. Because mutant data within each Western blot were normalized to the WT sample on the same blot, the WT value is always 1 and is without error bars. WT is included in the graph only for visual reference. B) hFpn-GFP mutants were induced overnight with dox and then incubated for 24 hours in the presence of 25 μM ferric ammonium citrate (FAC). The intracellular ferritin concentration was normalized to the total protein concentration. Ferritin was normalized to the uninduced sample (-dox) for each

cell line (uninduced = 1). Data shown are means ± SD of 3-5 independent experiments. Statistical analysis employed the two-tailed one-sample t-test (normally distributed data) or the two-tailed one-sample signed rank test (data with non-normal distribution) using 1 as the comparison (***P<0.001, **P<0.01, *P<0.05).

Gain-of-function Fpn-GFP mutants display hepcidin resistance either because of impaired hepcidin binding or impaired hepcidin-induced ubiquitination

Another potential mechanism for non-classical FD is resistance of Fpn mutants to downregulation by hepcidin, which manifests as continued cellular iron export despite exposure to hepcidin concentrations that cause iron retention in cells expressing WT Fpn. We therefore measured intracellular ferritin as an indicator of iron retention in cells treated with or without hepcidin for 24 h, and observed by microscopy the localization of Fpn after 24 h. Finally, we quantified the stability of WT and mutant Fpn over 24 h by Western blotting, as well as Fpn degradation after treatment with hepcidin for 24 h. All clinical mutants, with the exception of V72F, D270V, and S338R, were hepcidin-resistant compared to WT as demonstrated by lower ferritin retention after hepcidin treatment (Figure 1A-2A), and less Fpn-GFP degradation as assessed by both microscopy (Figure S1) and Western blotting compared to WT (Figure S3A representative blots and Figure S3B quantitation). To detect milder resistance, we exposed V72F and D270V mutants to a lower hepcidin concentration for a shorter time, and measured iron export using radioactive iron release for up to 10 h. V72F and D270V indeed displayed mild hepcidin resistance compared to WT Fpn (Figure S4; S71F and C326S mutants were added as controls manifesting strong resistance). We also examined S338R using the radioactive iron export assay, but with higher hepcidin concentrations (Figure S4), and also observed mild, but significant resistance to hepcidin (with N144D and C326S serving as controls for medium-to-strong resistance). Of note, several mutants (Y64N, H507R, D270V and S338R) had decreased stability

at 24 h compared to WT (Figure S3A, C), which could partially counteract hepcidin resistance *in vivo*, and modulate the patient phenotype.

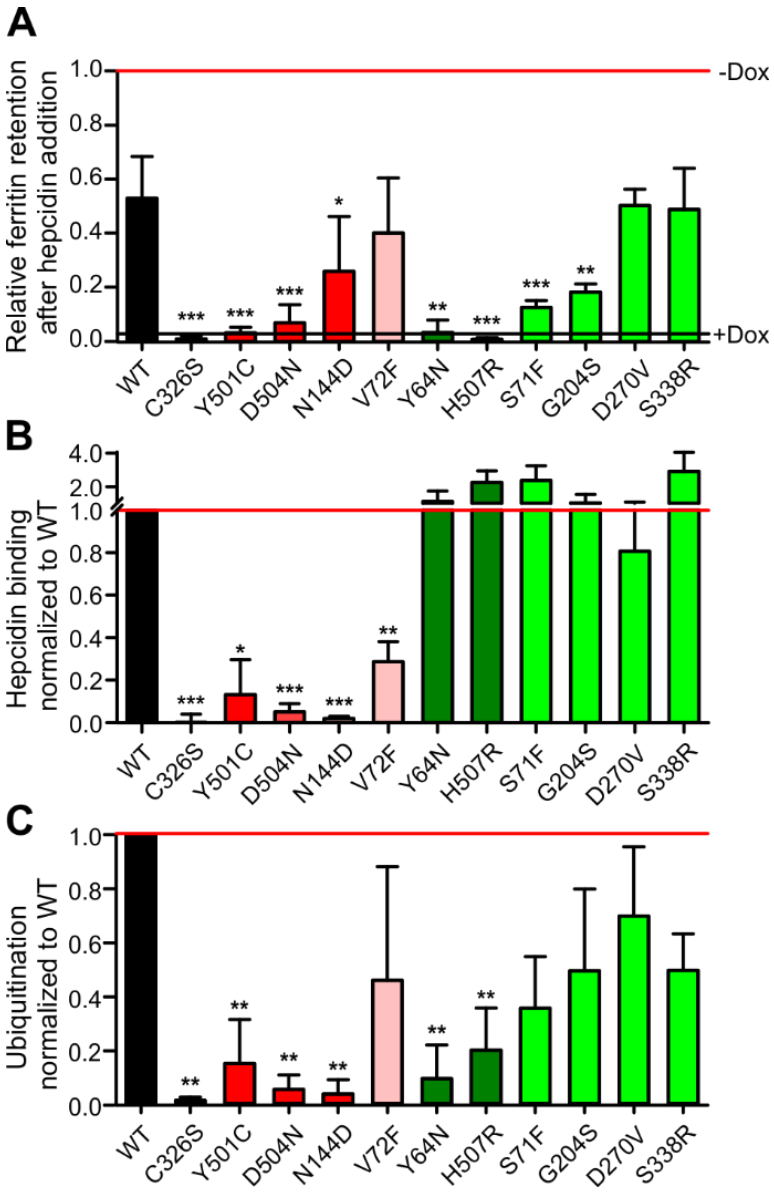

Figure 1A-2: Fpn mutants have either impaired hepcidin binding or impaired ubiquitination leading to varying hepcidin resistance. A) Expression of WT and mutant hFpn-GFP was induced overnight or not, and cells were then incubated for 24 hours with 25 μM FAC ±1μg/mL hepcidin. The intracellular ferritin concentration was normalized to total protein concentration, and expressed relative to uninduced cells (i.e. maximal ferritin levels for each mutant, -dox). B) HEK293T expressing WT and mutant hFpn-GFP were treated with N-terminally biotinylated hepcidin for 30 minutes, immunoprecipitated with anti-GFP Ab, and immunoblotted with streptavidin-HRP or anti-GFP Abs. Streptavidin signal was first normalized to total GFP, and then mutant hepcidin binding values is expressed as a fraction of hepcidin binding to WT Fpn. Because mutant data within each Western blot were normalized to the WT sample on the same blot, the WT value is always 1 and is without error bars. WT is included in the graph only for visual reference. C) hFpn-GFP WT and mutants were treated with hepcidin for 30 minutes, immunoprecipitated with anti-GFP Ab, and immunoblotted with anti-poly/mono ubiquitin (FK2) Ab or anti-GFP Ab. The ubiquitination signal was first normalized to the GFP signal and then the mutant ubiquitination was expressed as a fraction of WT Fpn ubiquitination. As in B, WT is included only for visual reference. Statistical analysis employed the two-tailed one-sample t-test using 1 as the comparison for B and C and the two-tailed t-test (normally distributed data) or the Mann-Whitney rank sum test (data with non-normal distribution) using the WT as the comparison for A (***P<.001, **P<.01, *P<.05). Data shown are means ± SD of 3-6 independent experiments. Hepcidin-binding mutants were denoted by red shades and ubiquitination mutants by

green shades. Severely impaired mutants were denoted by bolder colors. Severe impairment was defined as ≤ 25% of WT values.

The two major possible mechanisms of functional hepcidin resistance are i) decreased hepcidin binding to Fpn or ii) decreased hepcidin-induced endocytosis of Fpn despite intact hepcidin binding. To determine if the Fpn-GFP mutants bind hepcidin, we treated mutant cell lines with biotinylated hepcidin for 30 min, immunoprecipitated Fpn with anti-GFP antibody, and detected bound hepcidin by immunoblotting with streptavidin-HRP, taking advantage of the stability of the hepcidin-ferroportin complex in nonreducing SDS-PAGE (21, 22). We identified 5 mutants that showed impaired hepcidin binding compared to WT (quantitation showed in Figure 1A-2B and representative Western blots in Figure S5): C326S, Y501C, D504N, N144D and V72F.

After hepcidin binding to Fpn, ubiquitination of several cytoplasmic lysines is required for endocytosis of Fpn (17). To assess hepcidin-induced ubiquitination, we treated Fpn-GFP mutants with hepcidin, immunoprecipitated them with anti-GFP antibody, and probed for ubiquitin with an antibody that recognizes both poly-and mono-ubiquitinated proteins. We identified 6 mutants that had normal hepcidin binding, but variably deficient hepcidin-induced ubiquitination: Y64N and H507R showed a severe impairment in ubiquitination, and S71F, G204S, D270V and S338R were less impaired (quantitation shown in Figure 2C and representative Western blots in Figure S6).

Results shown in Figures 1A-2B (hepcidin binding) and 1A-2C (Fpn ubiquitination) were used as the basis for color assignment in all the figures and structures in this manuscript: red/pink indicates mutants with impaired hepcidin binding, and light/dark green indicates mutants that bind hepcidin normally but have variably impaired ubiquitination. The intensity of the color denotes the severity of the impairment.

Fpn-GFP mutants map out a hepcidin-binding site in the central cavity and reveal peripheral hindrance of conformation-dependent ubiquitination

We next mapped the mutations causing impaired hepcidin binding (C326S, Y501C, D504N, N144D, and V72F) or impaired hepcidin-dependent ubiquitination (Y64N, H507R, S71F, G204S, D270V, and S338R) onto a computational structural model of human ferroportin (hFpn) (Figure 1A-3). All the hepcidin-binding mutants localized within the main cavity of Fpn, implicating four helices in the hepcidin binding site (helices 2, 4, 7 and 11). All of the ubiquitination mutants localized to the periphery of Fpn, at the helix-helix interfaces, suggesting that these substitutions interfere with appropriate conformational change after hepcidin binding. A second computational model (Figure S7) which included the crystal structure of BdFPN in the modeling led to the same conclusion.

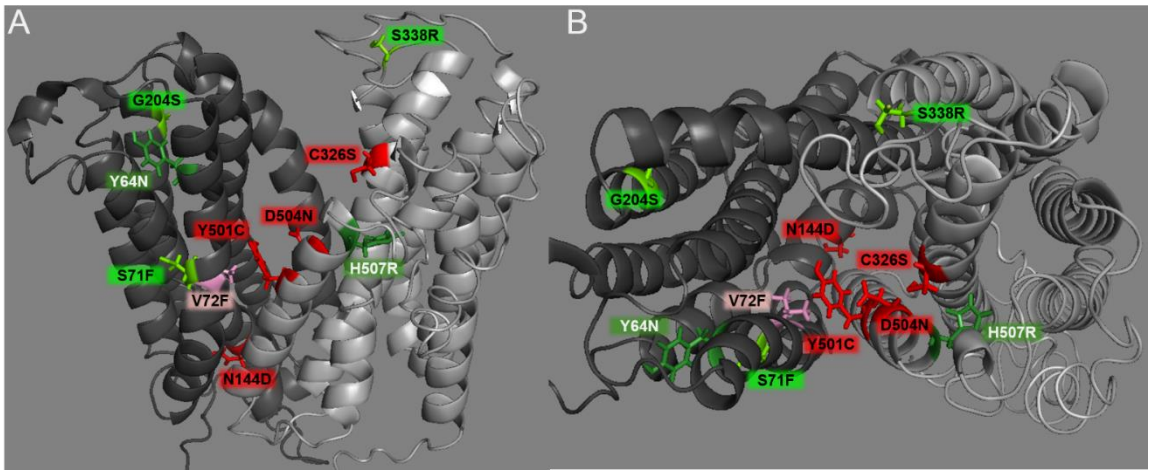

Figure 1A-3: hFpn structure depicting clinically relevant mutant residues. (A) A side-view of hFpn in its outward-facing state, with the N-terminus on the left and C-terminus on the right. (B) Top-down view of hFpn in its outward-facing state. D270V is not modeled because it is in the unstructured intracellular loop of Fpn. The red/pink color denotes mutants with impaired hepcidin binding, and the green color denotes mutants with variably impaired ubiquitination.

To refine the model of hepcidin binding to Fpn, we generated additional nonclinical mutations within helices 7 and 11 as our data suggest that these helices contribute most strongly to hepcidin binding. We tested F324A, F324Y, Y333A, Y333F, and F508Y as before and showed that all were displayed on the membrane and exported iron (Figure 1A-4A and -4B). Only F508Y strongly impaired hepcidin binding, whereas the others had impaired ubiquitination compared to the WT (Figure 1A-4C and -4D). Ferritin retention as a marker of functional resistance to hepcidin showed that F508Y was strongly resistant despite conservative amino acid substitutions (Figure 1A-4E and S8), whereas for other residues, non-conservative substitutions (F324A and Y333A) were required for significant resistance (Figure 1A-4E). Interestingly, even though F508Y bound hepcidin very poorly and failed to retain intracellular ferritin or radiolabeled iron, it was mostly degraded by 24 h (Figure S9A and B), suggesting delayed internalization and degradation. The only unstable nonclinical mutant was F324A (Figure S9C), a ubiquitination-impaired mutant. Mapping the 5 nonclinical Fpn-GFP mutants onto our computational hFpn model (Figure S10 and Figure S7) indicates that the deduced hepcidin-binding site may include F508. The model also highlights the role of peripheral Fpn mutations in impeding ubiquitination and thereby causing variable resistance to hepcidin-induced Fpn endocytosis and degradation.

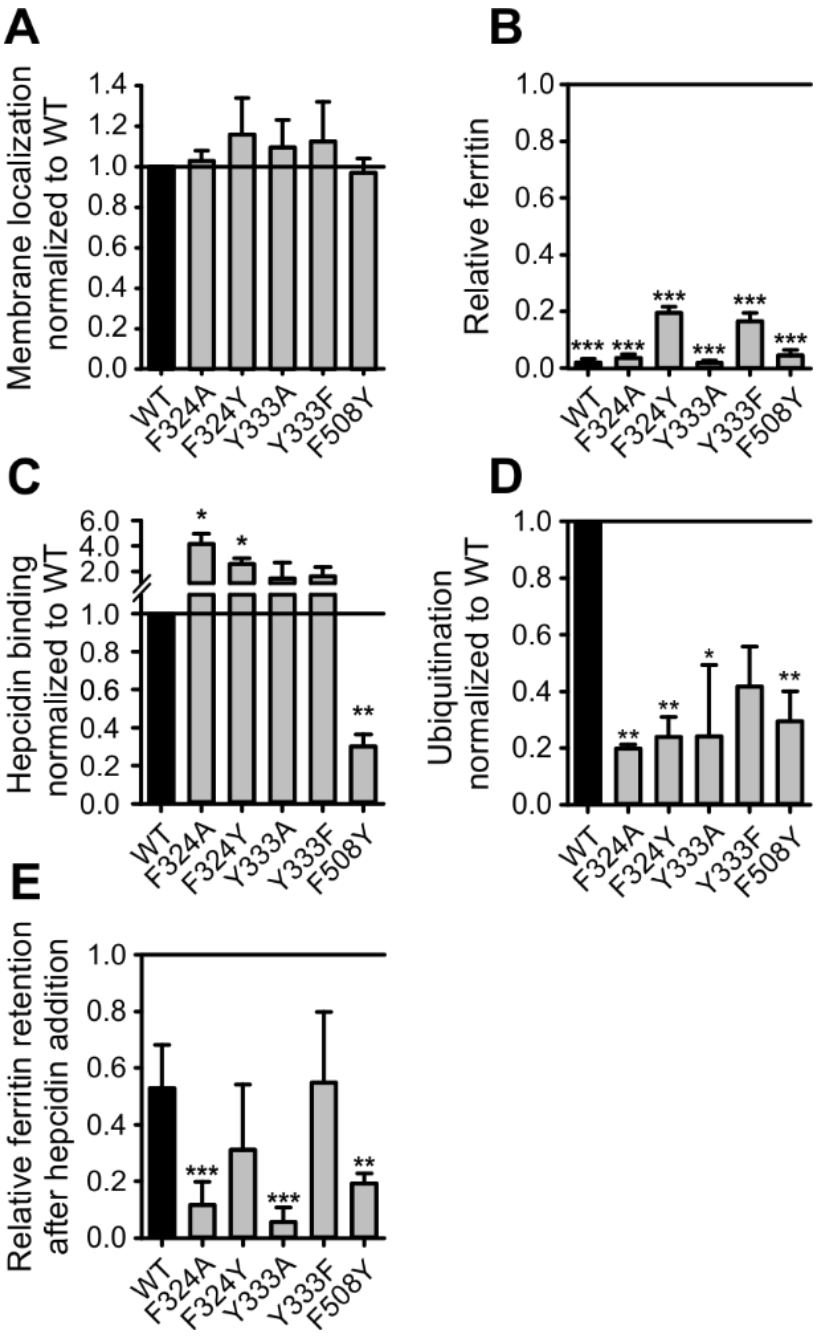

Figure 1A-4: Analysis of nonclinical hFpn-GFP mutants. Cells expressing inducible nonclinical Fpn mutants were analyzed with the same approaches as those expressing clinical mutants. A) All mutants were displayed on the cell membrane. Membrane localization was determined as in Figure 1A-1A. B) All mutants exported iron. Ferritin was determined as in Figure 1A-1B by normalizing it to the uninduced (-dox) condition for each cell line (thus, uninduced ferritin levels = 1). C) Hepcidin binding was determined as in Figure 1A-2B. D) Ubiquitination was determined as in Figure 1A-2C. E) Relative ferritin retention after hepcidin addition was determined as in Figure 1A-2A. Data shown are means ± SD of 3-6 independent experiments. Statistical analysis employed the two-tailed one-sample t-test using 1 as the comparison for A-D and the two-tailed t-test (normally distributed data) or the Mann-Whitney rank sum test (data with non-normal distribution) using the WT as the comparison for E (***P<0.001, **P<0.01, *P<0.05).

Characterization of K8R Fpn mutant and evidence of its occlusion by hepcidin and minihepcidin

Our structural model of Fpn implies that hepcidin binding deep in the Fpn central cavity should impede iron export, even if hepcidin-induced endocytosis of Fpn is disabled. To test this, we designed a Fpn variant deficient in ligand-induced endocytosis through mutations that disable ubiquitination but have a minimal effect on the intramembrane domains of Fpn. The cytoplasmic loop that connects the two six-helix bundle lobes of Fpn contains lysines that undergo hepcidin-dependent ubiquitination (17), so we generated a cell line stably expressing inducible K8R Fpn-GFP, in which 8 lysines of the loop were mutated to arginines (Figure S7E). K8R localized on the cell membrane (Figure 1A-5A), exported iron similarly to WT as measured by loss of intracellular ferritin after Fpn induction (Figure 1A-5B), and bound hepcidin, though at about 30% of WT Fpn binding (Figure 1A-5C). K8R had severely impaired hepcidin-induced ubiquitination as expected (Figure 1A-5D), even at very high hepcidin concentrations (Figure S11). Despite the complete loss of hepcidin-dependent ubiquitination, K8R ^{55}Fe iron export was still decreased by hepcidin treatment (Figure 1A-5E). We compared ferritin retention and Fpn degradation in WT, C326S (a mutant that cannot bind hepcidin), and K8R in response to a range of hepcidin concentrations. After hepcidin addition, K8R Fpn retained ferritin in a dose-dependent manner, and higher hepcidin concentrations achieved maximal iron retention comparable to WT (Figure 1A-6A). The C326S mutant was resistant to hepcidin-induced iron retention. The profound block of iron export through K8R was achieved despite impaired Fpn degradation as determined by Western blotting (Figure 1A-6B) and microscopy (Figure 1A-6C). PR73, (23) a minihepcidin, was 10x more potent than hepcidin in inducing ferritin retention without endocytic degradation of K8R Fpn (Figure S12).

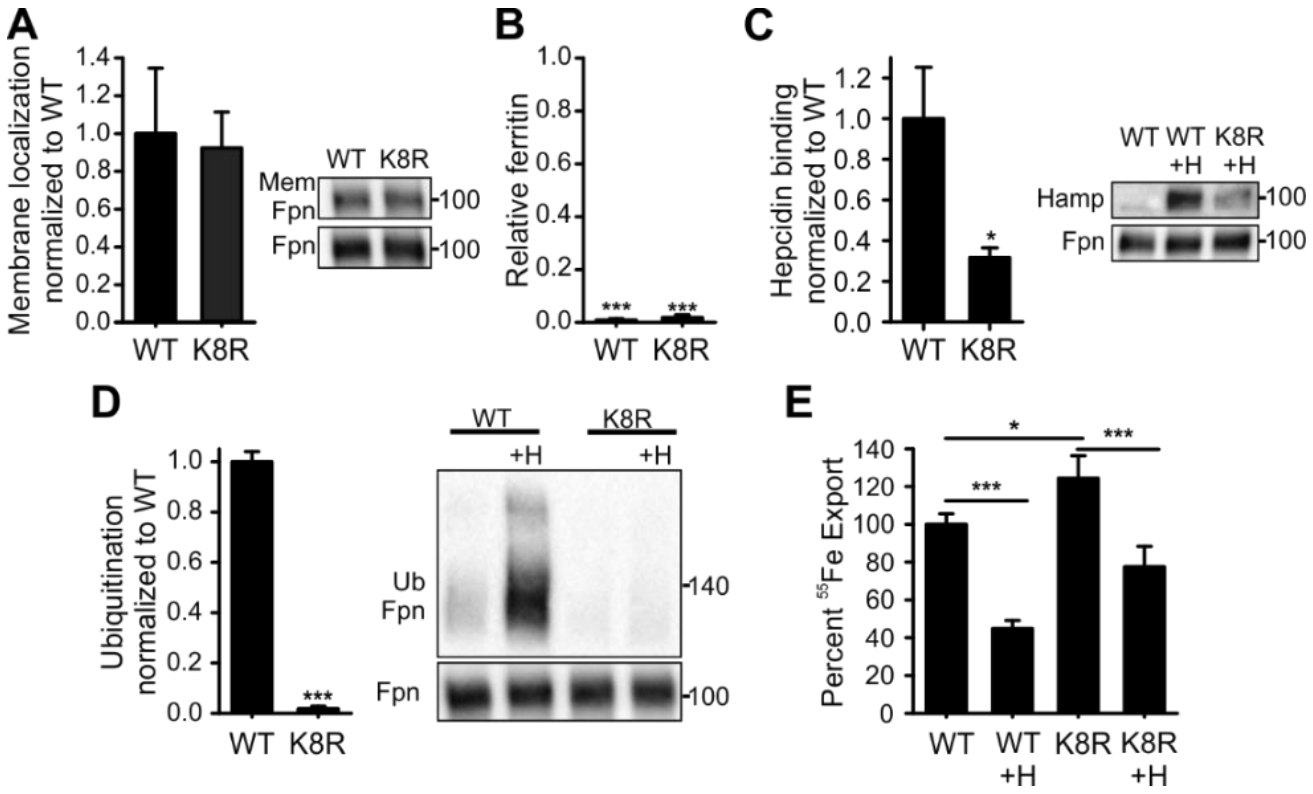

Figure 1A-5: Iron export by the K8R mutant is inhibited by hepcidin despite the absence of ligand-induced ubiquitination. A) Cells were treated as in Figure 1A-1A. K8R localized to the cell membrane similarly to WT. Mem= membrane. B) Cells were treated as in Figure 1A-1B. K8R exported iron and decreased ferritin similarly to WT. Statistical analysis employed the one-sample t test compared to one (normally distributed data) or one-sample signed rank test (data with non-normal distribution). C) Cells were treated as in Figure 1A-2B. Hepcidin bound less to K8R compared to WT. D) Cells were treated as in Figure 1A-2C. The K8R mutant was not ubiqitinated after hepcidin addition. For A, C, and D, statistical analysis employed the two-tailed t-test compared to WT. E) Cells were loaded with 2mM ^{55}Fe for 48 hours, washed, re-plated, induced overnight, washed again, and ± 3 μg/ml hepcidin was added. Extracellular radioactivity was measured at 0, 2, 4 and 8 hours. The "uninduced" measurement at each time point was subtracted as background, and the slope for each sample determined and used to calculate the percent iron export by normalizing the slopes to the untreated WT. For E, Statistical analysis employed the two-tailed t-test (normally distributed data) and Mann-Whitney rank sum test (data with non-normal distribution) compared to WT. Data shown are means ± SD of 3-4 biological replicates where ***P<0.001, **P<0.01, *P<0.05.

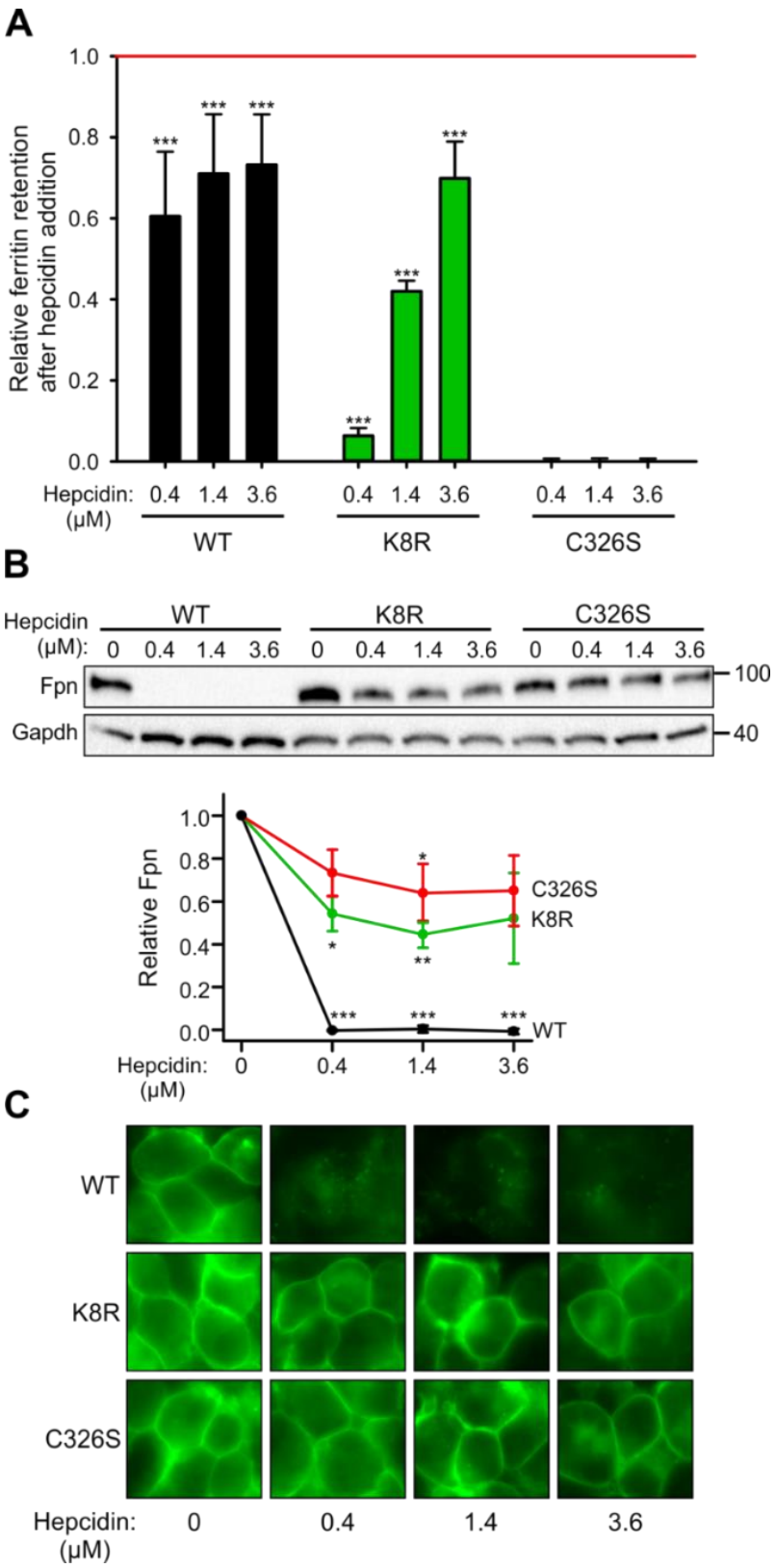

Figure 1A-6: Evidence for Fpn occlusion by hepcidin. Cells expressing inducible non-ubiquitinating K8R mutant were compared to those expressing WT Fpn or C326S mutant which does not bind hepcidin. A) Ferritin retention after hepcidin addition was determined as in Figure 1A-2A. Statistical analysis employed the two-tailed t-test using the respective untreated control for comparison (***P<0.001, **P<0.01, *P<0.05). B) Lysates from A were analyzed by Western blotting. Top: representative Western blot. Bottom: densitometry of triplicate Western blots. Fpn signal was first normalized to GAPDH, then expressed as the fraction of respective untreated control (no hepcidin treatment). Statistical analysis employed the two-tailed one-sample t-test using 1 as the comparison (***P<0.001, **P<0.01, *P<0.05). C) Microscopy of samples in A after 24 hours. Data shown are the mean ± SD of 3 independent experiments.

To further confirm that hepcidin can inhibit iron export without causing Fpn endocytosis but by occluding Fpn, we used *Xenopus* oocytes expressing WT or K8R Fpn-GFP. Oocytes expressing WT Fpn-GFP were pre-treated with hepcidin for up to 4 h to determine the time-course of the hepcidin effect on iron export. In contrast to mammalian cells in which hepcidin treatment results in a progressively greater inhibition of iron export up to 10 h, maximal inhibition of iron export in oocytes was observed after only 30 min pre-treatment (Figure 1A-7A). We found that 30 min hepcidin treatment inhibited ^{55}Fe efflux from oocytes expressing K8R Fpn to the same degree as it did for WT Fpn (Figure 1A-7B). Live-imaging of oocytes revealed that 30-min hepcidin treatment did not induce endocytosis of either WT or K8R Fpn (Figure 1A-7C). Whereas some reduction in the intensity of GFP fluorescence at the oocyte perimeter was observed in WT and K8R oocytes over time (presumably due to photobleaching), hepcidin did not stimulate a loss of fluorescence from the oocyte perimeter either for WT or K8R. These data reveal that hepcidin can directly inhibit Fpn-mediated iron transport activity independently of Fpn internalization not only in the K8R mutant but also in WT Fpn.

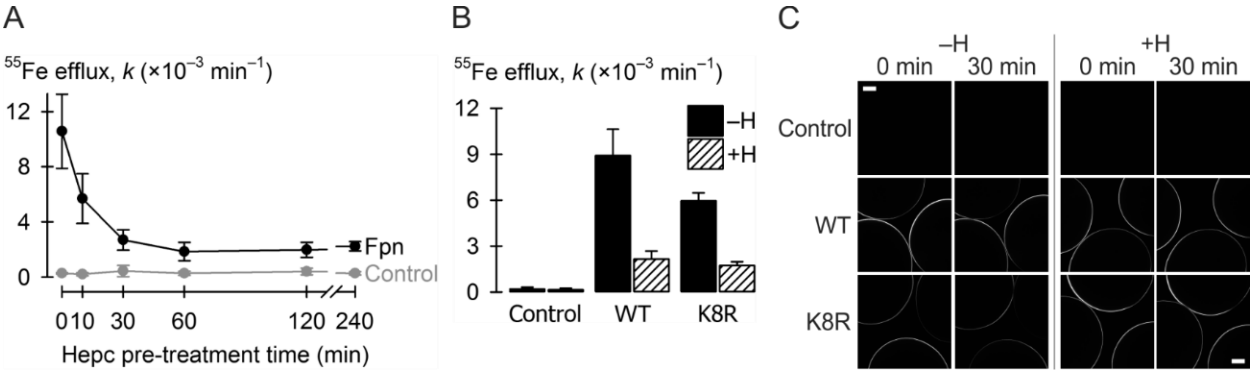

Figure 1A-7: Effect of hepcidin on WT and mutant Fpn expressed in *Xenopus* oocytes. (A) First-order rate constants (k) describing ^{55}Fe efflux (assayed over 30 min) from control oocytes (*gray*) and oocytes expressing WT Fpn (*black*) pre-treated with 10 μM hepcidin for 0–240 min (n = 8–12 per group). Two-way ANOVA revealed an interaction ($P < 0.001$); within Fpn, 0 and 10 min differed from all other time points ($P < 0.001$), and 30–240 min time points did not differ from one another ($P \geq 0.35$). (B) ^{55}Fe efflux in control oocytes, and oocytes expressing WT or K8R Fpn that were untreated (−H) or pre-treated 30 min with 10 μM hepcidin (+H) (n = 9–12 per group).

Two-way ANOVA revealed an interaction ($P < 0.001$). Percent inhibition of ^{55}Fe efflux by hepcidin did not differ between WT (76% ± SEM 6%) and K8R (71% ± 3%) ($P = 0.47$). (C) Live-cell imaging of control oocytes and oocytes expressing WT or K8R Fpn before *and* after 30 min treatment without hepcidin (−H) or with 10 μM hepcidin (+H), in the same oocyte preparation as used in (B). Each frame captures portions of 3 oocytes, and the image plane approximately bisects the oocytes. Scale bars, 0.2 mm. Two-way ANOVA of the change in fluorescence intensity (ΔF) over time revealed a greater loss of fluorescence in untreated oocytes (−H) compared with hepcidin-treated (+H) ($P = 0.005$) and that ΔF did not differ between WT and K8R ($P = 0.75$).

DISCUSSION

In this study, we characterized the mechanisms by which known clinical Fpn mutations (Table 1) cause non-classical Ferroportin Disease, and extended these findings to gain insights into the structural basis of Fpn function and its regulation by hepcidin. Our cellular models revealed that non-classical FD mutations do not increase the amount of Fpn in the cell membrane or their iron export capacity at baseline, but cause resistance to hepcidin by variably impairing the binding of hepcidin to Fpn or hepcidin-induced ubiquitination required for endocytosis. Although all of the mutations were associated with a clinical phenotype of non-classical FD, the mutants varied considerably in their degree of hepcidin resistance. In particular, V72F, D270V, and S338R show only very mild hepcidin resistance in our cellular model, suggesting that additional factors may modify the phenotype of FD caused by these mutations. One such factor could be the decreased stability of some mutants including Y64N, H507R, D270V, and S338R (Figure S3). Such instability could decrease Fpn cell surface expression and iron export at baseline, perhaps accounting for the frequent reports of a mixed form of FD (Table 1) manifesting restriction of iron export leading to iron accumulation in Kupffer cells with simultaneous resistance to hepcidin leading to systemic and hepatocyte iron overload. Other modifiers may include gender, age, and comorbidities such as alcohol abuse, obesity, and metabolic syndrome, which are all known to affect the iron status of patients with FD (24, 25). Although our cellular model faithfully

documents profound hepcidin resistance in the more severe mutations, it lacks the complex cellular and systemic regulatory factors that could amplify the effects of the weakest mutations.

Our structural models indicate that hepcidin binding occurs within the main cavity of Fpn where hepcidin interacts with as many as 4 different helices. Additionally, we conclude that peripheral amino acids, positioned at helix-helix interfaces, influence the hepcidin-induced conformational change that leads to the ubiquitination of Fpn. They may even affect Fpn conformation in the absence of hepcidin, explaining how some of the ubiquitination-impaired mutants (Y64N, H507R, D270V, S338R, and F324A), but none of the hepcidin binding-impaired mutants are unstable. Although the alternative structure generated by adding BdFPN to the threading set displays small differences from our earlier model (Figure S7), it does not alter the conclusions of our analysis.

Using the model as a guide to design informative nonclinical mutants, we examined F508Y, the nearest residue that could contribute to the binding site based on its location on helix 11 immediately above Y501 and D504. F508Y was a milder hepcidin-resistant mutant than Y501C and D504N, likely because the amino acid substitution we chose was very conservative. We previously showed that hepcidin binding to Fpn involves a disulfide-thiol interaction between hepcidin and Fpn C326 residue, because the isosteric C326S substitution results in the complete loss of hepcidin binding (7, 21). However, our current study implicates several additional residues on multiple helices in stabilizing the binding between the ligand and its receptor. We also examined F324 and Y333 Fpn residues, because we had previously noted that mutants at these locations did not internalize radiolabeled hepcidin (21). In the present study, we found that these mutants bound hepcidin, but displayed impaired ubiquitination and endocytosis. Our proposed Fpn structural model is consistent with all our experimental data classifying residues as those involved in

hepcidin binding versus those that affect the conformational change leading to ubiquitination of Fpn. After we completed the cellular analyses and modeling, Praschberger et al. described a partially hepcidin-resistant clinical hFpn mutant A69T (26) in a patient with iron-overloaded hepatocytes. Another group described a patient with the A69T mutation as having severe hyperferritinemia (6,242 μg/L) and elevated serum transferrin saturation (95.4%) (27). According to our hFpn computational model, this mutation would be expected to affect hepcidin binding based on the residue location in the central cavity (Figure S7).

Chung et al. previously observed in Caco-2 cells that hepcidin treatment inhibited iron efflux, but failed to decrease Fpn protein levels, and hypothesized that hepcidin could directly block iron export through in these cells (28). Taniguchi et al. (15) similarly proposed Fpn occlusion by hepcidin based on the structure of the prokaryotic homolog BbFPN. Our refined models also predict that hepcidin binds to Fpn in the main cavity and our mutagenesis data experimentally identified a patch of Fpn residues critical for hepcidin binding. Furthermore, we provide evidence that hepcidin binding occludes Fpn and directly blocks iron export even without causing Fpn internalization. We report that the engineered Fpn mutant, K8R, shows severely impaired hepcidin-induced Fpn internalization and degradation but its ability to export iron is completely inhibited by hepcidin, although requiring higher concentrations than WT. Furthermore, using *Xenopus* oocytes, which do not endocytose Fpn in response to hepcidin, we show that hepcidin blocks iron export by occlusion of not only K8R, but also WT Fpn. We surmise that high concentrations of hepcidin are necessary to demonstrate the occlusion of iron transport, because at lower concentrations, many Fpn molecules may not be stably occupied by hepcidin. If so, hepcidin-induced endocytosis serves to amplify the effect of transiently-bound hepcidin. The relative contribution of Fpn occlusion and endocytosis may differ depending on the cell type, its

endocytic machinery, and even Fpn glycosylation, perhaps explaining the reported differences between tissues in sensitivity to hepcidin and discrepancies between the effects of hepcidin on iron export compared with endocytosis (29). Occlusion by hepcidin may be the critical mechanism of regulation of iron efflux in Fpn-expressing cells that lack endocytic machinery, such as mature red blood cells (30). Furthermore, the high potency of minihepcidin PR73 in inhibiting iron export by Fpn K8R suggests that assays of Fpn iron export and FPN endocytosis measure potentially distinct activities of hepcidin agonists, and that engineered hepcidin agonists may exert a therapeutic effect even in patients exhibiting Fpn resistance to hepcidin.

SUPPLEMENTAL MATERIALS

Table S1. Primers for site-directed mutagenesis of human Fpn-GFP

Mutation	Forward primer	Reverse primer
S71F	ctggtggtggcagggtttgttctggtcctg	caggaccagaacaaaccctgccaccaccag
V72F	ggtggcagggtcttttctggtcctggg	cccaggaccagaaaagaccctgccacc
G204S	tggctccccagtcatcagctgtggctttatttc	gaaataaagccacagctgatgactggggagcca
D270V	catctaatgggtgtgaaagtctctaacatccatgagctt	aagctcatggatgttagagactttcacacccattagatg
S338R	cactcagggactgaggggttccatcctcagt	actgaggatggaacccctcagtccctgagtg
Y501C	ggtgtacagaactccatgaactgtcttcttgatcttctgc	gcagaagatcaagaagacagttcatggagttctgtacacc
D504N	gtacagaactccatgaactatcttcttaatcttctgcatttcatcat	atgatgaaatgcagaagattaagaagatagttcatggagttctgtac
H507R	ctatcttcttgatcttctgcgtttcatcatggtcatcctgg	ccaggatgaccatgatgaaacgcagaagatcaagaagatag
F508Y	atcttcttgatcttctgcattatatcatggtcatcctggctcc	ggagccaggatgaccatgatataatgcagaagatcaagaagat
Y64N	ccaccaccagcccgttgactgctgtcaaaag	cttttgacagcagtcaacgggctggtggtgg
N144D	ctattgcaaatattgcagatttggccagtactgc	gcagtactggccaaatctgcaatatttgcaatag
Y333A	accacagggtacgccgccactcagggactgag	ctcagtccctgagtggcggcgtaccctgtggt
Y333F	cacagggtacgccttcactcagggactga	tcagtccctgagtgaaggcgtaccctgtg
F324A	tatatgactgtcctgggcgctgactgcatcaccacagg	cctgtggtgatgcagtcagcgcccaggacagtcatata
F324Y	tatgactgtcctgggctatgactgcatcaccac	gtggtgatgcagtcatagcccaggacagtcata
C326S	tcctgggcttgacagcatcaccacaggg	ccctgtggtgatgctgtcaaagcccagga

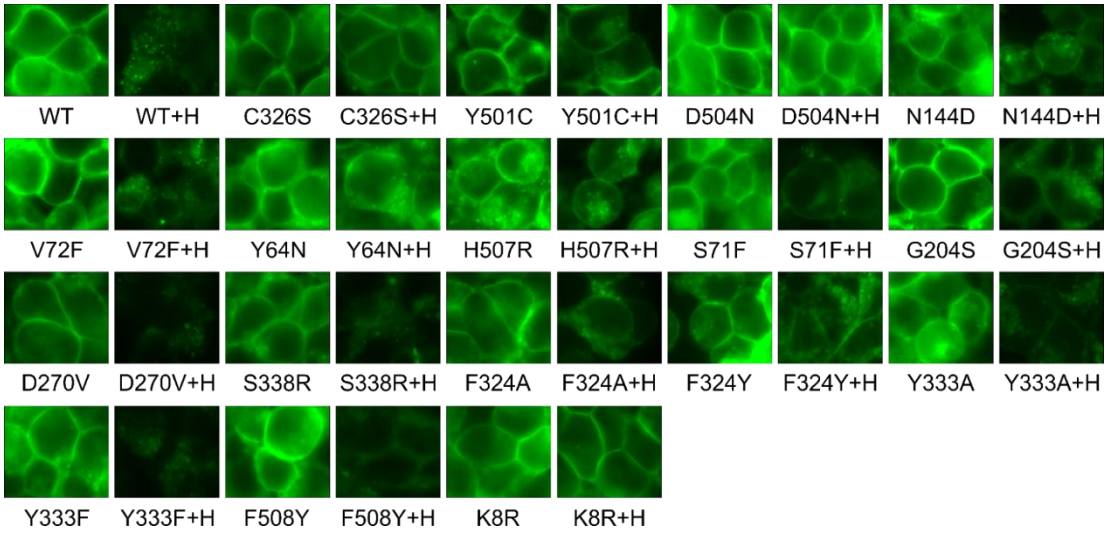

Figure S1: Microscopy of human Fpn (hFpn) mutant cells ± hepcidin treatment. HEK293T cells stably transfected with doxycycline (dox)-inducible hFpn-GFP mutants were induced with 100 ng/ml dox overnight. The cells were then washed, incubated with ±1 µg/ml hepcidin for 24 hours, and imaged by fluorescent microscopy.

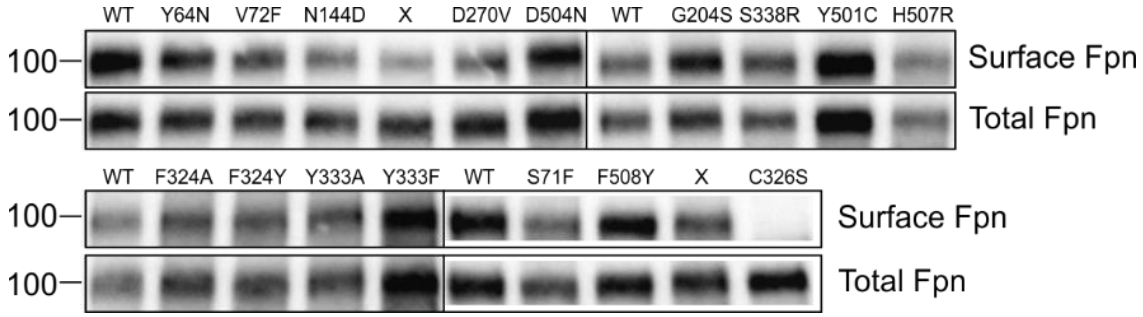

Figure S2: Representative Western blots: cell surface biotinylation of hFpn. HEK293T cells stably expressing doxycycline (dox)-inducible hFpn-GFP mutants were induced with dox to express Fpn, treated with maleimide-biotin for 30 minutes, immunoprecipitated using anti-GFP Ab, and immunoblotted with streptavidin-HRP or anti-GFP Ab. X denotes mutants not discussed in the paper.

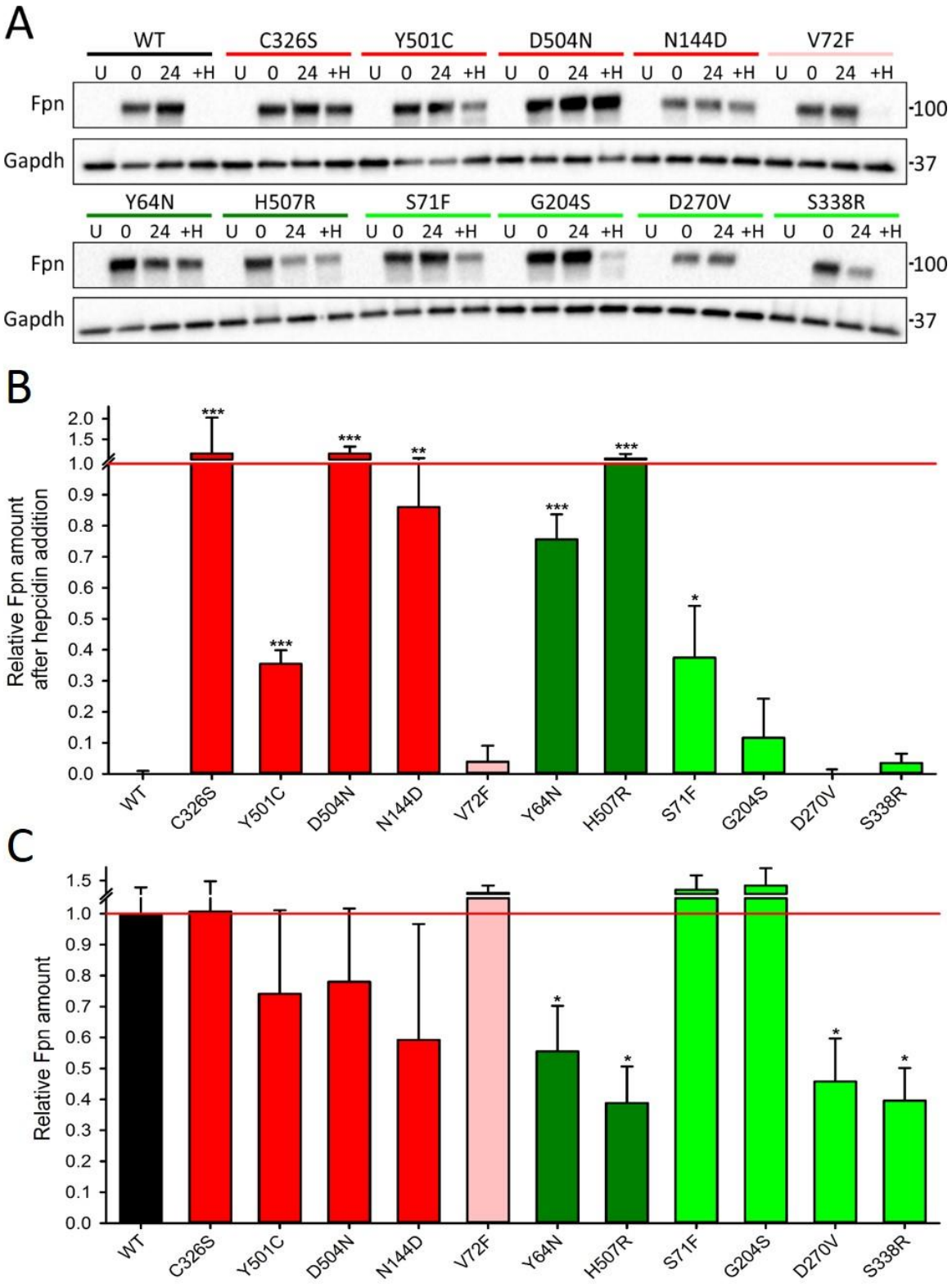

Figure S3: Stability and hepcidin-induced degradation of WT and mutant Fpn. Cells were induced overnight to express hFpn-GFP. The inducer was removed, the cells were washed, and some wells were harvested for the 0 h time point, or incubated for another 24 hours ±1 μg/mL

hepcidin. A) Representative Western blot of WT and mutant hFpn-GFP. Fpn was detected using anti-GFP Ab and GAPDH was used for normalization. U= uninduced Fpn cells, 0= 0 h time-point, 24= 24 h time-point without hepcidin treatment, and H= hepcidin treatment for 24 h. B) Quantification of Fpn degradation by hepcidin. Densitometry was performed on triplicate Western blots from A. GAPDH was used for normalization of the GFP signal. Values of hepcidin-treated samples were further normalized to their respective untreated 24 h control to express results as relative Fpn amount after hepcidin treatment. The two-tailed t-test comparing mutants to WT was employed (***P<0.001, **P<0.01, *P<0.05). C) Quantification of Fpn stability. Densitometry was performed on triplicate Western blots from A, and GAPDH was used for normalization of GFP signal. Fpn values at 24 h (non-hepcidin treated) were expressed as a fraction of their respective controls at 0 h. 1= amount of Fpn at the 0 h time point for each respective mutant. Statistical analysis employed the two-tailed one-sample t-test using 1 as the comparison (***P<0.001, **P<0.01, *P<0.05). Data shown are means ± SD of 3 independent experiments.

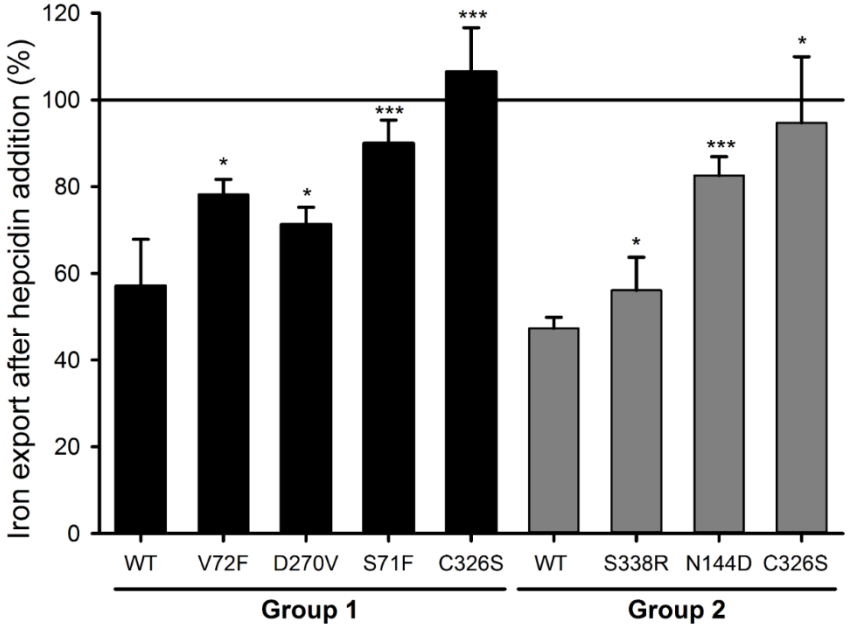

Figure S4: Iron export after hepcidin addition. Cells were loaded with 2mM ^{55}Fe for 48 hours, washed, re-plated, and either left uninduced or were induced by adding doxycycline overnight. Cells were washed again and medium was sampled at multiple time points to measure iron export up to 10 hours ± hepcidin (Group 1: 0.1 µg/ml, Group 2: 3 µg/ml). The "uninduced" measurement at each time point was subtracted as background. The slope for each "induced" and "induced + hepcidin" sample was determined, and % export after hepcidin treatment calculated. Statistical analysis employed the two tailed t-test comparing each mutant to its respective WT. Data shown are means ± SD of at least 4 biological replicates. *** P < 0.0005, **P < 0.005, *P < 0.05 by t-test or t-test on ranks if not normally distributed. C326S, a highly hepcidin-resistant mutant, was used in each experiment as a control for assay integrity.

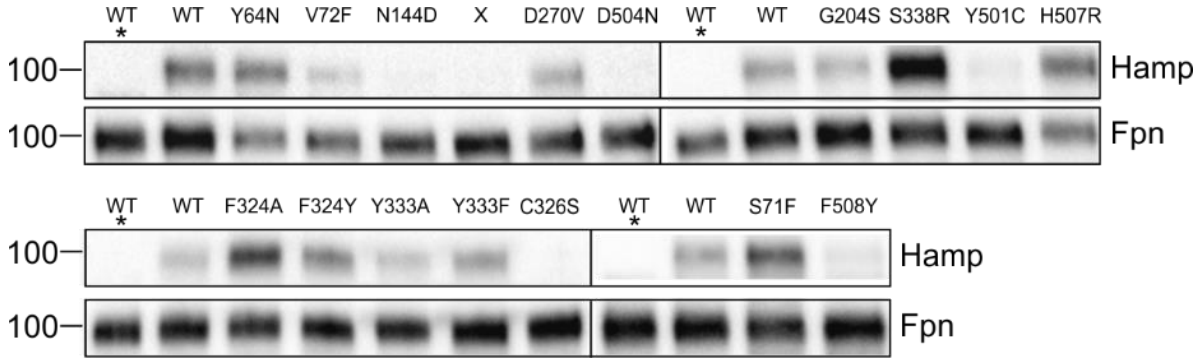

Figure S5: Representative Western blots: hepcidin binding to hFpn. Cells induced to express WT or mutant hFpn-GFP were treated with N-terminally biotinylated hepcidin for 30 minutes, immunoprecipitated with anti-GFP Ab, and immunoblotted with streptavidin-HRP or anti-GFP Ab. *= WT with no hepcidin added. X denotes a mutant not discussed in the paper.

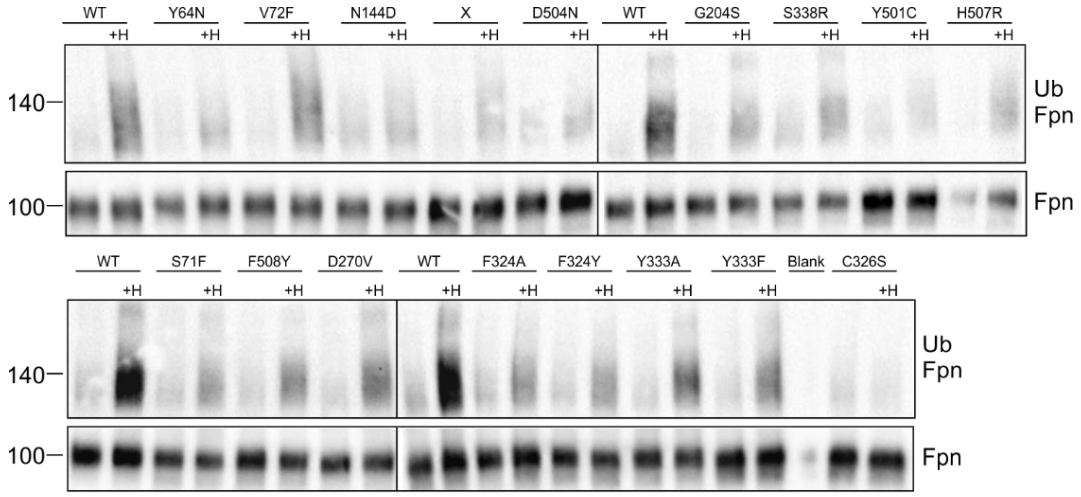

Figure S6: Representative Western blots: ubiquitination of hFpn. Cells expressing WT and mutant hFpn-GFP were treated with hepcidin for 30 minutes, immunoprecipitated with anti-GFP Ab, and immunoblotted with anti-poly/mono ubiquitin Ab (FK2) or anti-GFP Ab. X denotes a mutant not discussed in the paper.

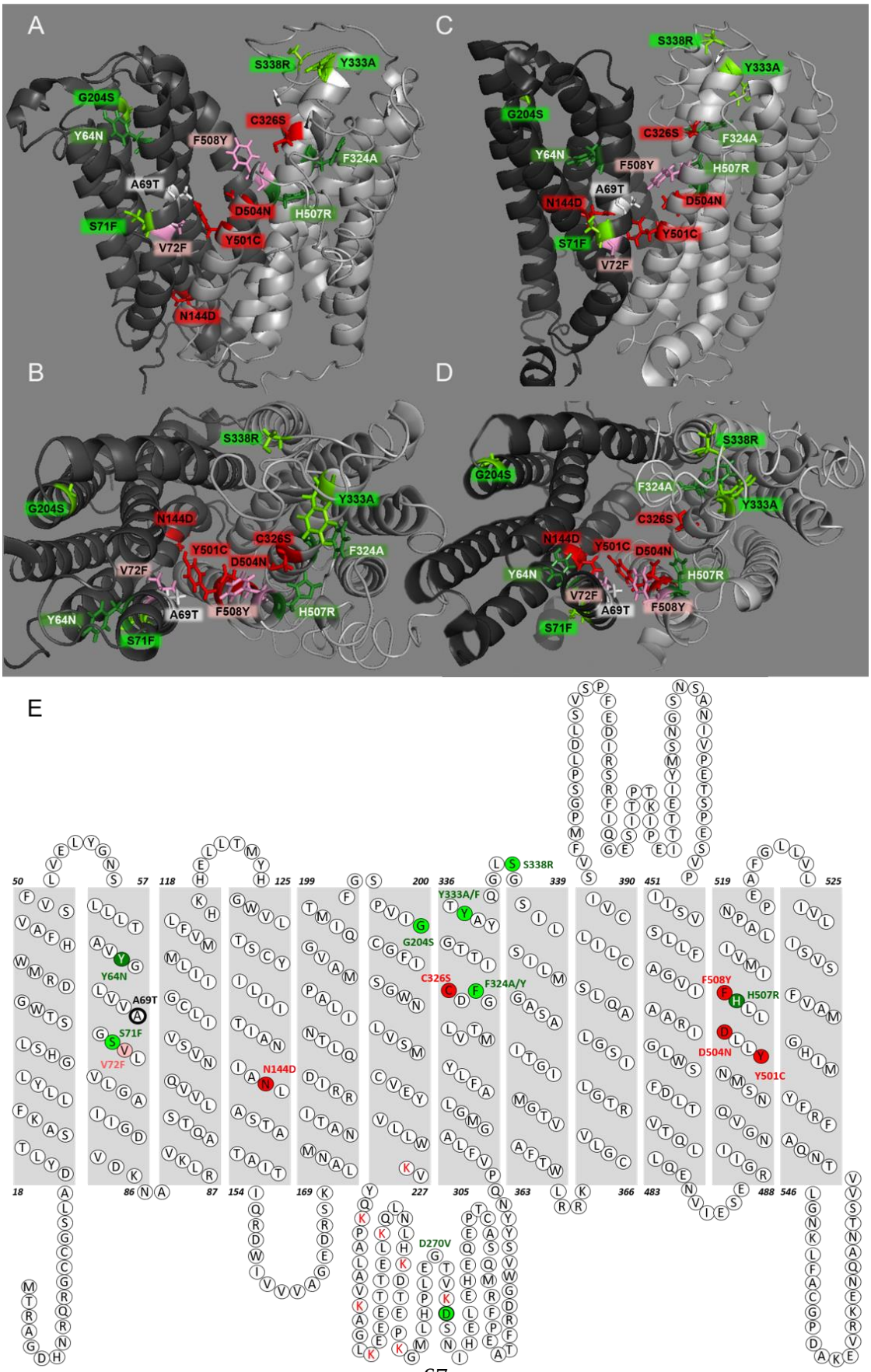
A
S338R
Y333A
G204S
Y64N
C326S
F508Y
F324A
A69T
D504N
H507R
S71F
V72F
Y501C
N144D
B
S338R
G204S
Y333A
N144D
C326S
Y501C
F324A
D504N
V72F
A69T
F508Y
H507R
Y64N
S71F
C
S338R
Y333A
G204S
C326S
F324A
Y64N
F508Y
H507R
A69T
D504N
N144D
Y501C
S71F
V72F
D
S338R
G204S
F324A
Y333A
C326S
N144D
Y501C
D504N
Y64N
H507R
V72F
A69T
F508Y
S71F
E
S338R
Y333A/F
G204S
C326S
F324A/Y
Y64N
A69T
S71F
V72F
N144D
F508Y
H507R
D504N
Y501C
D270V

Figure S7: hFpn I-TASSER modeling without or with BdFPN among templates. (A and B) Model generated without the Bd2109 crystal structure; side-view and top-view of hFpn in its outward-facing state are shown. (C and D) Model generated by including the Bd2109 crystal structure among templates; side-view and top-down view of hFpn in its outward-facing state are shown. D270V is not modeled because it is in the disordered intracellular loop of Fpn. Red/pink color denotes mutants with impaired hepcidin binding, and green color denotes mutants with variably impaired ubiquitination. A69T, the white colored mutant, is a recently discovered clinical mutation causing non-classical ferroportin disease that was not experimentally examined in our study. E) 2D Fpn model of A and B. Red Ks (lysines) indicate the residues mutated in the K8R Fpn mutant.

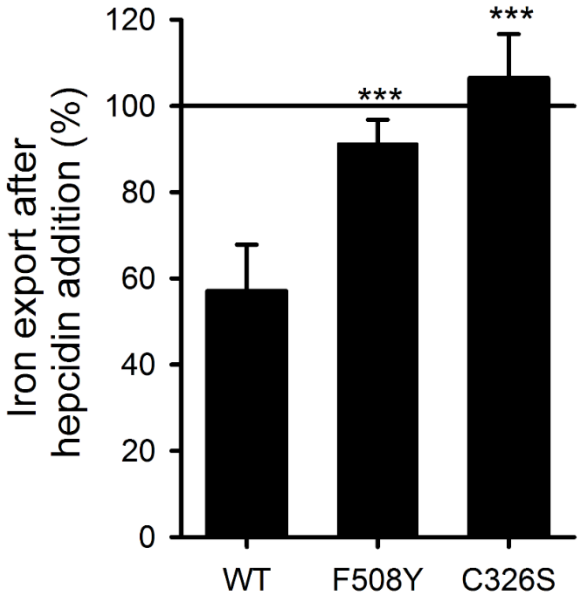

Figure S8: F508Y Fpn mutant is functionally resistant to hepcidin as determined by radiolabeled iron export. Cells were loaded with 2mM ^{55}Fe for 48 hours, washed, re-plated, and either left uninduced or were induced by adding doxycycline overnight. Cells were washed again, and medium sampled at multiple time points to measure iron export up to 10 hours ± 0.1 µg/ml hepcidin. The "uninduced" measurement at each time point was subtracted as background. The slope for each "induced" and "induced + hepcidin" sample was determined, and % export after hepcidin treatment calculated. Statistical analysis employed the two tailed t-test comparing each mutant to its respective WT. Data shown are means ± SD of at least 4 biological replicates. *** $P < 0.0005$, ** $P < 0.005$, * $P < 0.05$ by t-test or t-test on ranks if not normally distributed. C326S, a highly hepcidin-resistant mutant, was used in each experiment as a control for assay integrity.

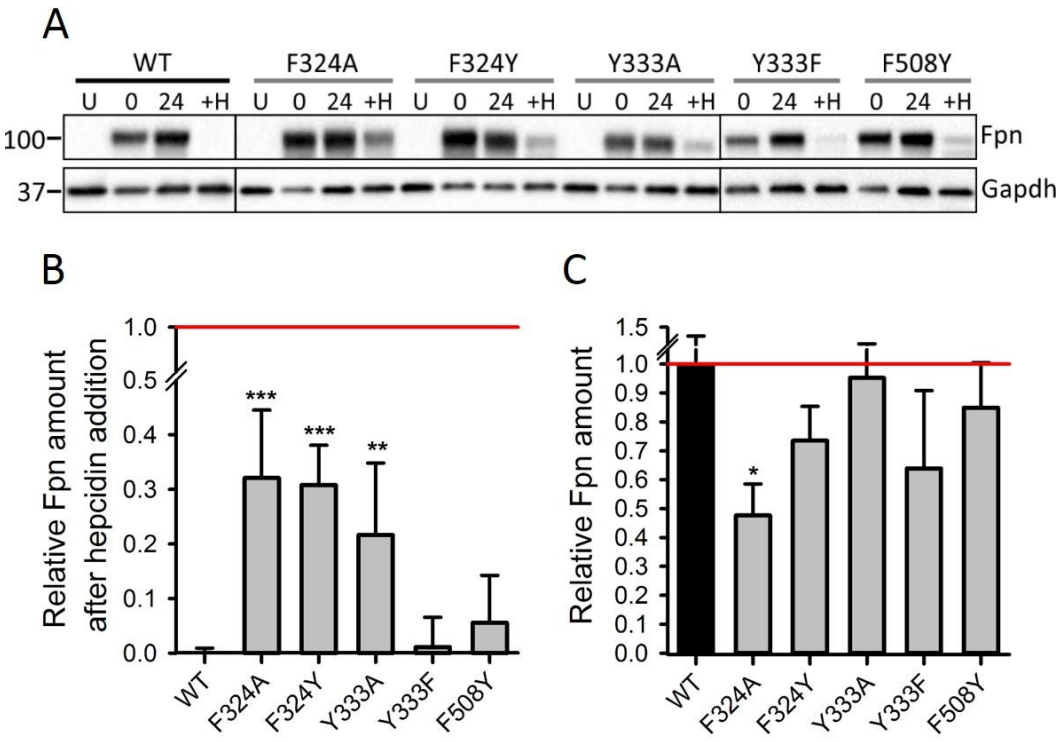

Figure S9: Stability and hepcidin-induced degradation of hFpn. Cells expressing inducible nonclinical Fpn mutants were analyzed with the same approaches as described in Figure S3. Cells were induced overnight to express WT and mutant hFpn-GFP. Doxycycline was removed and cells harvested for the 0 h time point or incubated for another 24 hours ±1 μg/mL hepcidin. A) Representative Western blots. B) Quantification of Fpn degradation by hepcidin. C) Quantification of Fpn stability. Densitometry in B and C was performed on triplicate Western blots from A, and an average of two housekeeping proteins was used for normalization (GAPDH and actin). Statistical analysis employed the two-tailed t-test comparing the mutants to WT (B) or the two-tailed one-sample t-test using 1 as the comparison (C) (***P<0.001, **P<0.01, *P<0.05). Data shown are means ± SD of 3 independent experiments.

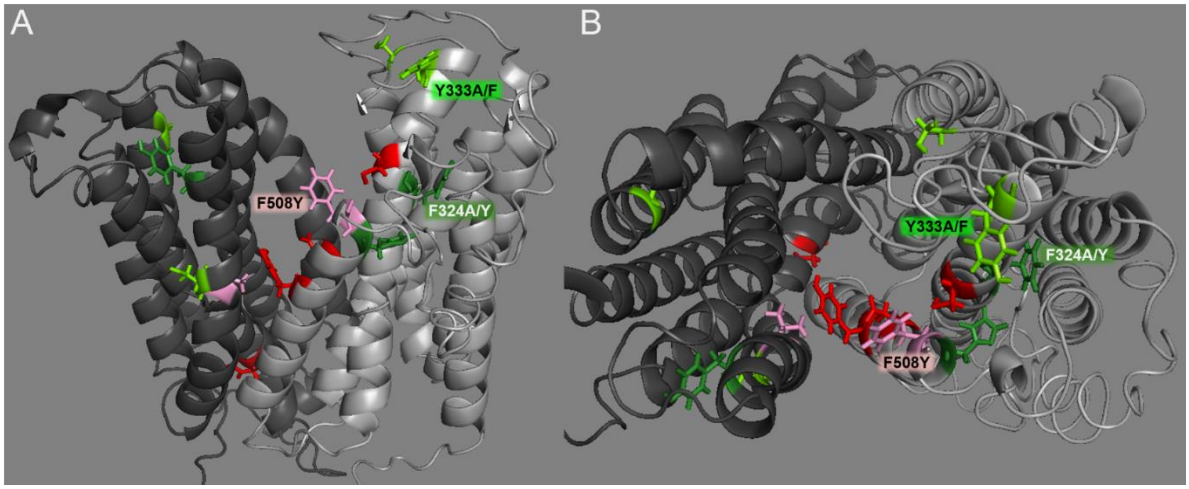

Figure S10: hFpn structure depicting nonclinical mutant residues. (A) A side-view of hFpn in its outward-facing state, with the N-terminus on the left and C-terminus on the right. (B) Top-down view of hFpn in its outward-facing state.

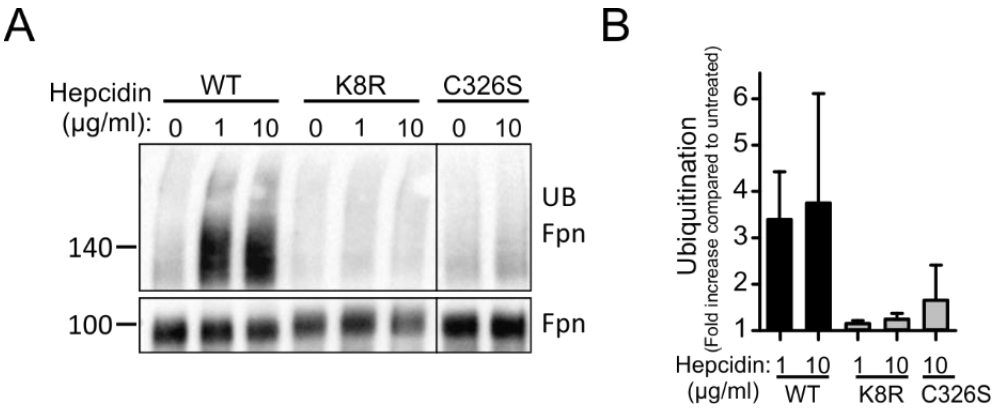

Figure S11: High concentrations of hepcidin do not cause ubiquitination of K8R Fpn. A) hFpn-GFP WT and mutants were treated with hepcidin for 30 minutes, immunoprecipated with anti-GFP Ab, and immunoblotted with anti-poly/mono ubiquitin Ab (FK2) or anti-GFP Ab. The C326S mutant, which does not bind hepcidin, was used as a control. B) Quantification of triplicate Western blots from A. Ubiquitination was normalized to total Fpn in each sample and then expressed as fold increase over hepcidin-untreated sample. 1= the amount of basal ubiquitination for each respective untreated mutant in the absence of hepcidin. Results are shown as the mean ± standard deviation of 3 independent experiments. No statistical significance for mutants was achieved when employing the two-tailed one-sample t-test using 1 as a comparison.

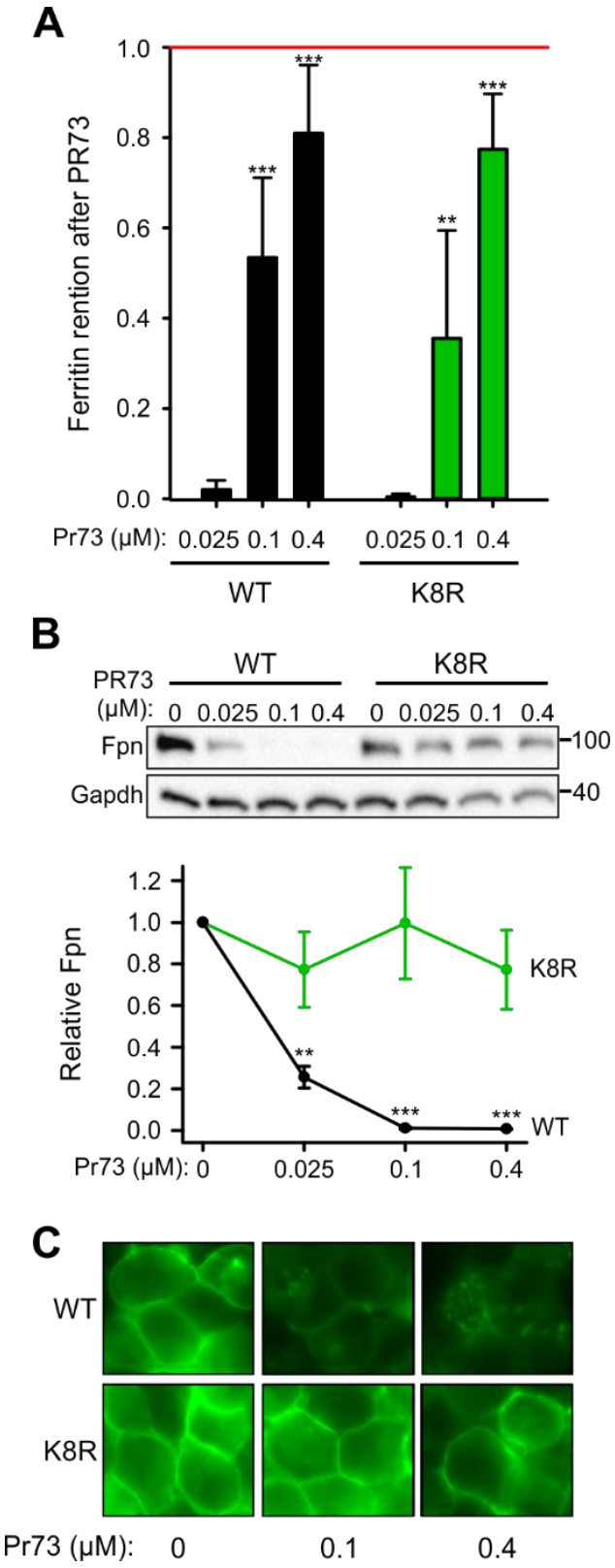

Figure S12: Evidence for Fpn occlusion by minihepcidin. Cells expressing inducible non-ubiquitinated K8R mutant were compared to those expressing WT Fpn. A) Ferritin retention after hepcidin addition was determined as in Figure 1A-2A. Statistical analysis employed the two-tailed t-test using the respective untreated control for comparison (***P<0.001, **P<0.01, *P<0.05). Data shown are the mean ± SD of 3 independent experiments. B) Lysates from A were analyzed by Western blotting. Top: representative Western blot. Bottom: densitometry of triplicate Western blots. Fpn signal was first normalized to GAPDH, then expressed as the fraction of respective untreated control (no hepcidin treatment). Data shown are the mean ± SEM of 3 independent experiments. For A and B, statistical analysis employed the two-tailed one-sample t-test using 1 as the comparison (***P<0.001, **P<0.01, *P<0.05). C) Microscopy of samples in A after 24 hours.

SUPPLEMENTAL MATERIAL AND METHODS

Fpn stability Western blot

Cells were induced with 100ng/ml doxycycline overnight in 12-well poly-D-lysine coated plates (BD). Next, the medium was removed, cells were washed 2x with 1xPBS, and treated with 25 μM ferric ammonium citrate (FAC) either with or without 1 μg/ml hepcidin for 24 hours, except the zero-time point sample which occurred after the PBS wash and was harvested. The protein concentration was measured using the BCA assay and 25 μgs of protein was used for Western blots. Anti-GFP Ab (Roche) measured total FPN and was normalized using an anti-GAPDH Ab or anti-actin Ab when specified.

Radioactive iron export

Adherent cells were loaded with 2 mM ^{55}Fe for 48 hours, washed 3x with medium, re-plated, induced overnight, washed 2x with medium, and then 3 μg/ml of hepcidin was added to some wells. Aliquots of the medium were taken up to 10 hours to measure iron export. The "uninduced" measurement at each time point was subtracted as background. The slope of each line was determined and used to calculate the percent iron export by comparing the slopes to that of untreated WT.

SUPPLEMENTAL REFERENCES

S1. Lok CY, Merryweather-Clarke AT, Viprakasit V, Chinthammitr Y, Srichairatanakool S, Limwongse C *et al.* Iron overload in the Asian community. *Blood* 2009; 114(1)**:** 20-25. doi: 10.1182/blood-2009-01-199109

S2. Sham RL, Phatak PD, West C, Lee P, Andrews C, Beutler E. Autosomal dominant hereditary hemochromatosis associated with a novel ferroportin mutation and unique clinical features. *Blood Cells Mol. Dis.* 2005; 34(2)**:** 157-161.

S3. Letocart E, Le GG, Majore S, Ka C, Radio FC, Gourlaouen I *et al.* A novel missense mutation in SLC40A1 results in resistance to hepcidin and confirms the existence of two ferroportin-associated iron overload diseases. *Br.J Haematol.* 2009; 147(3)**:** 379-385.

S4. Callebaut I, Joubrel R, Pissard S, Kannengiesser C, Gérolami V, Ged C *et al.* Comprehensive functional annotation of 18 missense mutations found in suspected hemochromatosis type 4 patients. *Hum. Mol. Genet.* 2014; 23(17)**:** 4479-4490. doi: 10.1093/hmg/ddu160

S5. Wallace DF, Clark RM, Harley HA, Subramaniam VN. Autosomal dominant iron overload due to a novel mutation of ferroportin1 associated with parenchymal iron loading and cirrhosis. *J. Hepatol.* 2004; 40(4)**:** 710-713. doi: 10.1016/j.jhep.2003.12.008

S6. Pelucchi S, Mariani R, Salvioni A, Bonfadini S, Riva A, Bertola F *et al.* Novel mutations of the ferroportin gene (SLC40A1): analysis of 56 consecutive patients with unexplained iron overload. *Clin. Genet.* 2008; 73(2)**:** 171-178. doi: 10.1111/j.1399-0004.2007.00950.x

S7. Rivard SR, Lanzara C, Grimard D, Carella M, Simard H, Ficarella R *et al.* Autosomal dominant reticuloendothelial iron overload (HFE type 4) due to a new missense mutation in the FERROPORTIN 1 gene (SLC11A3) in a large French-Canadian family. *Haematologica* 2003; 88(7)**:** 824-826.

S8. Mayr R, Griffiths WJ, Hermann M, McFarlane I, Halsall DJ, Finkenstedt A *et al.* Identification of mutations in SLC40A1 that affect ferroportin function and phenotype of human ferroportin iron overload. *Gastroenterology* 2011; 140(7)**:** 2056-2063, 2063. doi: S0016-5085(11)00279-4 [pii];10.1053/j.gastro.2011.02.064 [doi]

S9. Yamakawa N, Oe K, Yukawa N, Murakami K, Nakashima R, Imura Y *et al.* A Novel Phenotype of a Hereditary Hemochromatosis Type 4 with Ferroportin-1 Mutation, Presenting with Juvenile Cataracts. *Intern. Med.* 2016; 55(18)**:** 2697-2701. doi: 10.2169/internalmedicine.55.6565

S10. Le Lan C, Mosser A, Ropert M, Detivaud L, Loustaud-Ratti V, Vital-Durand D *et al.* Sex and acquired cofactors determine phenotypes of ferroportin disease. *Gastroenterology* 2011; 140(4)**:** 1199-1207 e1191-1192. doi: 10.1053/j.gastro.2010.12.049

S11. Santos PC, Cancado RD, Pereira AC, Schettert IT, Soares RA, Pagliusi RA *et al.* Hereditary hemochromatosis: mutations in genes involved in iron homeostasis in Brazilian patients. *Blood Cells Mol. Dis.* 2011; 46(4)**:** 302-307. doi: 10.1016/j.bcmd.2011.02.008

S12. Zaahl MG, Merryweather-Clarke AT, Kotze MJ, van der Merwe S, Warnich L, Robson KJ. Analysis of genes implicated in iron regulation in individuals presenting with primary iron overload. *Hum. Genet.* 2004; 115(5)**:** 409-417. doi: 10.1007/s00439-004-1166-y

S13. Lee PL, Gaasterland T, Barton JC. Mild iron overload in an African American man with SLC40A1 D270V. *Acta Haematol.* 2012; 128(1)**:** 28-32. doi: 10.1159/000337034

S14. Wallace DF, Dixon JL, Ramm GA, Anderson GJ, Powell LW, Subramaniam VN. A novel mutation in ferroportin implicated in iron overload. *J.Hepatol.* 2007; 46(5)**:** 921-926.

REFERENCES

1. Pietrangelo A. The ferroportin disease. *Blood Cells Mol. Dis.* 2004; 32(1)**:** 131-138.

2. Schimanski LM, Drakesmith H, Merryweather-Clarke AT, Viprakasit V, Edwards JP, Sweetland E *et al.* In vitro functional analysis of human ferroportin (FPN) and hemochromatosis-associated FPN mutations. *Blood* 2005; 105(10)**:** 4096-4102. doi: 10.1182/blood-2004-11-4502

3. Rice AE, Mendez MJ, Hokanson CA, Rees DC, Bjorkman PJ. Investigation of the biophysical and cell biological properties of ferroportin, a multipass integral membrane protein iron exporter. *J Mol.Biol* 2009; 386(3)**:** 717-732. doi: S0022-2836(08)01596-9 [pii];10.1016/j.jmb.2008.12.063 [doi]

4. Drakesmith H, Schimanski LM, Ormerod E, Merryweather-Clarke AT, Viprakasit V, Edwards JP *et al.* Resistance to hepcidin is conferred by hemochromatosis-associated mutations of ferroportin. *Blood* 2005; 106(3)**:** 1092-1097.

5. Letocart E, Le GG, Majore S, Ka C, Radio FC, Gourlaouen I *et al.* A novel missense mutation in SLC40A1 results in resistance to hepcidin and confirms the existence of two ferroportin-associated iron overload diseases. *Br.J Haematol.* 2009; 147(3)**:** 379-385.

6. Callebaut I, Joubrel R, Pissard S, Kannengiesser C, Gérolami V, Ged C *et al.* Comprehensive functional annotation of 18 missense mutations found in suspected hemochromatosis type 4 patients. *Hum. Mol. Genet.* 2014; 23(17)**:** 4479-4490. doi: 10.1093/hmg/ddu160

7. Fernandes A, Preza GC, Phung Y, De Domenico I, Kaplan J, Ganz T *et al.* The molecular basis of hepcidin-resistant hereditary hemochromatosis. *Blood* 2009; 114(2)**:** 437-443. doi: blood-2008-03-146134 [pii];10.1182/blood-2008-03-146134 [doi]

8. Mayr R, Griffiths WJ, Hermann M, McFarlane I, Halsall DJ, Finkenstedt A *et al.* Identification of mutations in SLC40A1 that affect ferroportin function and phenotype of human ferroportin iron overload. *Gastroenterology* 2011; 140(7)**:** 2056-2063, 2063. doi: S0016-5085(11)00279-4 [pii];10.1053/j.gastro.2011.02.064 [doi]

9. Wallace DF, Harris JM, Subramaniam VN. Functional analysis and theoretical modeling of ferroportin reveals clustering of mutations according to phenotype. *Am. J. Physiol. Cell Physiol.* 2010; 298(1)**:** C75-C84.

10. Wallace DF, Dixon JL, Ramm GA, Anderson GJ, Powell LW, Subramaniam VN. A novel mutation in ferroportin implicated in iron overload. *J.Hepatol.* 2007; 46(5)**:** 921-926.

11. Detivaud L, Island ML, Jouanolle AM, Ropert M, Bardou-Jacquet E, Le Lan C *et al.* Ferroportin diseases: functional studies, a link between genetic and clinical phenotype. *Hum. Mutat.* 2013; 34(11)**:** 1529-1536. doi: 10.1002/humu.22396

12. Liu XB, Yang F, Haile DJ. Functional consequences of ferroportin 1 mutations. *Blood Cells Mol. Dis.* 2005; 35(1)**:** 33-46.

13. Le Gac G, Ka C, Joubrel R, Gourlaouen I, Lehn P, Mornon JP *et al.* Structure-function analysis of the human ferroportin iron exporter (SLC40A1): effect of hemochromatosis type 4 disease mutations and identification of critical residues. *Hum. Mutat.* 2013; 34(10)**:** 1371-1380. doi: 10.1002/humu.22369

14. Bonaccorsi di Patti MC, Polticelli F, Cece G, Cutone A, Felici F, Persichini T *et al.* A structural model of human ferroportin and of its iron binding site. *FEBS J* 2014; 281(12)**:** 2851-2860. doi: 10.1111/febs.12825

15. Taniguchi R, Kato HE, Font J, Deshpande CN, Wada M, Ito K *et al.* Outward- and inward-facing structures of a putative bacterial transition-metal transporter with homology to ferroportin. *Nat Commun* 2015; 6**:** 8545. doi: 10.1038/ncomms9545

16. Hilton KB, Lambert LA. Molecular evolution and characterization of hepcidin gene products in vertebrates. *Gene* 2008; 415(1-2)**:** 40-48.

17. Qiao B, Sugianto P, Fung E, Del-Castillo-Rueda A, Moran-Jimenez MJ, Ganz T *et al.* Hepcidin-induced endocytosis of ferroportin is dependent on ferroportin ubiquitination. *Cell Metab.* 2012; 15(6)**:** 918-924. doi: S1550-4131(12)00139-8 [pii];10.1016/j.cmet.2012.03.018 [doi]

18. Yang J, Yan R, Roy A, Xu D, Poisson J, Zhang Y. The I-TASSER Suite: protein structure and function prediction. *Nat Methods* 2015; 12(1)**:** 7-8. doi: 10.1038/nmeth.3213

19. Roy A, Kucukural A, Zhang Y. I-TASSER: a unified platform for automated protein structure and function prediction. *Nat. Protoc.* 2010; 5(4)**:** 725-738. doi: 10.1038/nprot.2010.5

20. Mitchell CJ, Shawki A, Ganz T, Nemeth E, Mackenzie B. Functional properties of human ferroportin, a cellular iron exporter reactive also with cobalt and zinc. *Am. J. Physiol. Cell Physiol.* 2014; 306(5)**:** C450-459. doi: 10.1152/ajpcell.00348.2013

21. Preza GC, Ruchala P, Pinon R, Ramos E, Qiao B, Peralta MA *et al.* Minihepcidins are rationally designed small peptides that mimic hepcidin activity in mice and may be useful for the treatment of iron overload. *J Clin.Invest* 2011; 121(12)**:** 4880-4888. doi: 57693 [pii];10.1172/JCI57693 [doi]

22. Nemeth E, Tuttle MS, Powelson J, Vaughn MB, Donovan A, Ward DM *et al.* Hepcidin regulates cellular iron efflux by binding to ferroportin and inducing its internalization. *Science* 2004; 306(5704)**:** 2090-2093.

CHAPTER 1B:

Therapeutic potential of minihepcidins to treat non-classical Ferroportin Disease

INTRODUCTION

Hepcidin is a 25 amino acid hormone peptide which regulates ferroportin (Fpn), the only known iron exporter (Figure 1B-1). Hepcidin binds to Fpn which triggers Fpn to undergo a conformational change that results in ubiquitination of Fpn on its intracellular loop, causing Fpn to be endocytosed and degraded in lysosomes (1). Some Fpn mutations cause a gain-of-function dominantly-acting Fpn phenotype, leading to an iron overload disease known as non-classical Ferroportin Disease. In these patients, Fpn is hepcidin resistant, meaning Fpn continues to export iron even in the presence of hepcidin. Gain-of-function Fpn mutants differ in severity. The most severe Fpn mutation is at position 326 on Fpn where the cysteine is mutated to a serine, an amino acid with the same shape and size but different chemistry. Remarkably, the cysteine at this position is critical for hepcidin binding to Fpn (2, 3). The patients with heterozygous C326S Fpn develop iron overload which causes liver cirrhosis and arthritis at a young age (3). Native hepcidin is not a promising treatment for these patients since it cannot bind the C326S Fpn mutant.

Minihepcidins, hepcidin analogs, consist only of 7-9 N-terminal amino acids of hepcidin (2) but share the activity of full-length hepcidin. PR65 and PR73 (Figure 1B-1) are closely related minihepcidins that have been engineered to have a greater affinity for Fpn than the N-terminal segment of native hepcidin, and they potently induce the endocytosis and degradation of Fpn. When injected into WT or hepcidin KO mice, PR-65 and PR-73 lower serum iron and in hepcidin KO mice, prevent iron overload (4, 5). They are in phase 1 clinical trials to treat patients with iron overload, such as β-thalassemia and hereditary hemochromatosis type I, but not patients with non-classical Ferroportin Disease (6). Since minihepcidins were engineered to bind more strongly to Fpn than native hepcidin, we explored the possibility that PR73 could degrade even C326S Fpn, a hepcidin non-binding mutant.

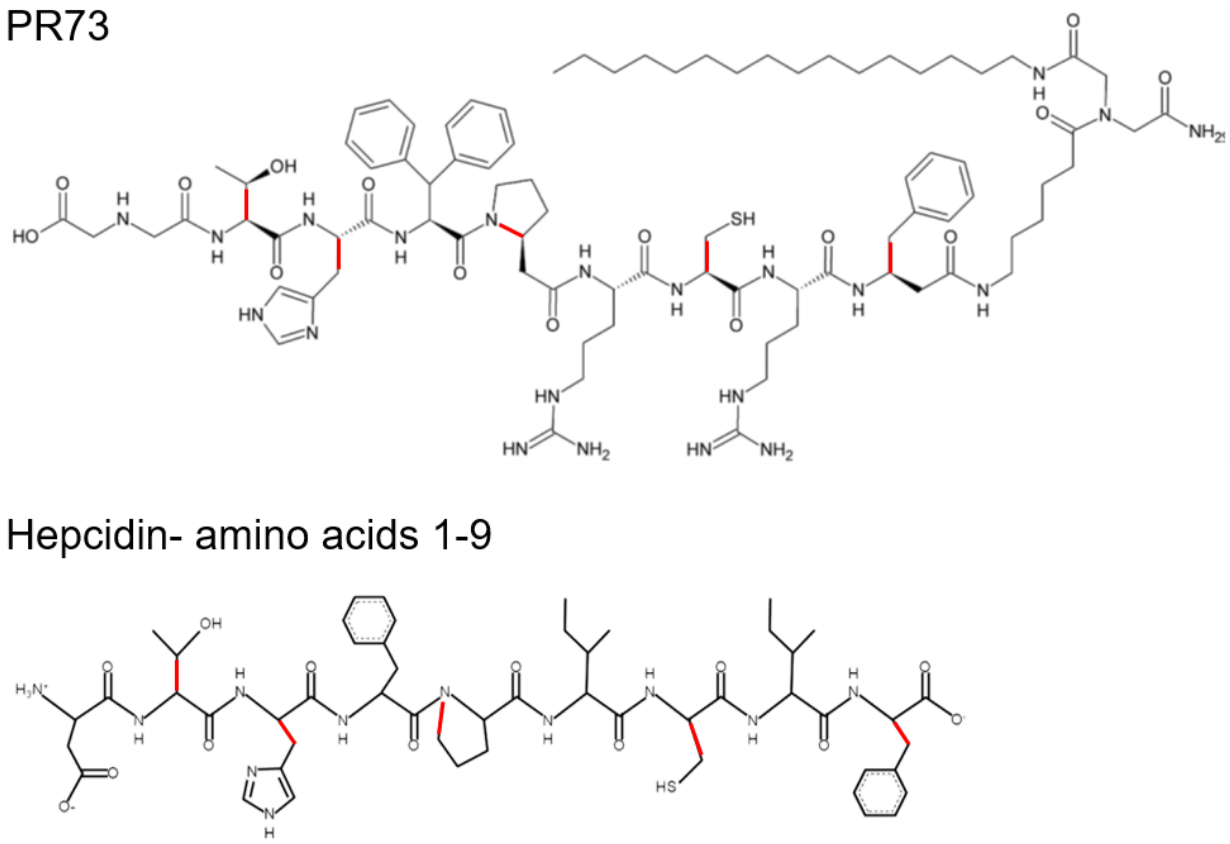

Figure 1B-1 (adapted from (5)): Amino acid primary structure of PR73 and the first 9 amino acids of hepcidin. Top: the amino acid structure of PR73 from N-to C-terminus. Its sequence is iminodiacetic acid, L-threonine, L-histidine, L-3,3-diphenylalanine, L-β-homoproline, L-arginine, L-cysteine, L-arginine, L-β-homophenylalanine, 6-aminohexanoic acid, iminodiacetic acid palmitylamide (Ida-T-H-Dpa-bhPro-R-C-R-bhPhe-Ahx-Ida(NHPal)-$CONH_2$). Bottom: the amino acid structure of hepcidin (amino acids 1-9 only) from the N- to C- terminus using PepDraw (7). Its sequence is D-T-H-F-P-I-C-I-F. The red lines indicate the amino acids that are the same in both PR73 and hepcidin or similar.

MATERIALS AND METHODS

Site-directed mutagenesis

Human Fpn-GFP in the pGFP-N3 vector (3) was transferred into the pcDNA5/FRT/TO vector (Invitrogen). Single mutations were introduced using QuikChange Lightning Site-Directed Mutagenesis Kit (Agilent Technologies) and confirmed by sequencing. Primers used for

mutagenesis of C326S were F: tcctgggcttgacagcatcaccacaggg and R: ccctgtggtgatgctgtcaaagcccagga

Stably transfected inducible cell lines

All mutant human Fpn-GFP pcDNA5/FRT/TO vector constructs were verified by sequencing. Using the Flp-In T-Rex system (Invitrogen K5600-01), HEK293T cells were transfected with the pcDNA5/FRT/TO vector encoding WT or mutant Fpn and pOG44 vector. Stable cell lines were established according to the manufacturer's protocol. Doxycycline (dox) was used to induce expression of Fpn-GFP.

Microscopy in mammalian cells

Cells were induced with 100 ng/ml dox overnight in 12-well poly-D-lysine coated plates (BD). Cells were washed with PBS, and treated with 25 μM ferric ammonium citrate (FAC) ±1 μg/ml hepcidin (Peptide International) for 24 hours. Cells were visualized with an epifluorescence microscope (Nikon Eclipse), and images were acquired with a 40x objective, SPOT camera, and SPOT Advanced Imaging Software (Diagnostic Instruments).

Ferritin assay

Cells were processed the same as in the microscopy section. After 24 hours of treatment, cells were washed with PBS and harvested in RIPA with protease inhibitors. Ferritin levels were determined by an ELISA assay (Ramco Laboratories) according to the manufacturer's instructions and were normalized to the total protein concentration in each sample (BCA assay, Pierce). To adjust for variations of the absolute ferritin values between multiple experiments, we expressed the measurements as the relative change in ferritin, according to the formula I/U, where I is the ferritin value for the induced cell line and U is the ferritin value for the uninduced cell line. For

hepcidin-treated cells, we expressed the ferritin measurements as (H-I)/U, where H refers to the ferritin value for the induced cells treated with hepcidin.

Fpn Western blot

Protein was measured by BCA assay, 6x SDS-loading buffer was added to lysates which were then separated by SDS-PAGE on 4-20% Mini-PROTEAN TGX Precast Gels (BioRad), and transferred to PVDF membranes using Trans-Blot Turbo (Bio-Rad). Blocking was performed overnight at 4°C in 5% milk in TBST (50mM Tris-HCl, pH7.5, 150mM NaCl, 0.1% Tween 20). Anti-GFP (Roche) was used to detect Fpn and anti-GAPDH-HRP (Cell Signaling) were used for normalization.

Statistical analysis

We set critical significance level, $\alpha = 0.05$, and expressed our data as mean, SD of 3 independent experiments. Statistical analyses employed the two-tailed t-test (normally distributed data) or Mann-Whitney rank sum test (data with non-normal distribution), the two-tailed one-sample t-test (normally distributed data) or the two-tailed one-sample signed rank test (data with non-normal distribution) compared with a reference of 1 (SigmaPlot version 12.5, Systat Software).

RESULTS AND DISCUSSION

We treated Fpn-GFP WT or C326S mutant cells with either hepcidin or PR73 for 24 h and measured ferritin as a proxy for cellular iron content (Figure 1B-2). The hepcidin data shown in Figure 1B-2 is the same as in Figure 1A-6 and is shown here for comparative purposes. WT Fpn achieved maximal iron retention after treatment of either ~0.4 μM hepcidin or PR73 (Figure 1B-2A, B). As expected, even in the presence of high concentrations of hepcidin, C326S Fpn -

expressing cells did not retain iron nor was C326S Fpn degraded (Figure 1B-2A,C,E). However, in the presence of high PR73 concentrations, C326S Fpn retained ferritin in a dose-dependent manner and C326S Fpn was degraded (Figure 1B-2B,D,F). We interpret these studies as indicating that the interaction with the C326 residue on Fpn is dispensable, because minihepcidins bind to Fpn so strongly through alternative interactions. These alternative interactions make the dose-response relationships for PR-73 against WT versus C326S more similar than they are for hepcidin (Figure 1B-2C, D). Thus, minihepcidins at high doses could become an effective treatment for even the most severe form of Ferroportin Disease: patients with the C326S mutation.

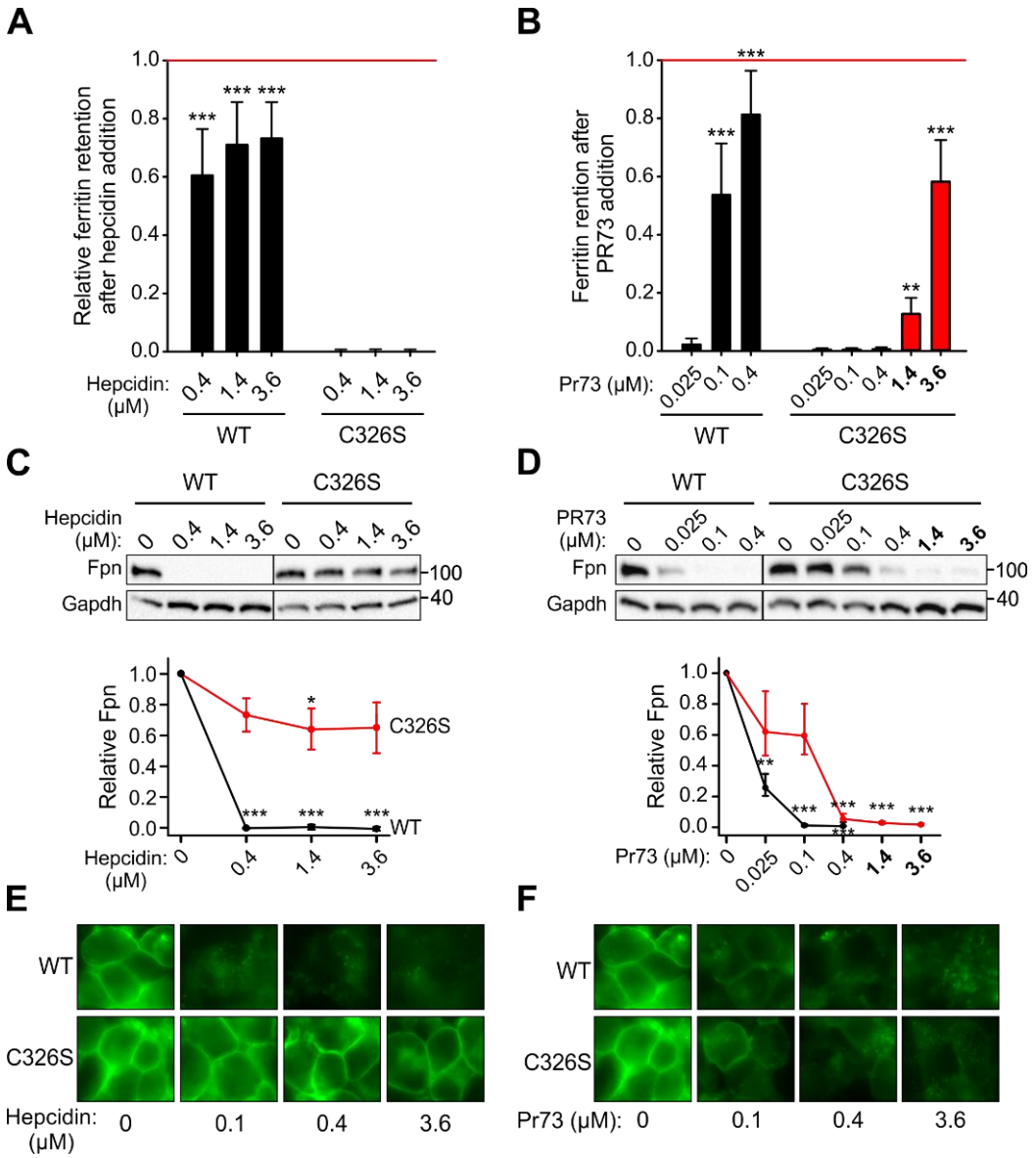

Figure 1B-2: High concentrations of PR73 degrade C326S in a dose dependent manner. Cells expressing inducible C326S Fpn were compared to those expressing WT Fpn. A,B) Ferritin retention after hepcidin or PR73 addition was determined as in Figure 1A-2A. Statistical analysis employed the two-tailed t-test using the respective untreated control for comparison (***P<0.001, **P<0.01, *P<0.05). C,D) Lysates from A and B were analyzed by Western blotting. Top: representative Western blot. Bottom: densitometry of triplicate Western blots. Fpn signal was first normalized to GAPDH, then expressed as the fraction of respective untreated control (no hepcidin treatment). Data shown are the mean ± SEM of 3 independent experiments. For A and B, statistical analysis employed the two-tailed one-sample t-test using 1 as the comparison (***P<0.001, **P<0.01, *P<0.05). D,F) Microscopy of samples in A and B after 24 hours. Data shown are the mean ± SD of 3 independent experiments.

FUTURE DIRECTIONS

In a potential extension of this project, we would also assess other gain-of-function Fpn mutants with PR73 in a dose dependent manner to determine if they also retain ferritin and degrade. This would help establish whether patients with these mutations could be treated with minihepcidin. In Chapter 1A, we classified non-classical Ferroportin Disease mutations into two groups: hepcidin non-binders and impaired ubiquitination mutants. Thus, we would test the most severe hepcidin non-binders: N144D, Y501C, and D504N and the most severe ubiquitination impaired mutants: Y64N and H507R. This experiment will determine if PR73 is a general treatment for any non-classical Ferroportin Disease mutation or if it is specific to only C326S Fpn mutants.

We also could assess how PR73 degrades C326S Fpn while native hepcidin does not and whether is it possible to modify native hepcidin to degrade C326S Fpn. PR73's truncated size cannot explain its C326S Fpn degrading ability, because treating Fpn cells with a truncated form of native hepcidin containing only the first 9 amino acids is 10x less active than full length hepcidin (8). To test if the hydrocarbon chain is necessary, we could treat C326S Fpn with PR73 containing or lacking the long hydrocarbon tail. We could also synthesize hepcidin-25, but instead of using all native amino acids for the first 9, we would use the same amino acids that comprise PR73 which we will call PR73-FL. Then we could treat WT and C326 Fpn with either PR73-FL, PR73, or native hepcidin, visualize them via microcopy, and measure ferritin retention after 24 h of treatment. PR73-FL should have similar activity to WT Fpn as PR73 and native hepcidin. If PR73-FL degrades C326S Fpn similarly to PR73 at high concentrations, this further suggests the amino acid composition of the first 9 amino acids of hepcidin is important in determining whether or not

a minihepcidin will interact with C326S Fpn. If PR73-FL does not degrade C326S Fpn, it could be that a combination of factors contribute to the potency of PR73.

Additionally, *in vivo* evidence is needed before developing PR73 as a treatment for non-classical Ferroportin Disease patients. C326S Fpn homozygous mice are iron overloaded and die between 7-14 months of age (9). We could treat both heterozygous and homozygous C326S Fpn mice with PR73 daily for several weeks to determine if PR73 prevents iron overload in these mice compared to solvent controls.

REFERENCES

1. Nemeth E, Tuttle MS, Powelson J, Vaughn MB, Donovan A, Ward DM *et al.* Hepcidin regulates cellular iron efflux by binding to ferroportin and inducing its internalization. *Science* 2004; 306(5704)**:** 2090-2093.

2. Preza GC, Ruchala P, Pinon R, Ramos E, Qiao B, Peralta MA *et al.* Minihepcidins are rationally designed small peptides that mimic hepcidin activity in mice and may be useful for the treatment of iron overload. *J Clin.Invest* 2011; 121(12)**:** 4880-4888. doi: 57693 [pii];10.1172/JCI57693 [doi]

3. Fernandes A, Preza GC, Phung Y, De Domenico I, Kaplan J, Ganz T *et al.* The molecular basis of hepcidin-resistant hereditary hemochromatosis. *Blood* 2009; 114(2)**:** 437-443. doi: blood-2008-03-146134 [pii];10.1182/blood-2008-03-146134 [doi]

4. Ramos E, Ruchala P, Goodnough JB, Kautz L, Preza GC, Nemeth E *et al.* Minihepcidins prevent iron overload in a hepcidin-deficient mouse model of severe hemochromatosis. *Blood* 2012; 120(18)**:** 3829-3836. doi: blood-2012-07-440743 [pii];10.1182/blood-2012-07-440743 [doi]

5. Arezes J, Jung G, Gabayan V, Valore E, Ruchala P, Gulig PA *et al.* Hepcidin-induced hypoferremia is a critical host defense mechanism against the siderophilic bacterium Vibrio vulnificus. *Cell Host Microbe* 2015; 17(1)**:** 47-57. doi: 10.1016/j.chom.2014.12.001

6. Sebastiani G, Wilkinson N, Pantopoulos K. Pharmacological Targeting of the Hepcidin/Ferroportin Axis. *Front. Pharmacol.* 2016; 7**:** 160. doi: 10.3389/fphar.2016.00160

7. Freeman T. PepDraw. http://www.tulane.edu/~biochem/WW/PepDraw. In: Tulane University, 2011.

8. Preza GC, Ruchala P, Pinon R, Qiao B, Peralta M, Sharma S *et al.* Analysis of the hepcidin-ferroportin interface yields minihepcidins, small peptides for the treatment of iron overload. In, 2011.

9. Altamura S, Kessler R, Groene HJ, Gretz N, Hentze MW, Galy B *et al.* Resistance of Ferroportin to Hepcidin Binding causes Exocrine Pancreatic Failure and Fatal Iron Overload. *Cell Metab.* 2014; 20(2)**:** 359-367.

CHAPTER 2:

Erythroferrone and matriptase-2 independently regulate hepcidin transcription

A shorter version of this chapter was published as a correspondence letter

(refer to pages 104-106)

INTRODUCTION

Iron is an essential functional component of heme and hemoglobin and is required for red blood cell production (erythropoiesis). During increased erythropoiesis which takes place after hemorrhage or erythropoietin (EPO) administration, intestinal iron absorption and the release of iron from stores are augmented, facilitating the production of new erythrocytes. The increase of iron supply is at least in part caused by suppression of the iron-regulatory hormone hepcidin. Our laboratory has shown that under the influence of erythropoietin, the hormone erythroferrone (ERFE) is secreted by erythroblasts (erythroid precursors) in the bone marrow and spleen, and suppresses hepcidin synthesis to facilitate the recovery from anemia (1, 2). Wang et al. discovered that both EPO and ERFE treatment suppress hepcidin at least in part by inhibiting the BMP/SMAD signaling pathway in hepatocytes (3). However, the mechanism by which ERFE suppresses the BMP/SMAD pathway is unknown.

Like ERFE, matriptase-2 (MT-2) is also a negative regulator of hepcidin. It is a GPI-linked membrane serine protease of hepatocytes, and it cleaves hemojuvelin (HJV), a BMP co-receptor, and therefore, blunts baseline BMP/SMAD signaling and decreases hepcidin transcription. Mutations in transmembrane serine protease 6 (TMPRSS6), the gene encoding matriptase-2 (MT-2), cause iron-refractory iron deficiency anemia (IRIDA) (4). In contrast with forms of anemia in which hepcidin is suppressed, IRIDA patients have pathological activation of the BMP/Smad signaling and increased hepcidin production despite a severe anemia and elevated EPO levels because MT-2 is not suppressing baseline BMP signaling by cleaving HJV. Previous studies have shown that hepcidin production was not affected by EPO in *Tmprss6* mutant mice (5) or IRIDA

patients (6). Lehmberg et al. reported that IRIDA patients administered EPO did not lower hepcidin to stimulate erythropoiesis, because their baseline levels of EPO were already high, suggesting a missing link between regulation of hepcidin by EPO and baseline regulation of hepcidin by MT-2. More recently, Nai and colleagues suggested that matriptase-2 may act downstream of EPO to dampen the signaling through the BMP-Smad regulatory pathway and allow ERFE to repress hepcidin production (7). We therefore examined the crosstalk between ERFE and matriptase-2 in mice.

MATERIALS AND METHODS

Mice

Experiments were conducted in accordance with the guidelines by the National Research Council and were approved by the Animal Research Committee of the University of California, Los Angeles. *Hbb*$^{th3/+}$ mice were obtained from The Jackson Laboratory (strain name B6;129P-*Hbb-b1*^{tm1Unc} *Hbb-b2*^{tm1Unc}/J) and bred onto a C57BL/6 background at UCLA. *Erfe*$^{+/-}$ mice on a mixed Sv129/C57BL/6 background (*Fam132b*^{tm1Lex}) were generated by Lexicon Pharmaceuticals (8) and bred onto a C57BL/6 background at UCLA. *Tmprss6-/-* mice (9) on a C57BL/6 background were kindly provided by Jodie Babitt (Massachusetts General Hospital). *Tmprss6*$^{-/-}$ mice were mated with *Erfe*$^{-/-}$ to generate *Erfe*$^{+/-}$, *Tmprss6*$^{+/-}$ mice and subsequent breeding of these mice generated littermates *Erfe*$^{-/-}$ *Tmprss6*$^{-/-}$ (E-/-,T-/-), *Erfe*$^{+/+}$ *Tmprss6*$^{-/-}$ (E+/+,T-/-) or *Erfe*$^{+/-}$ *Tmprss6*$^{-/-}$ (E+/-,T-/-) mice that were maintained at UCLA on a standard chow (200 ppm iron; Labdiet, MO) and studied at the age of 6 weeks. Wild type (WT) mice (males and females) were purchased separately from The Jackson Laboratory to simplify the breeding. At the age of 6 weeks,

WT mice were phlebotomized by retro-orbital puncture (500 μL) and analyzed 24 h after phlebotomy.

Measurement of iron and hematologic parameters

Serum iron, spleen, and liver non-heme iron concentrations were determined as previously described (10), using acid treatment followed by a colorimetric assay for iron quantitation (Sekisui Diagnostics, Charlottetown, Canada). Complete blood counts were obtained with a HemaVet blood analyzer (Drew Scientific). Spleen index was calculated as spleen weight (mg) / body weight (g).

ERFE enzyme-linked immunosorbent assay

Mouse ERFE monoclonal antibodies and recombinant mouse ERFE standard were produced by Silarus Therapeutics. High binding 96-well EIA plates (Corning) were coated overnight at 4°C with 100 μL/well of 1.0 μg/mL capture antibody in 50 mM sodium carbonate buffer (pH 9.6). Plates were washed (TBS, 0.5% Tween-20) and blocked for 45 minutes with 200 μL/well SuperBlock T20 blocking buffer (Pierce). Samples and standards diluted in SuperBlock T20 were incubated for 2 hours at room temperature. Plates were washed and incubated for one hour with 100 μL/well of 1.0 μg/mL biotinylated detection antibody, washed and then incubated for 45 minutes with Streptavidin-HRP conjugate (Invitrogen). *Erfe*$^{-/-}$ serum was used as a negative control. The limit of quantitation was determined at 500 pg/ml.

Mouse hepcidin-1 monoclonal antibodies, Ab2B10 (capture), AB2H4-HRP (detection) and synthetic mouse hepcidin-25, were a generous gift from Amgen (Thousand Oaks, CA). High binding 96-well EIA plates (Corning) were coated overnight at room temperature with 50 μL/well of 3.6 μg/mL Ab2B10 in 0.2 M carbonate-bicarbonate buffer pH 9.4 (Pierce). Plates were washed twice with wash buffer (PBS, 0.5% Tween-20) and blocked for 45 minutes with 200 μL/well

blocking buffer (PBS, 1% BSA, 1% normal goat serum, 0.5% Tween-20). Samples and standards were added and incubated 1 hour at room temperature. After four washes, plates were incubated an hour with 50 µL/well of 130 ng/mL Ab2H4-HRP.

For both assays, plates were developed with 100 µL/well Ultra-TMB substrate (Thermo Scientific) for 30 minutes in the dark at room temperature. The reaction was stopped by adding 50 µL 2M sulfuric acid and the absorbance was measured at 450 nm.

Recombinant protein production

HEK293T cells were transduced with a lentivirus encoding *Erfe* cDNA or a control GFP lentivirus cultured in William's E medium supplemented with 5% FBS. ERFE-containing and control supernatants were harvested after 5 days. To generate serum-free supernatants, Freestyle 293-F cells in protein-free Freestyle 293 expression medium (ThermoFisher Scientific) were transfected with a plasmid encoding *Erfe* cDNA using 293-fectin transfection reagent (ThermoFisher Scientific). ERFE-containing and control serum free supernatants were harvested after 72 hours to match the concentration of recombinant ERFE obtained in serum containing conditions (1 µg/ml). ERFE-expressing cells and control cells were cultured concomitantly and in the same conditions. *TMPRSS6* is not expressed in HEK293 or freestyle 293F cell lines (Tmprss6 mRNA expression is below the level of detection by qPCR).

Mouse primary hepatocyte isolation and treatment

Matriptase-2 is mostly expressed on hepatocytes. Hepatocytes were isolated from wild-type C57BL/6 and *Tmprss6*$^{-/-}$ mice by a two-step portal vein collagenase perfusion method as previously described[3] and incubated overnight (16 hours) in fresh Williams E Medium (Sigma Aldrich) supplemented with 5% FBS and 200 µM L-glutamine (Invitrogen) and 50% (v/v) supernatants from control HEK293T cells or HEK293T cells overexpressing ERFE (also

maintained in Williams E Medium/5%FBS/200 µM L-glutamine). For serum-free experiments, hepatocytes were incubated overnight (16 hours) in protein-free Freestyle 293 expression medium (ThermoFisher Scientific) and 50% (v/v) supernatants from control freestyle 293-F cells or 293F cells transfected with a plasmid encoding *Erfe* cDNA (also maintained in Freestyle 293 expression medium). Measurement of ERFE concentration showed that hepatocytes were treated with 500 ng of recombinant ERFE. Three independent experiments with 16 hour treatments in triplicate were performed.

Quantitation of mRNA levels

Total RNA from mouse tissues was extracted using Trizol (Invitrogen). cDNA was synthesized using iScript (Biorad). Quantitative PCR reactions were prepared with Sso advanced Sybr Green supermix (Biorad) and primers, and run in duplicate on a CFXconnect Instrument (Biorad). The following primers were used: *Hprt* F: CTG-GTT-AAG-CAG-TAC-AGC-CCC-AA R: CAG-GAG-GTC-CTT-TTC-ACC-AGC, *Hamp* F: TTG-CGA-TAC-CAA-TGC-AGA-AGA R: GAT-GTG-GCT-CTA-GGC-TAT-GTT, *Erfe* F: ATG-GGG-CTG-GAG-AAC-AGC R: TGG-CAT-TGT-CCA-AGA-AGA-CA, *Id1* F: ACC-CTG-AAC-GGC-GAG-ATC-A R: TCG-TCG-GCT-GGA-ACA-CAT-G, *Smad7* F: TTG-CCT-CGG-ACA-GCT-CAA-TTC R: CGC-ACT-TTC-TGT-ACC-AGC-TGA-C, and *Atoh8* F: CAC-CAT-CAG-CGC-AGC-CTT-C R: CCA-TAG-GAG-TAG-CAC-GGC-ACC. *Hamp, Erfe, Id1, Atoh8,* and *Smad7* mRNA transcript abundance was normalized to the reference gene *Hprt.* Results are expressed as -ΔCt ± standard error of the mean (i.e., the cycle threshold differences between reference and target genes within each group of mice).

Statistical analysis

The statistical significance of differences between groups was evaluated using Sigmaplot 12.5 package (Systat Software, San Jose, CA). The Student *t* test was used to compare 2 groups of normally distributed data. The Mann Whitney rank-sum test was used to compare data that were not normally distributed. A P value < 0.05 in a two-tailed test was considered as statistically significant.

RESULTS AND DISCUSSION

In agreement with Nai et al., we observed that *Erfe* mRNA expression was highly increased in the bone marrow and spleen of *Tmprss6*$^{-/-}$ mice (Figure 1). While WT mice have undetectable plasma ERFE, plasma ERFE concentration was elevated in *Tmprss6*$^{-/-}$ to levels comparable to those of WT animals 24 hours after phlebotomy (~3 ng/ml) but was lower than ERFE levels in thalassemic mice (~10 ng/ml) (Figure 2). To assess the contribution of ERFE to the phenotype of *Tmprss6*$^{-/-}$ mice, we generated *Tmprss6*$^{-/-}$ mice with disrupted *Erfe* (*Erfe*$^{-/-}$ *Tmprss6*$^{-/-}$; *Erfe*$^{+/-}$ *Tmprss6*$^{-/-}$ and *Erfe*$^{+/+}$ *Tmprss6*$^{-/-}$). Ablation of *Erfe* in *Tmprss6*$^{-/-}$ mice did not result in any change in hematological parameters compared to *Tmprss6*$^{-/-}$ animals at 6 weeks of age (Table 1). Mice deficient for *Tmprss6* had higher RBC and lower hemoglobin, hematocrit, and MCV compared to WT, regardless of the *Erfe* genotype. Liver hepcidin mRNA (Figure 3A) and serum hepcidin concentration (Figure 3B) were higher in *Tmprss6*$^{-/-}$ mice compared to WT mice and no difference was observed after manipulation of *Erfe*. One exception is that hepcidin mRNA in female mice is not significantly increased in *Tmprss6*-/- mice compared to WT mice. However, serum hepcidin levels indicate that hepcidin is highly increased in *Tmprss6*-/- females. Serum hepcidin levels are a better indicator of hepcidin production than mRNA since serum levels reflect the hepcidin output

of the whole organ rather than a fragment of it and take into account potential differences in hepcidin catabolism. Consistent with chronically increased hepcidin production, liver iron content (Figure 3C) was decreased in *Tmprss6*$^{-/-}$ mice compared to WT mice, but this was not influenced by the ablation of *Erfe*. No statistically significant difference in spleen iron content was observed between the genotypes (Figure 3D). *Erfe*-deficient *Tmprss6*$^{-/-}$ mice and *Tmprss6*$^{-/-}$ mice showed similarly increased spleen weight compared to WT mice (Figure 4A). However, we observed a decrease in body weight in double mutant animals at 6 weeks compared to *Tmprss6*$^{-/-}$ mice (Figure 4B), suggesting that ERFE may be important for normal development of *Tmprss6*$^{-/-}$ mice. As a consequence of smaller body size, spleen index was higher in *Erfe*$^{-/-}$, *Tmprss6*$^{-/-}$ mice compared to *Tmprss6*$^{-/-}$ mice (Figure 4C). Together, these results indicate that the disruption of *Erfe* has at most a very minor effect on the phenotype of *Tmprss6* deficiency in mice.

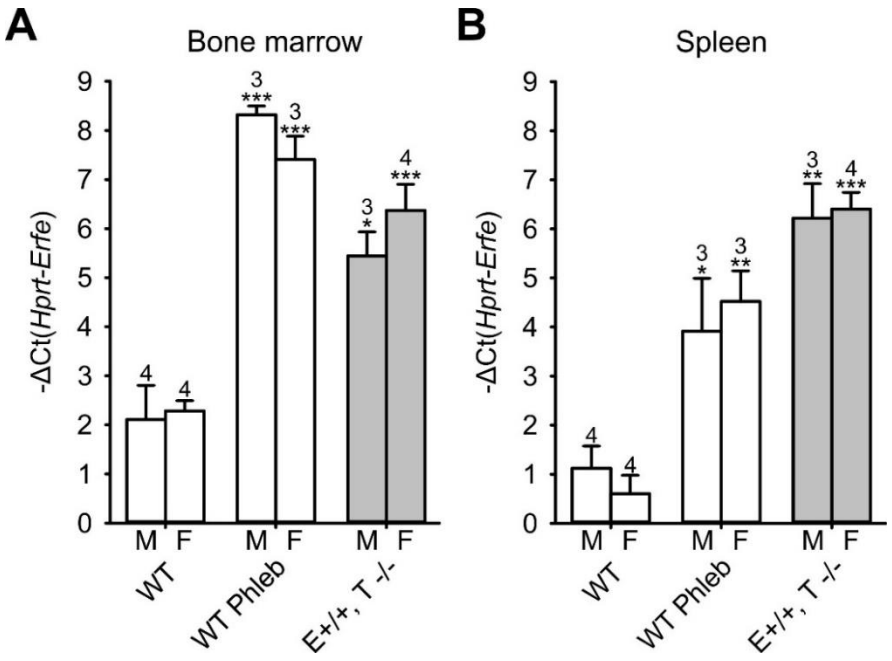

Figure 1: *Erfe* mRNA expression is increased in the bone marrow and spleen of *Tmprss6*$^{-/-}$ mice. *Erfe* mRNA expression in the bone marrow **(A)** and spleen **(B)** was highly increased in phlebotomized WT mice (24 h) and *Tmprss6*$^{-/-}$ mice compared to WT mice. The number of mice

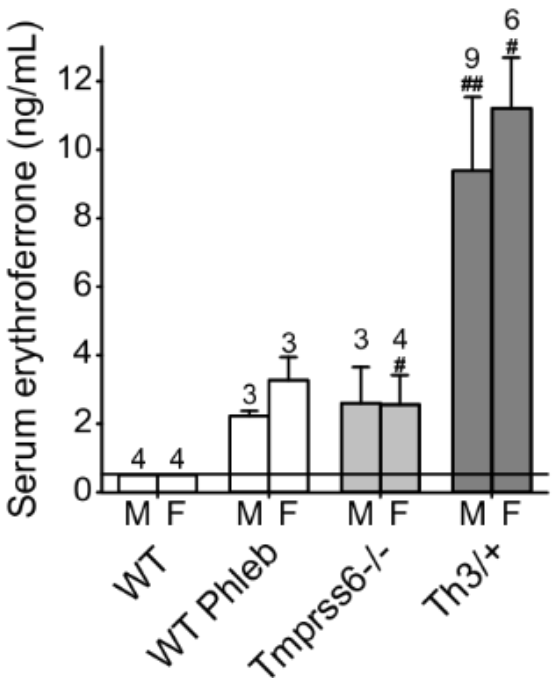

analyzed at 6 weeks of age is indicated for each group. Data shown are means ± SEM and were compared for each group to control WT mice by two-tailed Student t-test. ***P < .001, **P < .01, *P <.05.

Figure 2: Levels of ERFE in mice expressing high EPO. Serum ERFE concentration was elevated in *Tmprss6*$^{-/-}$ mice similarly to WT mice 24 hours after phlebotomy, but was lower than in thalassemic mice (Th3/+). The number of mice studied is shown for each group. Data shown are means ± SEM. Statistical analysis was performed compared to WT controls of the same gender, using the Mann-Whitney test ($^{\#\#}$P<.01, $^{\#}$P<.05). M=male, F=female.

Table 1: Hematological parameters are unchanged by ERFE ablation in *Tmprss6*$^{-/-}$ mice

	N	RBC (M/µL)	HB (g/dL)	HCT (%)	MCV (fL)
Males					
WT	4	9.4 ± 0.2	16.3 ± 0.5	45.7 ± 1.2	48.6 ± 0.2
WT phlebotomized	3	8.0** ± 0.1	13.9*± 0.4	38.7**± 0.4	48.3 ± 0.7
Erfe +/+ Tmprss6 -/-	5	10.3 ± 0.4	8.4*** ± 0.3	34.9***± 1.2	34.0** ± 0.4
Erfe +/- Tmprss6 -/-	12	10.7* ± 0.3	8.9*** ± 0.2	35.7*** ± 0.7	33.5** ± 0.4
Erfe -/- Tmprss6 -/-	5	10.8* ± 0.5	9.0*** ± 0.4	36.6* ± 1.3	34.0*** ± 0.2
Females					
WT	4	9.2 ± 0.1	16.3 ± 0.4	44.3 ± 0.6	48.1 ± 0.2
WT phlebotomized	3	6.8*** ± 0.3	11.8*** ± 0.4	33.3*** ± 1.1	48.6 ± 0.2
Erfe +/+ Tmprss6 -/-	5	11.4** ± 0.4	9.4*** ± 0.3	38.6** ± 1.1	33.9*** ± 0.2
Erfe +/- Tmprss6 -/-	4	10.2* ± 0.4	8.7*** ± 0.5	34.8*** ± 1.1	34.0*** ± 0.4
Erfe -/- Tmprss6 -/-	6	11.3*** ± 0.3	9.7** ± 0.2	37.6*** ± 0.9	33.3*** ± 0.1

RBC was increased while hemoglobin, hematocrit and MCV were decreased in *Tmprss6*$^{-/-}$ mice compared to WT mice at 6 weeks of age. Ablation of *Erfe* in *Tmprss6*$^{-/-}$ mice did not result in any change in hematological parameters compared to *Tmprss6*$^{-/-}$ animals at 6 weeks of age (two-tailed Student t-test comparison of *Erfe*$^{-/-}$ *Tmprss6*$^{-/-}$ and *Erfe*$^{+/-}$ *Tmprss6*$^{-/-}$ to *Erfe*$^{+/+}$ *Tmprss6*$^{-/-}$). None

of the CBC parameters were statistically different by gender or by genotype when comparing *Erfe*$^{-/-}$ *Tmprss6*$^{-/-}$ and *Erfe*$^{+/-}$ *Tmprss6*$^{-/-}$ to *Erfe*$^{+/+}$ *Tmprss6*$^{-/-}$ by two-way ANOVA. Data shown are means ± SEM and were compared for each group to control WT mice by two-tailed Student t-test (n=6 to 16 per group, gender combined). ***P < .001, **P < .01, *P < .05.

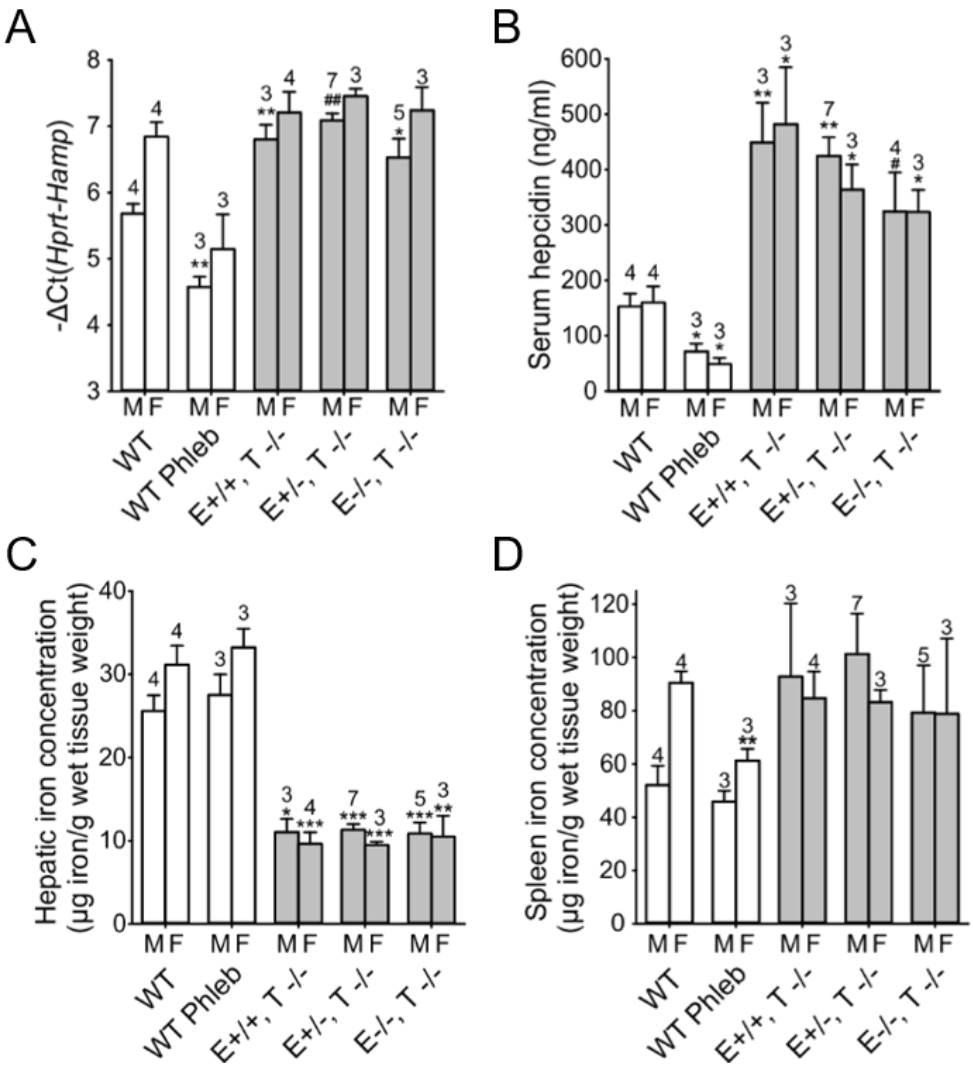

Figure 3: No major iron-related phenotypic differences between ablation of ERFE in Tmprss6-/- compared to *Tmprss6-/-* mice. (A,B) Neither liver hepcidin mRNA expression nor serum hepcidin were significantly different in *Erfe*$^{-/-}$ *Tmprss6*$^{-/-}$ (E-/-,T-/-) mice compared to *Erfe*$^{+/+}$ *Tmprss6*$^{-/-}$ (E+/+,T-/-) or *Erfe*$^{+/-}$ *Tmprss6*$^{-/-}$ (E+/-,T-/-) mice. **(C)** Liver iron content was similarly lower in *Tmprss6*$^{-/-}$ mice compared to WT mice regardless of the *Erfe* genotype whereas spleen iron content **(D)** was comparable to those of WT mice. **(A-D)** The number of mice studied is shown for each group. Data shown are means ± SEM. Statistical analysis was performed compared to WT controls of the same gender, using the two-tailed Student t-test (***P<.001, **P<.01, *P<.05) or Mann-Whitney test ($^{\#\#}$P<.01, $^{\#}$P<.05). M=male, F=female.

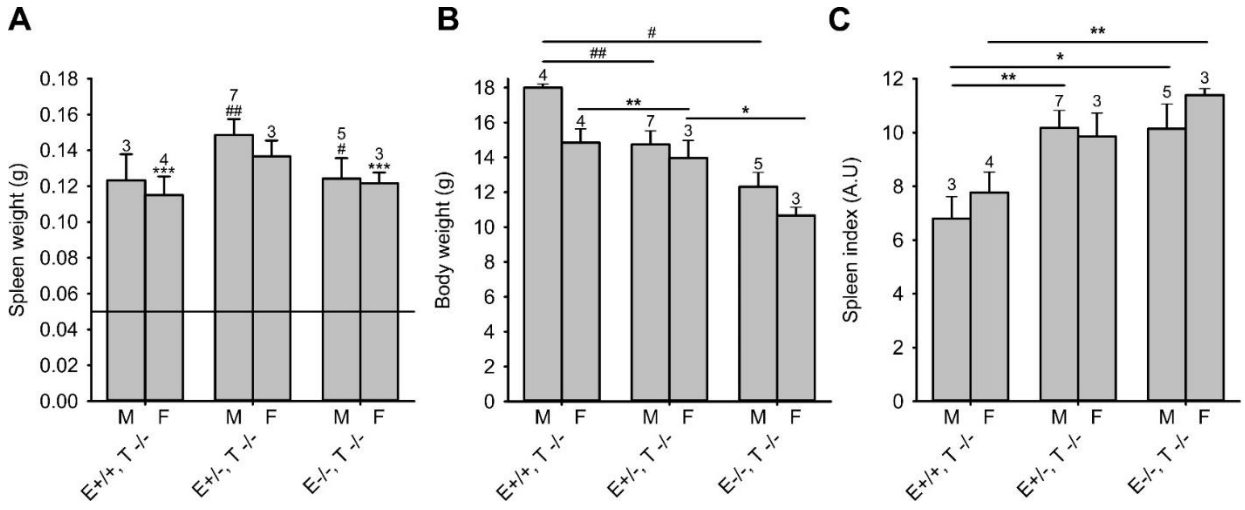

Figure 4: Spleen weight, body weight, and spleen index in *Tmprss6*$^{-/-}$ mice. *Tmprss6*$^{-/-}$ mice showed similarly increased spleen weight **(A)** compared to WT mice, regardless of their *Erfe* genotype. However, *Erfe*-deficient *Tmprss6*$^{-/-}$ mice were significant smaller than *Tmprss6*$^{-/-}$ mice **(B)** and presented higher spleen index **(C)** indicating that ablation of *Erfe* in *Tmprss6*$^{-/-}$ mice results in a more severe splenomegaly. **(A)** Data shown are means ± SEM and were compared for each group to control WT mice (black reference line) by two-tailed Student t-test. **(B, C)** Data shown are means ± SEM and were compared for each group to *Erfe*$^{+/+}$, *Tmprss6*$^{-/-}$. Statistical analysis was performed compared to WT controls of the same gender, using the two-tailed Student t-test (***P<.001, **P<.01, *P<.05) or Mann-Whitney test ($^{\#\#}$P<.01, $^{\#}$P<.05).

To determine whether ERFE requires TMPRSS6 to regulate hepcidin production, we treated freshly isolated hepatocytes from WT or *Tmprss6*$^{-/-}$ mice with conditioned medium from cells expressing recombinant ERFE or from control cells. Consistent with stimulated BMP/Smad signaling, baseline hepcidin expression was higher in *Tmprss6*$^{-/-}$ hepatocytes compared to WT hepatocytes in serum-containing and serum-free conditions (Figure 5). Hepcidin mRNA expression was reduced more than 12-fold in both WT and *Tmprss6*$^{-/-}$ hepatocytes after treatment with ERFE in serum-containing media. Similarly, treatment of hepatocytes with ERFE in serum-free media (i.e. in the absence of any soluble MT-2) resulted in a 2.5 and 5-fold decrease in hepcidin expression in WT and *Tmprss6*$^{-/-}$ hepatocytes, respectively. These results demonstrate *in vitro* that ERFE represses hepcidin independently of TMPRSS6. Interestingly, *Id1* mRNA expression (Figure 6A) was also reduced in primary mouse hepatocytes from WT and *Tmprss6*$^{-/-}$

mice after treatment with ERFE in serum-containing and serum-free conditions. Similarly, *Atoh8* and *Smad7* mRNA expression (Figure 6 B, C) was decreased in ERFE-treated WT and *Tmprss6*$^{-/-}$ hepatocytes in serum-containing conditions. In serum-free conditions, the decrease in *Atoh8* and *Smad7* mRNA expression was observed only in ERFE-treated *Tmprss6*$^{-/-}$ hepatocytes but not in WT hepatocytes. This suggests a potential crosstalk between BMP and ERFE signaling that is independent of TMPRSS6.

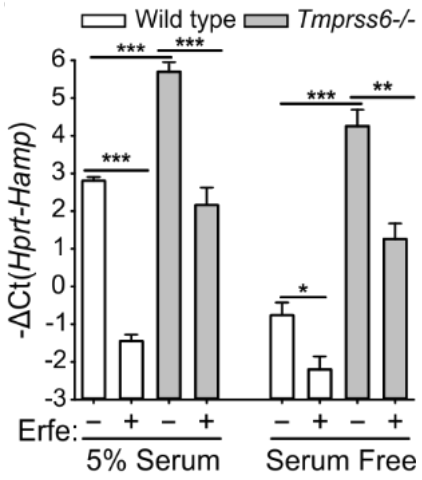

Figure 5: ERFE and MT-2 regulate hepcidin independently *in vitro*. Hepcidin mRNA expression was strongly reduced in primary hepatocytes from WT and *Tmprss6*$^{-/-}$ mice 16 hours after treatment with conditioned medium containing ERFE (final concentration 500 ng/ml of recombinant ERFE), both in 5% serum or serum-free conditions. Data shown are means ± SEM of three independent experiments. Statistical analysis was performed using two-tailed Student t-test (***P<.001, **P<.01, *P<.05).

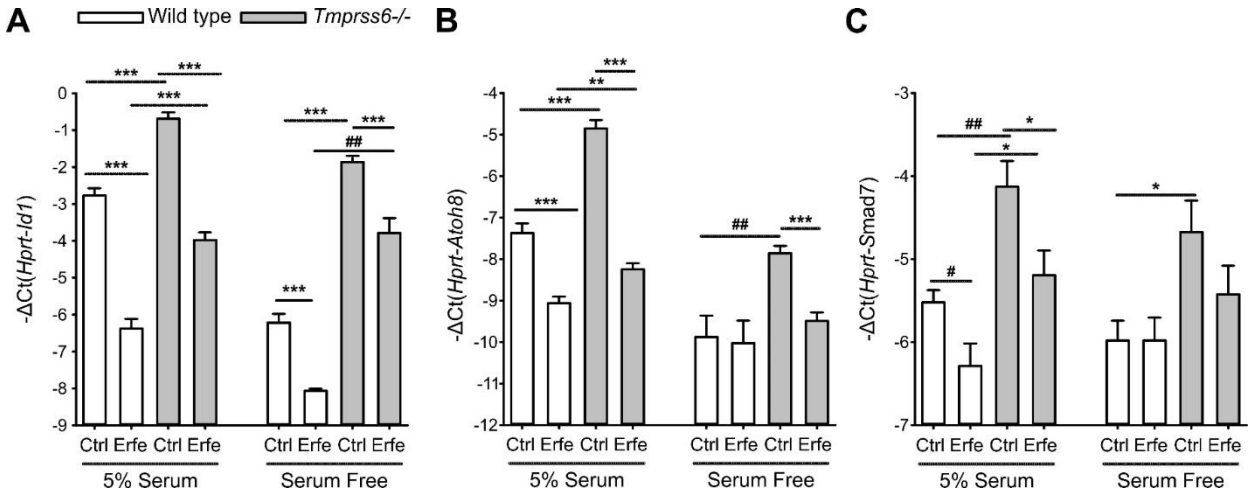

Figure 6: Markers of BMP signaling in primary mouse hepatocytes treated with ERFE. (A) *Id1* mRNA expression was reduced in primary mouse hepatocytes from WT and *Tmprss6*$^{-/-}$ mice 16 hours after treatment with ERFE in serum-containing and serum-free conditions. *Atoh8* **(B)** and

Smad7 **(C)** mRNA expression was decreased in ERFE-treated WT and *Tmprss6*$^{-/-}$ hepatocytes in serum-containing conditions. However, in serum-free conditions, the decrease in *Atoh8* and *Smad7* mRNA expression was observed only in ERFE-treated *Tmprss6*$^{-/-}$ hepatocytes, but not in WT hepatocytes. Data shown are means ± SEM of three independent experiments. Statistical analysis was performed compared to WT controls of the same gender, using the two-tailed Student t-test (***P<.001, **P<.01, *P<.05) or Mann-Whitney test ($^{\#\#}$P<.01, $^{\#}$P<.05).

CONCLUSION

The reason for the impairment of erythropoietic suppression of hepcidin in patients and mice with IRIDA may lie in the intense stimulation of hepcidin by the BMP pathway *in vivo*, opposing the effect of ERFE. In accordance with the findings by Nai and colleagues, we previously demonstrated that hepcidin suppression after phlebotomy is blunted in iron-overloaded WT mice and *Tfr2*$^{-/-}$ mice where the BMP pathway is strongly stimulated by iron (2). These observations indicate that physiologic erythroid regulators (including ERFE) act additively to BMP-signaling and have a smaller relative effect on hepcidin production when the BMP/Smad signaling is highly activated.

The relatively weak effect of erythroid suppressors of hepcidin in IRIDA must be reconciled with the dominant effect of erythroid suppressors of hepcidin despite the iron-overload stimulated BMP signaling in patients with β-thalassemia and other disorders with ineffective erythropoiesis. Here, three kinds of differences may be relevant. First, the concentrations of ERFE (and perhaps other erythroid suppressors) may be higher in conditions with ineffective erythropoiesis than in IRIDA, likely because of the greater number of ERFE-secreting erythroblasts in ineffective erythropoiesis. Secondly, in anemias other than IRIDA, erythropoietin stimulation may increase the production of matriptase 2 through a posttranslational mechanism, potentiating the suppressive effect of erythroferrone on hepcidin. Thirdly, there are important species differences in the observed effect of erythroid suppressors of hepcidin in the mouse models

of ineffective erythropoiesis vs. human patients. Young β-thalassemic mice exhibit suppressed hepcidin, but progressively increase hepcidin with age to levels comparable to those of adult WT mice as they become iron overloaded, despite elevated ERFE production (11). In contrast, adult human patients with β-thalassemia continue to have decreased to undetectable levels of hepcidin despite severe iron overload. Human studies will be needed to quantitate the effects of erythroid suppressors of hepcidin production.

STUDY LIMITATIONS

Our *in vitro* data indicate that ERFE acts on the liver to suppress hepcidin independently of MT-2. In contrast, our *in vivo* approach tested ablation of ERFE with an expectation that this would raise hepcidin further. However, in Tmprss6-/- mice, as a consequence of increased BMP signaling, hepcidin expression is already maximally induced and does not readily respond to additional stimuli, as seen with LPS challenge, an inflammatory activator which induces IL-6, causing increase hepcidin transcription under physiological conditions (12). Thus, ablation of ERFE in Tmprss6-/- mice may not be sufficient to further raise hepcidin levels. These observations indicate that, *in vivo*, physiologic erythroid regulators (including ERFE) act additively to BMP-signaling and have a smaller relative effect on hepcidin production when the BMP/Smad signaling is highly activated. In agreement with Nai and colleagues, our data do not exclude that, *in vivo*, MT-2 could dampen BMP signaling and allow ERFE to repress hepcidin production.

FUTURE DIRECTIONS

We have evidence that ERFE suppresses hepcidin by inhibiting the BMP/SMAD signaling pathway in hepatocytes, but how this occurs is still elusive. Exploring potential interactors for

ERFE, Kautz et al. initially proposed that TfR2 and HJV were not involved in ERFE signaling, because TfR2 and HJV knockout mice still suppress hepcidin after phlebotomy, (2) but this still left open the possibility that other molecules involved in BMP signaling may interact with ERFE. I would like to consider the possibility that ERFE does not bind to a receptor, but binds to BMP2, a ligand involved in the BMP/SMAD signaling leading to hepcidin transcription (13), to prevent BMP2 from binding to its BMP receptor and thus, dampening the BMP/SMAD signal. ERFE, also known as CTRP 15 (C1q-TNF-related protein 15) is an orphan member of the C1q-TNF (complement component 1, q subcomponent- tumor necrosis factor) family of proteins that contains a collagen binding domain (14). Another CTRP family member, CTRP1, has a collagen domain which has been shown to bind to collagen (15). ERFE also has a collagen domain, although it is quite short (2). BMP2 binds collagen as well (16). Thus, it is possible that ERFE binds BMP2. To test if ERFE and BMP2 interact, we could perform surface plasmon resonance (SPR) interaction study to measure ERFE's binding affinity for BMP2. We could coat a chip with ERFE and flow BMP2 over the chip. If BMP2 binds to ERFE, we will observe a change in surface plasmon resonance and can calculate the association and dissociation constant. However, it is possible that this binding could be nonspecific, because ERFE aggregates easily and could trap other proteins in the process. We would need a control protein, such as BSA (bovine serum albumin), to flow across the ERFE coated chip to ensure that our detection method can discriminate between nonspecific and specific binding. We could also flow ERFE after BMP2 incubation to determine if the free ERFE will compete BMP2 off the ERFE-coated chip.

If ERFE does not directly bind BMP2, ERFE could compete with BMP ligands by binding to BMP receptors. Though ERFE is not similar in structure to BMPs or growth factors, it may still be able to bind BMP receptors since the receptors tend to be highly promiscuous at least for BMP

and GDF (growth differentiaton factor) ligands (17), and we know that ERFE decreases BMP signaling. We could test this by determining if ERFE interacts with known BMP receptors: ActRIIa, BMPR2, Alk2, Alk3 (18). We would overexpress each receptor, treat with ERFE, and then try to detect the binding interaction by co-immunoprecipitation (co-IP). However, ActRIIa and BMPR2 form heterodimers with Alk2 or Alk3 (18), so we might have to overexpress combinations of two receptors in order for ERFE to bind.

If our co-IP approach examining BMP receptors does not identify a receptor, we could perform an unbiased screen of an expression library of 16,000 human cDNA clones transiently expressed in ERFE-unresponsive cells in 384-well plates (UCLA Molecular Screening Shared Resource). The plates could be stained with a labeled murine or human ERFE and wells analyzed by high throughput microscopy to identify those with cell-bound ERFE. This approach may not work if the candidate receptor is a product of two or more genes, requires a specific cell type for appropriate processing or trafficking, or is not among one of the cDNAs in the library.

Alternatively, if the unbiased screen does not yield the ERFE receptor, we could affinity-purify the receptor from Hep3Bs and use proteomic techniques to characterize it. This is an unbiased approach, which is also able to detect unknown receptors. ERFE could be immobilized on magnetic beads and used to extract any binding proteins from solubilized membranes or cell lysates of Hep3Bs. The complex could be identified using HPLC-mass spectrometry of tryptic digests. The same method has been successfully used in our laboratory to identify proteins interacting with ferroportin.

Received: 2 February 2017 | Accepted: 3 February 2017
DOI 10.1002/ajh.24672

CORRESPONDENCE

WILEY AJH

Erythroferrone and matriptase-2 independently regulate hepcidin expression

To the Editor:

The production of the iron-regulatory hormone hepcidin is physiologically suppressed during increased erythropoietic activity. Hepcidin suppression increases iron availability to meet the additional iron demand of expanded hemoglobin synthesis. Under the influence of erythropoietin (EPO), the hormone erythroferrone (ERFE) is secreted by erythroid precursors in the bone marrow and spleen, and suppresses hepcidin synthesis to facilitate the recovery from anemia.[1,2] However, the mechanism by which ERFE suppresses hepcidin is unknown. In contrast with forms of anemia in which hepcidin is suppressed, patients with iron-refractory iron deficiency anemia (IRIDA),[3] a disease caused by mutations in transmembrane serine protease 6 (TMPRSS6) which result in pathological activation of the BMP/Smad signaling, exhibit increased hepcidin production despite a severe anemia and elevated EPO levels. Previous studies have shown that hepcidin production was not affected by EPO in *Tmprss6* mutant mice.[4] More recently, Nai and colleagues suggested that matriptase-2 may act downstream of EPO to dampen the signaling through the BMP-Smad regulatory pathway and allow ERFE to repress hepcidin production.[5] We therefore examined the crosstalk between ERFE and matriptase-2 in mice.

In agreement with Nai et al, we observed that *Erfe* mRNA expression was highly increased in the bone marrow and spleen of *Tmprss6*$^{-/-}$ mice (Supporting Information Figure 1). While wild-type mice (WT) mice have undetectable plasma ERFE, plasma ERFE concentration was elevated in *Tmprss6*$^{-/-}$ to levels comparable to those of WT animals 24 h after phlebotomy (~3 ng/mL) but was lower than ERFE levels in thalassemic mice (~10 ng/mL) (Figure 1A). To assess the contribution of ERFE to the phenotype of *Tmprss6*$^{-/-}$ mice, we generated *Tmprss6*$^{-/-}$ mice with disrupted *Erfe* (*Erfe*$^{-/-}$ *Tmprss6*$^{-/-}$; *Erfe*$^{+/-}$ *Tmprss6*$^{-/-}$, and *Erfe*$^{+/+}$ *Tmprss6*$^{-/-}$). Ablation of *Erfe* in *Tmprss6*$^{-/-}$ mice did not result in any change in hematological parameters compared to *Tmprss6*$^{-/-}$ animals at 6 weeks of age (Table 1). Mice deficient for *Tmprss6* had higher RBC and lower hemoglobin, hematocrit, and MCV compared to WT, regardless of the *Erfe* genotype. Liver hepcidin mRNA (Figure 1B) and serum hepcidin concentration (Figure 1C) were higher in *Tmprss6*$^{-/-}$ mice compared to WT mice and no difference was observed after manipulation of *Erfe*. Consistent with chronically increased hepcidin production, liver iron content (Figure 1D) was decreased in *Tmprss6*$^{-/-}$ mice compared to WT mice, but this was not influenced by the ablation of *Erfe*. No statistically significant difference in spleen iron content was observed between the genotypes (Figure 1E). *Erfe*-deficient *Tmprss6*$^{-/-}$ mice and *Tmprss6*$^{-/-}$ mice showed similarly increased spleen weight compared to WT mice (Supporting Information Figure 2A). However, we observed a decrease in body weight in double mutant animals at 6 weeks compared to *Tmprss6*$^{-/-}$ mice (Supporting Information Figure 2B) suggesting that ERFE may be important for normal development of *Tmprss6*$^{-/-}$ mice. As a consequence of smaller body size, spleen index was higher in *Erfe*$^{-/-}$, *Tmprss6*$^{-/-}$ mice compared to *Tmprss6*$^{-/-}$ mice (Supporting Information Figure 2C). Together, these results indicate that the disruption of *Erfe* has at most a very minor effect on the phenotype of *Tmprss6* deficiency in mice.

To determine whether ERFE requires TMPRSS6 to regulate hepcidin production, we treated freshly isolated hepatocytes from WT or *Tmprss6*$^{-/-}$ mice with conditioned medium from cells expressing recombinant ERFE or from control cells. Consistent with stimulated BMP/Smad signaling, baseline hepcidin expression was higher in *Tmprss6*$^{-/-}$ hepatocytes compared to WT hepatocytes in serum-containing and serum-free conditions (Figure 1F). Hepcidin mRNA expression was reduced more than 12-fold in both WT and *Tmprss6*$^{-/-}$ hepatocytes after treatment with ERFE in serum-containing media. Similarly, treatment of hepatocytes with ERFE in serum-free media (ie, in the absence of any soluble matriptase-2) resulted in a 2.5 and 5-fold decrease in hepcidin expression in WT and *Tmprss6*$^{-/-}$ hepatocytes, respectively. These results demonstrate *in vitro* that ERFE represses hepcidin independently of TMPRSS6. Interestingly, *Id1* mRNA expression (Supporting Information Figure 3A) was also reduced in primary mouse hepatocytes from WT and *Tmprss6*$^{-/-}$ mice after treatment with ERFE in serum-containing and serum-free conditions. Similarly, *Atoh8* and *Smad7* mRNA expression (Supporting Information Figure 3B and 3C) was decreased in ERFE-treated WT and *Tmprss6*$^{-/-}$ hepatocytes in serum-containing conditions. In serum-free conditions, the decrease in *Atoh8* and *Smad7* mRNA expression was observed only in ERFE-treated *Tmprss6*$^{-/-}$ hepatocytes but not in WT hepatocytes. This suggests a potential crosstalk between BMP and ERFE signaling that is independent of TMPRSS6.

The reason for the impairment of erythropoietic suppression of hepcidin in patients and mice with IRIDA may lie in the intense stimulation of hepcidin by the BMP pathway *in vivo*, opposing the effect of ERFE. In accordance with the findings by Nai and colleagues, we previously demonstrated that hepcidin suppression after phlebotomy is blunted in iron-overloaded WT mice and *Tfr2*$^{-/-}$ mice where the BMP pathway is strongly stimulated by iron[2]. These

 © 2017 Wiley Periodicals, Inc.

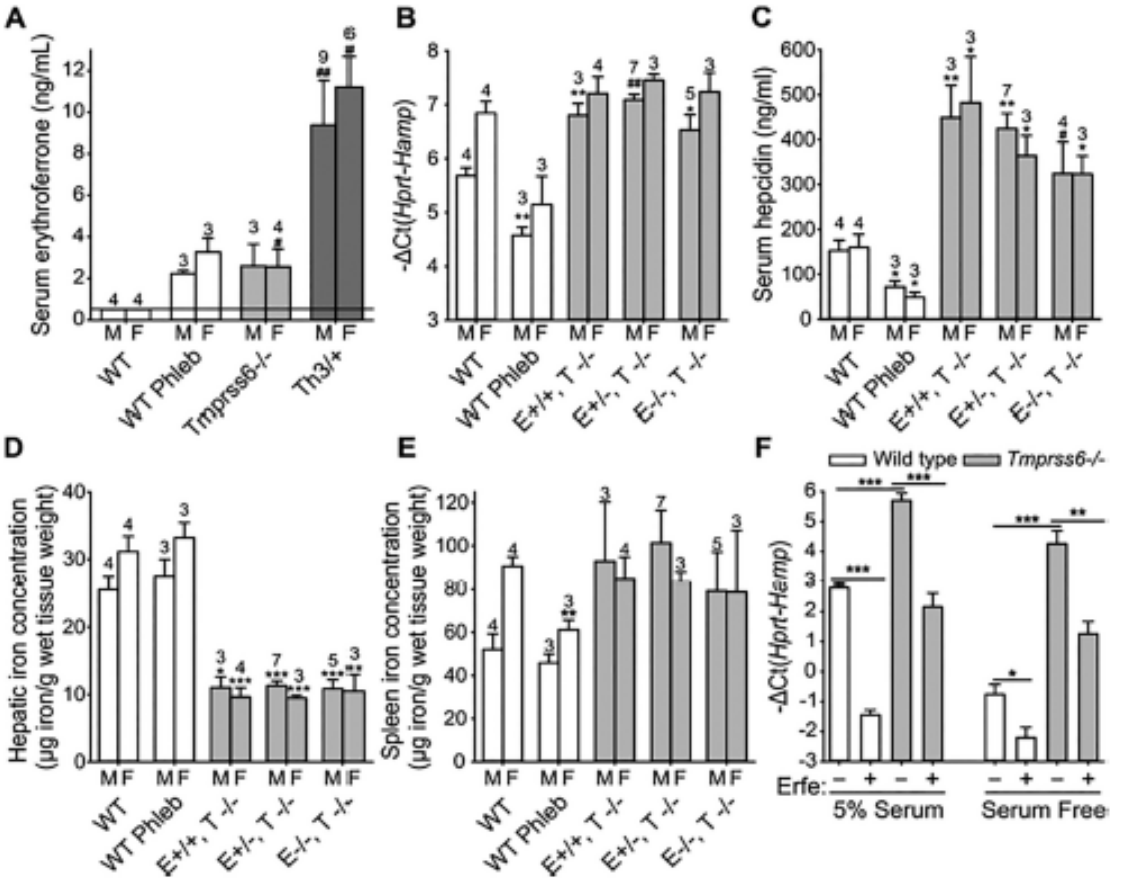

FIGURE 1 ERFE and Matriptase 2 regulate hepcidin independently. (A) Serum ERFE concentration was elevated in *Tmprss6*$^{-/-}$ mice similarly to WT (wild-type) mice 24 hours after phlebotomy, but was lower than in thalassemic mice (Th3/+). (B,C) Neither liver hepcidin mRNA expression nor serum hepcidin were significantly different in *Erfe*$^{-/-}$ *Tmprss6*$^{-/-}$ ($E^{-/-}$, $T^{-/-}$) mice compared to *Erfe*$^{+/+}$ *Tmprss6*$^{-/-}$ ($E^{+/+}$, $T^{-/-}$) or *Erfe*$^{+/-}$ *Tmprss6*$^{-/-}$ ($E^{+/-}$, $T^{-/-}$) mice. (D) Liver iron content was similarly lower in *Tmprss6*$^{-/-}$ mice compared to WT mice regardless of the *Erfe* genotype whereas spleen iron content (E) was comparable to those of WT mice. (A-E) The number of mice studied is shown for each group. Data shown are means ± SEM. Statistical analysis was performed compared to WT controls of the same gender, using the two-tailed Student *t* test (***$p < .001$, **$p < .01$, *$p < .05$) or Mann-Whitney test (##$p < .01$, #$p < .05$). *M* = male, *F* = female. (F) Hepcidin mRNA expression was strongly reduced in primary hepatocytes from WT and *Tmprss6*$^{-/-}$ mice 16 h after treatment with conditioned medium containing ERFE (final concentration 500 ng/mL of recombinant ERFE), both in 5% serum or serum-free conditions. Data shown are means ± SEM of three independent experiments. Statistical analysis was performed using two-tailed Student *t* test (***$p < .001$, **$p < .01$, *$p < .05$)

observations indicate that physiologic erythroid regulators (including ERFE) act additively to BMP-signaling and have a smaller relative effect on hepcidin production when the BMP/Smad signaling is highly activated.

The relatively weak effect of erythroid suppressors of hepcidin in IRIDA must be reconciled with the dominant effect of erythroid suppressors of hepcidin despite the iron-overload stimulated BMP signaling in patients with β-thalassemia and other disorders with ineffective erythropoiesis. Here, three kinds of differences may be relevant. First, the concentrations of ERFE (and perhaps other erythroid suppressors) may be higher in conditions with ineffective erythropoiesis than in IRIDA, likely because of the greater number of ERFE-secreting erythroblasts in ineffective erythropoiesis. Secondly, in anemias other than IRIDA, erythropoietin stimulation may increase the production of matriptase 2 through a posttranslational mechanism, potentiating the suppressive effect of erythroferrone on hepcidin. Thirdly, there are important species differences in the observed effect of erythroid suppressors of hepcidin in the mouse models of ineffective erythropoiesis vs. human patients. Young β-thalassemic mice exhibit suppressed hepcidin, but progressively increase hepcidin with age to levels comparable to those of adult WT mice as they become iron overloaded, despite elevated ERFE production.[6] In contrast, adult human patients with β-thalassemia continue to have decreased to undetectable levels of hepcidin despite severe iron overload. Human studies will be needed to quantitate the effects of erythroid suppressors of hepcidin production.

TABLE 1 Hematological parameters are unchanged by ERFE ablation in *Tmprss6*$^{-/-}$ mice

	N	RBC (M/μL)	HB (g/dL)	HCT (%)	MCV (fL)
Males					
WT	4	9.4 ± 0.2	16.3 ± 0.5	45.7 ± 1.2	48.6 ± 0.2
WT phlebotomized	3	8.0** ± 0.1	13.9*± 0.4	38.7**± 0.4	48.3 ± 0.7
Erfe$^{+/+}$ *Tmprss6*$^{-/-}$	5	10.3 ± 0.4	8.4*** ± 0.3	34.9***± 1.2	34.0** ± 0.4
Erfe $^{+/-}$ *Tmprss6*$^{-/-}$	12	10.7* ± 0.3	8.9*** ± 0.2	35.7*** ± 0.7	33.5** ± 0.4
Erfe$^{-/-}$ *Tmprss6*$^{-/-}$	5	10.8* ± 0.5	9.0*** ± 0.4	36.6* ± 1.3	34.0*** ± 0.2
Females					
WT	4	9.2 ± 0.1	16.3 ± 0.4	44.3 ± 0.6	48.1 ± 0.2
WT phlebotomized	3	6.8*** ± 0.3	11.8*** ± 0.4	33.3*** ± 1.1	48.6 ± 0.2
Erfe$^{+/+}$ *Tmprss6*$^{-/-}$	5	11.4** ± 0.4	9.4*** ± 0.3	38.6** ± 1.1	33.9*** ± 0.2
Erfe$^{+/-}$ *Tmprss6*$^{-/-}$	4	10.2* ± 0.4	8.7*** ± 0.5	34.8*** ± 1.1	34.0*** ± 0.4
Erfe$^{-/-}$ *Tmprss6*$^{-/-}$	6	11.3*** ± 0.3	9.7** ± 0.2	37.6*** ± 0.9	33.3*** ± 0.1

RBC was increased while hemoglobin, hematocrit and MCV were decreased in *Tmprss6*$^{-/-}$ mice compared to WT mice at 6 weeks of age. Ablation of *Erfe* in *Tmprss6*$^{-/-}$ mice did not result in any change in hematological parameters compared to *Tmprss6*$^{-/-}$ animals at 6 weeks of age (two-tailed Student *t* test comparison of *Erfe*$^{-/-}$ *Tmprss6*$^{-/-}$ and *Erfe*$^{+/-}$ *Tmprss6*$^{-/-}$ to *Erfe*$^{+/+}$ *Tmprss6*$^{-/-}$). None of the CBC parameters were statistically different by gender or by genotype when comparing *Erfe*$^{-/-}$ *Tmprss6*$^{-/-}$ and *Erfe*$^{+/-}$ *Tmprss6*$^{-/-}$ to *Erfe*$^{+/+}$ *Tmprss6*$^{-/-}$ by two-way ANOVA. Data shown are means ± SEM and were compared for each group to control WT mice by two-tailed Student *t* test (n = 6–16 per group, gender combined). ***$p < .001$, **$p < .01$, *$p < .05$.

ACKNOWLEDGMENTS

The authors thank Jodie Babitt (Massachusetts General Hospital) for providing the *Tmprss6*$^{-/-}$ mice and Xin Du, Justin Chapman, and Marc Nasoff of Silarus Therapeutics for providing the ERFE assay.

DISCLOSURES

E.N and T.G. are shareholders and scientific advisors of Intrinsic Life Sciences, Merganser Biotech, and Silarus Therapeutics. T.G. is a consultant to Keryx Biopharmaceuticals.

AUTHOR CONTRIBUTIONS

S.A. performed experiments, analyzed the data, and edited the manuscript, L.K. designed and performed the experiments, analyzed the data and wrote the paper, E.N. and T.G. supervised the project and wrote the paper.

Sharraya Aschemeyer[1,2], Victoria Gabayan[1], Tomas Ganz[1,2], Elizabeta Nemeth[1], Léon Kautz[4]

[1]*Departments of Medicine, David Geffen School of Medicine, University of California, Los Angeles, Los Angeles, California*

[2]*Departments of Pathology, David Geffen School of Medicine, University of California, Los Angeles, Los Angeles, California*

[3]*Departments of Molecular Biology Interdepartmental Doctoral Program, David Geffen School of Medicine, University of California, Los Angeles, Los Angeles, California*

[4]*IRSD, Université de Toulouse, INSERM U1220, INRA U1416, ENVT, UPS, Toulouse, France*

Correspondence

Léon Kautz, Inserm U1220 IRSD, CHU Purpan Place du Dr Baylac, CS60039, 31024 Toulouse Cedex 3, France.
Email: leon.kautz@inserm.fr

Funding Information

This research was supported by the ASH scolar award and ANR-16-ACHN-0002-01 to L.K. and the NHLBI award F31HL129760 and NIH Grant T32GM007185 to S.A.

REFERENCES

[1] Kautz L, Jung G, Nemeth E, Ganz T. Erythroferrone contributes to recovery from anemia of inflammation. *Blood*. 2014;124(16):2569–2574.

[2] Kautz L, Jung G, Valore EV, et al. Identification of erythroferrone as an erythroid regulator of iron metabolism. *Nat Genet*. 2014;46(7):678–684.

[3] De Falco L, Sanchez M, Silvestri L, et al. Iron refractory iron deficiency anemia. *Haematologica*. 2013;98(6):845–853.

[4] Nicolas G, Deschemin JC, Ramsay AJ, et al. Is EPO therapy able to correct iron deficiency anaemia caused by matriptase-2 deficiency? *Br J Haematol*. 2011;152(4):498–500.

[5] Nai A, Rubio A, Campanella A, et al. Limiting hepatic Bmp-Smad signaling by matriptase-2 is required for erythropoietin-mediated hepcidin suppression in mice. *Blood*. 2016;127(19):2327–2336.

[6] Kautz L, Jung G, Du X, et al. Erythroferrone contributes to hepcidin suppression and iron overload in a mouse model of beta-thalassemia. *Blood*. 2015;126(17):2031–2037.

SUPPORTING INFORMATION

Additional Supporting Information may be found in the online version of this article.

REFERENCES

1. Kautz L, Jung G, Nemeth E, Ganz T. Erythroferrone contributes to recovery from anemia of inflammation. *Blood* 2014; 124(16)**:** 2569-2574.

2. Kautz L, Jung G, Valore EV, Rivella S, Nemeth E, Ganz T. Identification of erythroferrone as an erythroid regulator of iron metabolism. *Nat. Genet.* 2014; 46(7)**:** 678-684. doi: ng.2996 [pii];10.1038/ng.2996 [doi]

3. Wang CY, Core AB, Canali S, Zumbrennen-Bullough KB, Ozer S, Umans L *et al.* Smad1/5 is required for erythropoietin-mediated suppression of hepcidin in mice. *Blood* 2017. doi: 10.1182/blood-2016-12-759423

4. De Falco L, Sanchez M, Silvestri L, Kannengiesser C, Muckenthaler MU, Iolascon A *et al.* Iron refractory iron deficiency anemia. *Haematologica* 2013; 98(6)**:** 845-853. doi: 10.3324/haematol.2012.075515

5. Nicolas G, Deschemin JC, Ramsay AJ, Mayeux P, Grandchamp B, Beaumont C *et al.* Is EPO therapy able to correct iron deficiency anaemia caused by matriptase-2 deficiency? *Br J Haematol* 2011; 152(4)**:** 498-500. doi: 10.1111/j.1365-2141.2010.08473.x

6. Lehmberg K, Grosse R, Muckenthaler MU, Altamura S, Nielsen P, Schmid H *et al.* Administration of recombinant erythropoietin alone does not improve the phenotype in iron refractory iron deficiency anemia patients. *Ann. Hematol.* 2013; 92(3)**:** 387-394. doi: 10.1007/s00277-012-1618-8

7. Nai A, Rubio A, Campanella A, Gourbeyre O, Artuso I, Bordini J *et al.* Limiting hepatic Bmp-Smad signaling by matriptase-2 is required for erythropoietin-mediated hepcidin suppression in mice. *Blood* 2016; 127(19)**:** 2327-2336. doi: 10.1182/blood-2015-11-681494

8. Tang T, Li L, Tang J, Li Y, Lin WY, Martin F *et al.* A mouse knockout library for secreted and transmembrane proteins. *Nat.Biotechnol.* 2010; 28(7)**:** 749-755. doi: nbt.1644 [pii];10.1038/nbt.1644 [doi]

9. Folgueras AR, de Lara FM, Pendas AM, Garabaya C, Rodriguez F, Astudillo A *et al.* Membrane-bound serine protease matriptase-2 (Tmprss6) is an essential regulator of iron homeostasis. *Blood* 2008; 112(6)**:** 2539-2545. doi: blood-2008-04-149773 [pii];10.1182/blood-2008-04-149773 [doi]

10. Goodnough JB, Ramos E, Nemeth E, Ganz T. Inhibition of hepcidin transcription by growth factors. *Hepatology* 2012; 56(1)**:** 291-299. doi: 10.1002/hep.25615 [doi]

11. Kautz L, Jung G, Du X, Gabayan V, Chapman J, Nasoff M *et al.* Erythroferrone contributes to hepcidin suppression and iron overload in a mouse model of beta-thalassemia. *Blood* 2015; 126(17)**:** 2031-2037. doi: 10.1182/blood-2015-07-658419

12. Pagani A, Nai A, Corna G, Bosurgi L, Rovere-Querini P, Camaschella C *et al.* Low hepcidin accounts for the proinflammatory status associated with iron deficiency. *Blood* 2011; 118(3)**:** 736-746. doi: blood-2011-02-337212 [pii];10.1182/blood-2011-02-337212 [doi]

13. Koch PS, Olsavszky V, Ulbrich F, Sticht C, Demory A, Leibing T *et al.* Angiocrine Bmp2 signaling in murine liver controls normal iron homeostasis. *Blood* 2017; 129(4)**:** 415-419. doi: 10.1182/blood-2016-07-729822

14. Schaffler A, Buechler C. CTRP family: linking immunity to metabolism. *Trends Endocrinol. Metab.* 2012; 23(4)**:** 194-204. doi: 10.1016/j.tem.2011.12.003

15. Lasser G, Guchhait P, Ellsworth JL, Sheppard P, Lewis K, Bishop P *et al.* C1qTNF-related protein-1 (CTRP-1): a vascular wall protein that inhibits collagen-induced platelet aggregation by blocking VWF binding to collagen. *Blood* 2006; 107(2)**:** 423-430. doi: 10.1182/blood-2005-04-1425

16. Sieron AL, Louneva N, Fertala A. Site-specific interaction of bone morphogenetic protein 2 with procollagen II. *Cytokine* 2002; 18(4)**:** 214-221.

17. Mueller TD, Nickel J. Promiscuity and specificity in BMP receptor activation. *FEBS Lett.* 2012; 586(14)**:** 1846-1859. doi: 10.1016/j.febslet.2012.02.043

18. Mayeur C, Leyton PA, Kolodziej SA, Yu B, Bloch KD. BMP type II receptors have redundant roles in the regulation of hepatic hepcidin gene expression and iron metabolism. *Blood* 2014; 124(13)**:** 2116-2123. doi: 10.1182/blood-2014-04-572644

CHAPTER 3

Nrf2 is does not regulate hepcidin in response to iron loading

INTRODUCTION

There are four main types of cells that comprise the liver: hepatocytes, sinusoidal endothelial cells (SECs), Kupffer cells, and stellate cells. SECs are endothelial cells that line the sinusoid blood vessels in the liver, Kupffer cells are liver-specific macrophages which monitor the blood stream and recycle iron from senescent red blood cells, and stellate cells store vitamin A and fat and participate in repair and scar formation (1-3). However, the predominant cell type in the liver is the hepatocyte (~60%) which specializes in intermediary metabolism, protein synthesis, and detoxification (4). Hepatocytes are the main producers of the iron-regulatory hormone hepcidin in the body.

Hepcidin is a small peptide hormone that regulates iron, analogous to glucose regulation by the hormone insulin (5). By regulating the entry of iron into plasma, hepcidin controls plasma iron concentrations, and thus, iron availability for erythropoiesis and other processes. Iron is transported into plasma by the only known cellular iron exporter, ferroportin, which is expressed on enterocytes absorbing dietary iron, macrophages recycling aged erythrocytes, and hepatocytes which store iron. Ferroportin is the hepcidin receptor: hepcidin binds to ferroportin, causing its endocytosis and degradation, thus inhibiting the entry of iron into plasma (6).

Regulation of hepcidin production is crucial to iron homeostasis. Hepcidin transcription is increased by the element whose concentration it regulates, iron. This feedback mechanism ensures that when body iron is sufficient, no further absorption of iron will occur. When this feedback mechanism is impaired and hepcidin is not adequately increased by iron, unrestrained iron absorption leads to excess iron deposition in organs and their destruction, resulting in the iron overload disease, hereditary hemochromatosis (7, 8).

Our lab previously demonstrated that both extracellular and intracellular iron concentrations provide signals for hepcidin regulation. The mechanism by which extracellular iron increases hepcidin transcription is better understood: holo-transferrin (iron-bound transferrin) concentrations are sensed by two transferrin receptors (TfR1 and TfR2) on the cell membrane of hepatocytes, which stimulate the BMP pathway to increase hepcidin transcription (9, 10). In our experiments *in vivo*, however, chronic iron loading in hemojuvelin (HJV) knockout (KO) or TfR2 KO mice, mice models where BMP signaling is severely impaired, still increased hepcidin mRNA in the liver despite unchanged holo-transferrin (10). Intracellular iron sensing and subsequent signaling is not well understood, but the circuitry involves production of BMP6 and BMP2 by sinusoidal endothelial cells within the liver. These ligands act on hepatocytes to stimulate Smad1/5/8 signaling and hepcidin transcription (11, 12). How and in which cell type intracellular iron is sensed, and how this increases BMP production in endothelial cells remains to be determined.

We hypothesized that Nrf2, a sensor of oxidative stress, could also effectively function as an intracellular iron sensor. Excessive intracellular iron can cause oxidative stress, because iron catalyzes production of reactive oxygen species (ROS) (13). Nrf2 is a transcription factor that induces expression of antioxidant genes in response to oxidative stress (14). Nrf2 is in the cytosol and at baseline, is readily ubiquitinated and degraded by an ubiquitination complex that includes homodimers of KEAP1, an E3 ubiquitin ligase that sequesters Nrf2. Keap1 homodimers each contain cysteine residues which become modified under oxidative stress conditions, causing Keap1 to undergo a conformational change. This conformational change inactivates Keap1's ability to facilitate ubiquitination of Nrf2. As a consequence, Nrf2 accumulates and translocates into the nucleus to activate antioxidant genes which prevent oxidative damage (15-17). Nrf2 is

important for healthy liver function, because Nrf2 KO mice experience delayed recovery after a short term toxin-induced liver injury and develop much more inflammation and fibrosis after a long term toxin-induced liver injury compared to wild-type (WT) mice (18).

Moon et al. observed that elevated hepatic iron activates Nrf2 in a dietary overloaded mouse model (19) and Tanaka et al., while studying fat-induced liver disease, indicated that Nrf2 KO mice do not upregulate hepcidin when they are iron loaded on a high fat diet (20). Both these studies suggest that Nrf2 may mediate hepcidin regulation by iron. We examined the role of Nrf2 in hepcidin regulation by removing the confounder of the high fat diet and using dietary iron as the only variable.

MATERIALS AND METHODS

Animals and diets

Experiments were conducted in accordance with guidelines by the National Research Council and were approved by the University of California, Los Angeles. *Nrf2 -/-* mice on a C57BL/6J background were obtained from Dr. Jesus Araujo from the University of California, Los Angeles. WT (*Nrf2 +/+*) C57BL/6J mice were purchased from the Jackson Laboratory.

Iron depleted mice were placed on a 4 ppm iron diet (TD 80396, Harlan Labs/Envigo) for three weeks and either given 1 day of standard chow (TD 8604, Harlan Labs/Envigo) for acute iron loading or three weeks of 10,000 ppm iron diet for chronic iron loading (TD 8043, Harlan Labs /Envigo). In Figure 3-2, the mice were on mice on a 10,000 ppm iron diet (TD 8043, Harlan Labs /Envigo) for 6 weeks.

Measurement of iron

Liver non-heme iron concentrations were determined as previously described (21), using acid treatment followed by a colorimetric assay for iron quantitation (Sekisui Diagnostics/Genzyme). To obtain total liver iron, the liver iron concentration was multiplied by the liver weight.

Quantitation of mRNA levels

Total RNA was extracted from mouse tissues using Trizol (Invitrogen) according to the manufacturer's instructions and iScript (Biorad) was used to synthesize cDNA. Quantitative PCR reactions were made using Sso advanced Sybr Green supermix (Biorad) and run in duplicate on a CFX Connect or CFX96 Touch instrument (Biorad). The following primers were used: *Hprt F:* CTG-GTT-AAG-CAG-TAC-AGC-CCC-AA R: CAG-GAG-GTC-CTT-TTC-ACC-AGC and *Hamp F:* TTG-CGA-TAC-CAA-TGC-AGA-AGA and R: GAT-GTG-GCT-CTA-GGC-TAT-GTT. Hamp mRNA was normalized to the reference gene Hprt. Results are expressed as –ΔCt which is the difference between the cycle thresholds for the reference and target gene within each group of mice.

Statistical analysis

Either two-way or three-way ANOVAs were utilized to determine the statistical differences between groups using Sigmaplot 12.5 (Systat Software). Two-way ANOVAs examined the interaction between genotype and gender whereas the three-way ANOVAs examined the interaction between genotype, gender, and diet.

RESULTS AND DISCUSSION

Nrf2 does not regulate hepcidin in response to iron loading

Nrf2-/- or Nrf2+/+ mice were placed on a 4ppm iron diet for 3 weeks (iron depleted) and then either sacrificed after 1 day of standard diet (acute loading) or after 3 weeks on a 10,000ppm iron diet (chronic loading). Hepcidin mRNA (Figure 3-1A) and liver iron concentration (Figure 3-2B) were measured. Though males and females on a 4ppm iron diet had lower liver iron concentrations compared to the chronic loading condition (Figure 3-2B), most of the female mice and some of the male mice were not fully iron-depleted, considering that hepcidin mRNA was not uniformly suppressed (Figure 3-2A). When comparing hepcidin mRNA response in the acute versus chronically loaded mice, there was no difference between the *Nrf2 -/-* or *Nrf2 +/+* mice. Only the diet and gender, but not genotype, affected hepcidin levels as assessed by three-way ANOVA. Interestingly, there was a significant difference in the liver iron concentration between *Nrf2 -/-* and *Nrf2 +/+* mice, but only during chronic iron loading. To determine if Nrf2 senses iron and subsequently regulates hepcidin, we plotted hepcidin mRNA as a function of liver iron concentration for both *Nrf2 -/-* and *Nrf2 +/+* mice. With increasing iron levels in the liver, hepcidin is increased until it reaches saturation around 7 Δcts, which occurs in both *Nrf2 -/-* and *Nrf2 +/+* mice, suggesting that both regulate hepcidin in response to iron loading similarly (Figure 3-2A). Although greater proportion of *Nrf2 +/+* mice had a more profound hepcidin suppression on the 4 ppm diet, differences in hepcidin expression below 0 Δct do not translate into biologically-relevant differences in serum hepcidin levels as serum hepcidin becomes undetectable (Figure 3-2B). The acute loading data was not plotted in this graph due to the additional signals that regulate hepcidin during acute iron stimulation (holo-transferrin increase).

If Nrf2 were a biologically relevant sensor of iron loading, the *Nrf2 -/-* mice would have displayed a blunted hepcidin response to iron loading compared to *Nrf2 +/+* when given a high iron diet, but they did not. Thus, Nrf2 is not required for hepcidin regulation by iron.

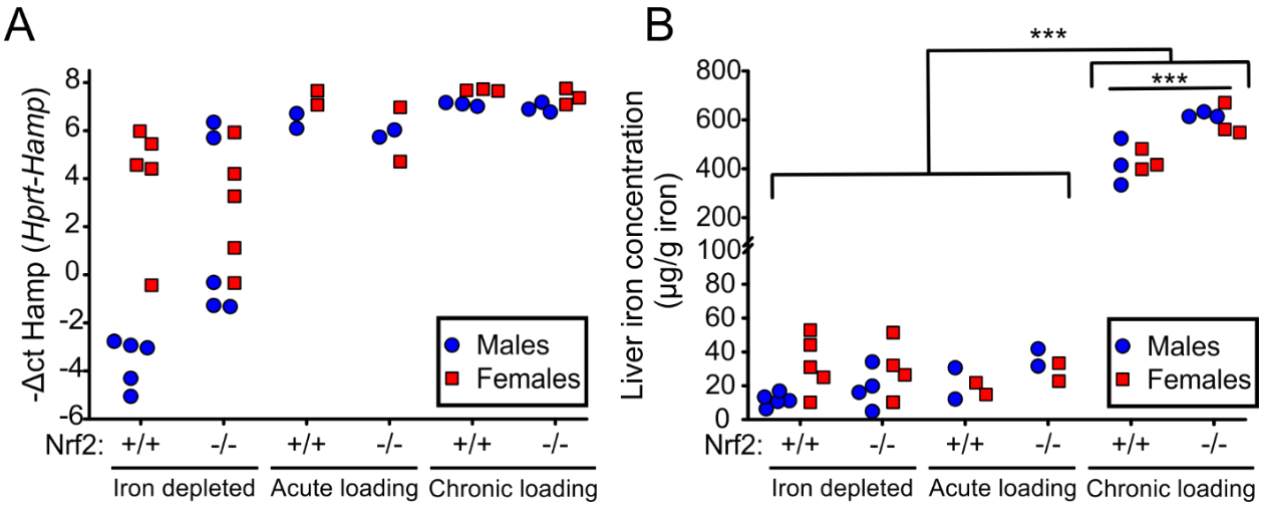

Figure 3-1: Nrf2 does not regulate hepcidin in response to iron loading.
A&B) Nrf2-/- or Nrf2+/+ mice were placed on a 4ppm iron diet for 3 weeks (iron depleted) and then either sacrificed after 1 day of standard diet (acute loading) or after 3 weeks on a 10,000 ppm iron diet (chronic loading). Hepcidin mRNA (A) and liver iron concentration (B) were measured. Statistical analysis employed a three-way ANOVA and determined that diet and gender, but not genotype, affected hepcidin levels in A). Genotype did affect liver iron concentration on 10,000ppm diet in B). ***P<0.001, **P<0.01, *P<0.05.

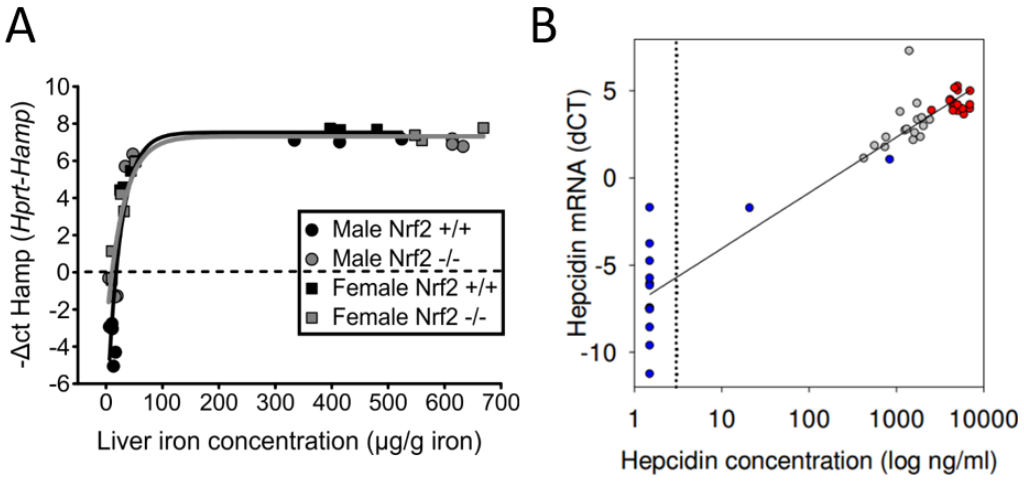

Figure 3-2: Nrf2 KO mice increase hepcidin in response to increasing iron concentration similarly to WT mice. A) The effect of liver iron concentration on hepcidin mRNA expression

using values from iron-depleted or chronically iron-loaded animals in Figure 3-1. The dashed line represents hepcidin mRNA levels at which hepcidin protein reaches its limit of detection (based on Figure 3-2B). B) Correlation between serum hepcidin protein and liver hepcidin mRNA concentrations. Data are from (22). Mice were placed on either an iron deficient diet (blue), iron replete diet (gray), or iron-loaded diet (red). Hepcidin mRNA was measured by qPCR and protein was measured by ELISA. The dotted line indicates 50% of the lower limit of detection for the hepcidin ELISA. The values below that limit were all assigned a concentration of 1.5 ng/ml.

Nrf2 does not alter total liver iron

In order to further investigate the difference in liver iron concentration between *Nrf2 +/+* and *Nrf2 -/-* mice on a chronic high iron diet, we placed *Nrf2 +/+* and *Nrf2 -/-* mice for 6 weeks on a 10,000 ppm iron diet and measured liver iron concentration (Figure 3-3A) and liver weight (Figure 3-3B). The liver iron concentration in *Nrf2 -/-* mice was significantly higher in both males and females compared to *Nrf2 +/+* mice. However, the liver weights in *Nrf2 -/-* mice were significantly lower than the *Nrf2 +/+* mice. Thus, when the total amount of iron in the liver was calculated by multiplying liver weight with liver iron concentration, there was no difference in total liver iron in either male or female Nrf2-/- mice compared to *Nrf2 +/+* mice (Figure 3-3C). Silva-Gomez et al. also compared *Nrf2 -/-* and *Nrf2 +/+* mice placed on an iron rich diet and found no difference in total liver iron as well (23). Though Nrf2 is necessary for healthy liver function after a toxic insult, it does not appear to play a role in iron homeostasis.

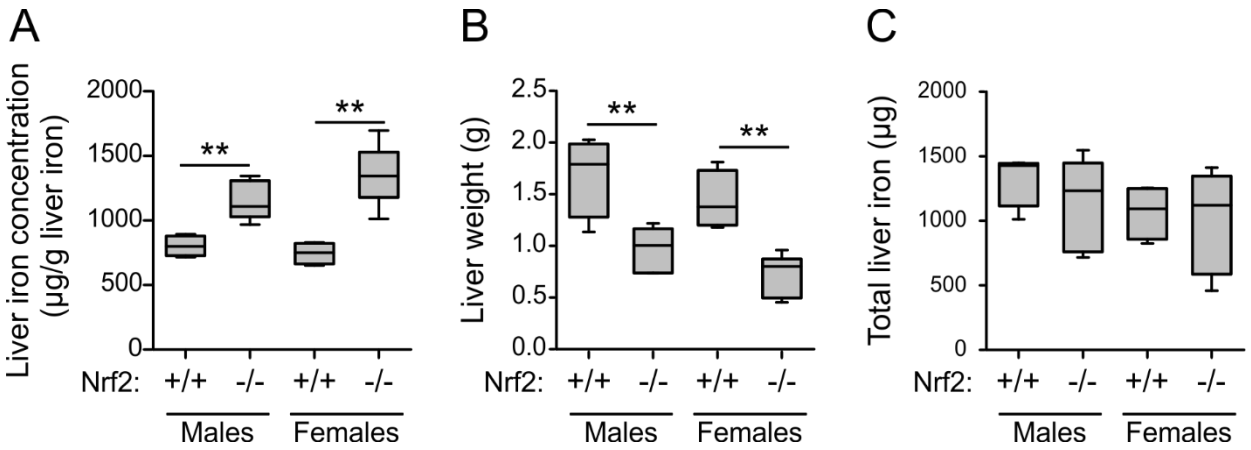

Figure 3-3: *Nrf2 -/-* mice have smaller livers but do not have increased total liver iron compared to *Nrf2 +/+* mice. A-C) Nrf2-/- or Nrf2+/+ mice were placed on a 10,000 ppm iron diet for 6 weeks and liver iron concentration (A), liver weight (B), and total liver iron (C) were measured. 4-6 mice were used per group. Statistical analysis employed a two-way ANOVA for significance (***P<0.001, **P<0.01, *P<0.05).

LIMITATIONS OF THIS STUDY

Our pilot study has some limitations. It is possible that only very high levels of iron elicit oxidative stress leading to Nrf2 activation which our iron loading diet did not reach. We did not determine in our iron-overloaded Nrf2 +/+ mouse model whether nuclear Nrf2 was sufficiently activated to increase transcription of any of its target genes. This could have been done by measuring expression of the downstream targets of Nrf2: *Nqo1* (NAD(P)H:quinone oxidoreductase 1) and *Gclc* (glutamate-cysteine ligase, catalytic subunit). Longer exposure to a high iron diet or injection with iron dextran may also produce a more severe iron overload and generate reactive oxygen species. Alternatively, we could have crossed Nrf2 KO mice with HJV KO mice as a model of severe iron overload. However, we were interested in identifying a physiologically-relevant iron sensor that regulates hepcidin over a large range of intracellular iron concentrations. Our mouse model showed increased hepcidin transcription with increasing amounts of stored iron despite the absence of Nrf2. Thus, we conclude that Nrf2 is not a physiologically relevant regulator of hepcidin expression in response to iron loading.

FUTURE DIRECTIONS

Nrf2 was a logical candidate intracellular iron sensor based on its function and on other publications that suggested it might participate in iron homeostasis and transcriptional regulation of hepcidin. If we were to continue our search for the intracellular iron sensor, our strategy would

be to start with the most likely candidates and deploy progressively more general approaches until the intracellular iron sensor is identified. The next candidate intracellular iron sensor would be iron-containing ferritin. In 2012, Feng et al. proposed that iron-containing ferritin may be the intracellular iron sensor since young mice treated with exogenous iron-containing ferritin increased both BMP6 and hepcidin transcription in the liver whereas iron-deficient ferritin did not (24). Serum ferritin is a good candidate, because serum ferritin is increased with increasing iron load and is correlated with increasing hepcidin transcription (25). Most serum ferritin is iron-depleted and secreted by macrophages (26), so it would not be effective in regulating hepcidin. However, patients with thalassemia had measurable serum ferritin that resembled tissues ferritin which likely leaked from the cytosol of iron-loaded cells (27), and primary human hepatocytes loaded with iron also release ferritin into the medium in a dose-dependent manner (28). Thus, it is possible that iron-containing ferritin is either secreted or leaks out from iron-loaded hepatocytes and is then endocytosed by ferritin receptors on the sinusoidal endothelial cells, signaling for the production of BMP6 and BMP2.

If iron-containing ferritin did not induce BMP6 or BMP2 transcription in cultured SECs, the cells that line blood vessels in the liver and are in close contact with hepatocytes, we would take a more open-ended approach to identify candidate intracellular iron sensors and their signaling pathways. Ferritin was an ideal candidate since it could have both sensed iron and been the signaling mediator between hepatocytes and SECs. If ferritin is not the sensor/mediator, potentially two or more proteins could be involved in a pathway sensing intracellular iron and mediating the signal between SECs and hepatocytes. Also, it is possible that some other liver cell type is involved as well. Since much is still unknown about the intracellular iron sensing pathway, we would first focus on the mediator between hepatocytes and SECs, and the signaling pathway in the SECs

causing BMP production. We would treat cultured SECs with conditioned media (CM) from either iron-loaded (IL-CM) or iron-depleted (ID-CM) hepatocytes, Kupffer cells, or hepatic stellate cells and quantify BMP2/6 mRNA. We also can compare BMP2/6 expression in SECs versus SECs co-cultured with hepatocytes, Kupffer cells, and stellate cells in a dual-chamber containing a permeable support. If one of these treatments induces BMP2/6 mRNA, then we will perform RNA sequencing or differential mass spectrometry on the SECs treated with the active IL-CM compared to its respective ID-CM to look for a potential signaling pathway. We could also fractionate the CM to determine a molecular weight range for the putative mediator and perform differential mass spectrometric profiling on the active fraction from the IL-CM versus the respective fraction from the ID-CM to identify new candidate intracellular iron sensor pathways and mediators.

REFERENCES

1. Braet F, Wisse E. Structural and functional aspects of liver sinusoidal endothelial cell fenestrae: a review. *Comp. Hepatol.* 2002; 1(1)**:** 1.

2. Kondo H, Saito K, Grasso JP, Aisen P. Iron metabolism in the erythrophagocytosing Kupffer cell. *Hepatology* 1988; 8(1)**:** 32-38. doi: S0270913988000205 [pii]

3. Friedman SL. Hepatic stellate cells: protean, multifunctional, and enigmatic cells of the liver. *Physiol. Rev.* 2008; 88(1)**:** 125-172. doi: 10.1152/physrev.00013.2007

4. Jungermann J, Sasse D. Heterogeneity of liver parenchymal cells. *Trends Biochem. Sci.* 1978; 3**:** 198-202.

5. Ganz T. Hepcidin and iron regulation, 10 years later. *Blood* 2011; 117(17)**:** 4425-4433. doi: blood-2011-01-258467 [pii];10.1182/blood-2011-01-258467 [doi]

6. Ward DM, Kaplan J. Ferroportin-mediated iron transport: expression and regulation. *Biochim. Biophys. Acta* 2012; 1823(9)**:** 1426-1433. doi: 10.1016/j.bbamcr.2012.03.004

7. Bridle KR, Frazer DM, Wilkins SJ, Dixon JL, Purdie DM, Crawford DHG *et al.* Disrupted hepcidin regulation in *HFE*-associated haemochromatosis and the liver as a regulator of body iron homoeostasis. *Lancet* 2003; 361**:** 669-673.

8. Papanikolaou G, Samuels ME, Ludwig EH, MacDonald ML, Franchini PL, Dube MP *et al.* Mutations in HFE2 cause iron overload in chromosome 1q-linked juvenile hemochromatosis. *Nat. Genet.* 2004; 36(1)**:** 77-82.

9. Lin L, Valore EV, Nemeth E, Goodnough JB, Gabayan V, Ganz T. Iron transferrin regulates hepcidin synthesis in primary hepatocyte culture through hemojuvelin and BMP2/4. *Blood* 2007; 110(6)**:** 2182-2189.

10. Ramos E, Kautz L, Rodriguez R, Hansen M, Gabayan V, Ginzburg Y *et al.* Evidence for distinct pathways of hepcidin regulation by acute and chronic iron loading in mice. *Hepatology* 2011; 53(4)**:** 1333-1341. doi: 10.1002/hep.24178 [doi]

11. Koch PS, Olsavszky V, Ulbrich F, Sticht C, Demory A, Leibing T *et al.* Angiocrine Bmp2 signaling in murine liver controls normal iron homeostasis. *Blood* 2017; 129(4)**:** 415-419. doi: 10.1182/blood-2016-07-729822

12. Canali S, Zumbrennen-Bullough KB, Core AB, Wang CY, Nairz M, Bouley R *et al.* Endothelial cells produce bone morphogenetic protein 6 required for iron homeostasis in mice. *Blood* 2017; 129(4)**:** 405-414. doi: 10.1182/blood-2016-06-721571

13. Brissot P, Ropert M, Le LC, Loreal O. Non-transferrin bound iron: A key role in iron overload and iron toxicity. *Biochim. Biophys. Acta* 2012; 1820(3)**:** 403-410. doi: S0304-4165(11)00180-2 [pii];10.1016/j.bbagen.2011.07.014 [doi]

14. Kang KW, Lee SJ, Kim SG. Molecular mechanism of nrf2 activation by oxidative stress. *Antioxid Redox Signal* 2005; 7(11-12)**:** 1664-1673. doi: 10.1089/ars.2005.7.1664

15. Colin-Gonzalez AL, Santana RA, Silva-Islas CA, Chanez-Cardenas ME, Santamaria A, Maldonado PD. The antioxidant mechanisms underlying the aged garlic extract- and S-allylcysteine-induced protection. *Oxid. Med. Cell. Longev.* 2012; 2012**:** 907162. doi: 10.1155/2012/907162

16. Zhang DD, Hannink M. Distinct cysteine residues in Keap1 are required for Keap1-dependent ubiquitination of Nrf2 and for stabilization of Nrf2 by chemopreventive agents and oxidative stress. *Mol. Cell. Biol.* 2003; 23(22)**:** 8137-8151.

17. Itoh K, Mimura J, Yamamoto M. Discovery of the negative regulator of Nrf2, Keap1: a historical overview. *Antioxid Redox Signal* 2010; 13(11)**:** 1665-1678. doi: 10.1089/ars.2010.3222

18. Xu W, Hellerbrand C, Kohler UA, Bugnon P, Kan YW, Werner S *et al.* The Nrf2 transcription factor protects from toxin-induced liver injury and fibrosis. *Lab. Invest.* 2008; 88(10)**:** 1068-1078. doi: 10.1038/labinvest.2008.75

19. Moon MS, McDevitt EI, Zhu J, Stanley B, Krzeminski J, Amin S *et al.* Elevated hepatic iron activates NF-E2-related factor 2-regulated pathway in a dietary iron overload mouse model. *Toxicol. Sci.* 2012; 129(1)**:** 74-85. doi: 10.1093/toxsci/kfs193

20. Tanaka Y, Ikeda T, Yamamoto K, Ogawa H, Kamisako T. Dysregulated expression of fatty acid oxidation enzymes and iron-regulatory genes in livers of Nrf2-null mice. *J Gastroenterol.Hepatol.* 2012. doi: 10.1111/j.1440-1746.2012.07180.x [doi]

21. Kautz L, Gabayan V, Wang X, Wu J, Onwuzurike J, Jung G *et al.* Testing the Iron Hypothesis in a Mouse Model of Atherosclerosis. *Cell Rep.* 2013; 5(5)**:** 1436-1442. doi: PMCID: PMC3880128

22. Kim A, Fung E, Parikh SG, Valore EV, Gabayan V, Nemeth E *et al.* A mouse model of anemia of inflammation: complex pathogenesis with partial dependence on hepcidin. *Blood* 2014; 123(8)**:** 1129-1136. doi: blood-2013-08-521419 [pii];10.1182/blood-2013-08-521419 [doi]

23. Silva-Gomes S, Santos AG, Caldas C, Silva CM, Neves JV, Lopes J *et al.* Transcription factor NRF2 protects mice against dietary iron-induced liver injury by preventing hepatocytic cell death. *J. Hepatol.* 2014; 60(2)**:** 354-361. doi: 10.1016/j.jhep.2013.09.004

24. Feng Q, Migas MC, Waheed A, Britton RS, Fleming RE. Ferritin upregulates hepatic expression of bone morphogenetic protein 6 and hepcidin in mice. *Am. J. Physiol. Gastrointest. Liver Physiol.* 2012; 302(12)**:** G1397-G1404. doi: ajpgi.00020.2012 [pii];10.1152/ajpgi.00020.2012 [doi]

25. Wang W, Knovich MA, Coffman LG, Torti FM, Torti SV. Serum ferritin: Past, present and future. *Biochim.Biophys.Acta* 2010; 1800(8)**:** 760-769. doi: S0304-4165(10)00085-1 [pii];10.1016/j.bbagen.2010.03.011 [doi]

26. Cohen LA, Gutierrez L, Weiss A, Leichtmann-Bardoogo Y, Zhang DL, Crooks DR *et al.* Serum ferritin is derived primarily from macrophages through a nonclassical secretory pathway. *Blood* 2010; 116(9)**:** 1574-1584. doi: blood-2009-11-253815 [pii];10.1182/blood-2009-11-253815 [doi]

27. Cazzola M, Borgna-Pignatti C, de Stefano P, Bergamaschi G, Bongo IG, Dezza L *et al.* Internal distribution of excess iron and sources of serum ferritin in patients with thalassemia. *Scand. J. Haematol.* 1983; 30(4)**:** 289-296.

28. Lescoat G, Hubert N, Moirand R, Jego P, Pasdeloup N, Brissot P. Iron load increases ferritin synthesis and secretion in adult human hepatocyte cultures. *Liver* 1991; 11(1)**:** 24-29.

CONCLUDING REMARKS

This work concentrated on two key aspects of hepcidin: its mechanism of action and its regulation. Chapter 1 elucidated the hepcidin-Fpn interaction and described a new mode of hepcidin action while Chapters 2 and 3 focused on the regulation of hepcidin.

The structure of ferroportin was analyzed in Chapter 1 to provide a comprehensive understanding of the molecular mechanism underlying non-classical Ferroportin Disease and the mechanism of hepcidin action. Non-classical Ferroportin Disease is caused either by Fpn mutants that have impaired hepcidin binding or impaired ubiquitination. Furthermore, we provided evidence that hepcidin binds in the central cavity of Fpn which inhibits iron export by occlusion, a newly described mechanism regulating iron export. However, the contribution of Fpn occlusion to controlling iron export *in vivo* remains to be determined, and the relative role of the canonical mechanism, endocytosis, and our newly described mechanism, occlusion, could vary from tissue to tissue. Despite these uncertainties, we provide evidenced that minihepcidins, which are more potent Fpn occluders than hepcidin and are capable of degrading hepcidin-resistant Fpn mutants, can potentially be used to treat patients with non-classical Ferroportin Disease.

Regulation of hepcidin by erythropoiesis and more specifically, by ERFE was the focus of Chapter 2. Since erythropoiesis suppresses hepcidin by ERFE via the BMP/SMAD pathway, and MT-2 is a negative regulator of the BMP pathway, it was crucial to examine whether or not ERFE suppresses hepcidin through MT-2. We demonstrated that ERFE does not require MT-2 to regulate hepcidin production. We also verified that there is some crosstalk between ERFE and BMP signaling. Though MT-2 and ERFE suppress hepcidin by the BMP/SMAD signaling pathway through different mechanisms, it remains to be determined whether ERFE is a plausible therapeutic for IRIDA patients. In this regard, studies of transgenic ERFE-overexpressing, Tmprss6 -/- mice

would be informative. Also, ERFE may contribute to the disease phenotype of β-thalassemic patients, because they have high ERFE levels due to expanded and ineffective erythropoiesis. Thus, antibodies against ERFE may be a therapeutic approach for β-thalassemic patients.

Lastly, in Chapter 3 we examined the regulation of hepcidin by intracellular iron. We focused on Nrf2 as a candidate intracellular iron sensor because of its role in sensing reactive oxygen species which cause oxidative stress. Since iron overload produces oxidative stress, we hypothesized that Nrf2 could be the link between increasing iron stores and hepcidin regulation, increasing hepcidin transcription in response to iron loading. Contrary to our hypothesis, Nrf2 is not required for hepcidin regulation nor is it involved in the regulation of iron homeostasis.

Overall, this work has provided better understanding of the two most important aspects of the molecular physiology of hepcidin: its mechanism of action and its regulation. Our insights into these two areas should provide the basis for better treatments for iron disorders.